



INSTITUTO SUPERIOR TÉCNICO
Universidade Técnica de Lisboa

**ELECTROMAGNETIC BRAKING SYSTEM FOR AIRCRAFT
APPLICATION
PROTOTYPE DESIGN**

Dário Gonçalo Ribeiro da Silva

Dissertação para a obtenção do Grau de Mestre em
Engenharia Aeroespacial

Júri

Presidente: Doutor João Manuel Lage de Miranda Lemos

Orientador: Doutor Horácio João Matos Fernandes

Vogal: Doutor Agostinho Rui Alves da Fonseca

Novembro de 2010

RESUMO

Do estudo de veículos eléctricos e das soluções utilizadas por estes para aumentar a sua eficiência, houve um sistema que se destacou como passível de ser aplicado a aeronaves - a travagem regenerativa. Travagem regenerativa é utilizada em praticamente todos os veículos eléctricos ou híbridos e contribui significativamente para aumentar a eficiência global do veículo.

Considerando que o táxi eléctrico de aeronaves já é uma solução testada e até expectável de ser uma realidade nos próximos anos, o estudo sobre a viabilidade de um sistema de travagem electromagnética em aeronaves impõem-se. A fim de realizar este estudo e de modo a comprovar a aplicabilidade do sistema, foi desenhado, simulado e produzido um sistema de travagem eléctrico para um veículo protótipo de menor dimensões.

Os resultados obtidos com as simulações mostram que o controlo da travagem electromagnética do protótipo é possível. Os testes experimentais serviram para validar os modelos criados. É possível concluir que apesar de conceptualmente este sistema ser interessante, a tecnologia necessária para a realizar ainda não está disponível, sobretudo devido à limitação do peso. Uma solução a mais curto prazo só será possível com um controlo integrado deste tipo de travagem com os travões de fricção, de modo a atingir valores de desaceleração relevantes.

PALAVRAS-CHAVE: Travagem electromagnética, Táxi eléctrico, Aeronave, protótipo, Travagem regenerativa.

ABSTRACT

The study of electric vehicles and the technologies involved in the continuous search for efficiency improvement, showed that there was a system likely to be applied to aircrafts - regenerative braking. Regenerative braking is used virtually in all electric or hybrid vehicles and contributes significantly to increase the overall efficiency of the vehicle.

Whereas the electric taxi aircraft is already a solution tested and expected to be a reality in the coming years, the study on the feasibility of an electromagnetic braking system for aircraft arises. In order to accomplish this study and prove the applicability of the system it was designed, simulated and produced an electromagnetic braking system for a prototype vehicle of smaller size.

The results obtained with simulations show that control of the electromagnetic braking of the prototype is possible. Experimental tests served to validate the models created. It is possible to conclude that although this system is conceptually interesting, the technology required to perform is not yet available, mainly due to the weight restriction. A shorter term solution is only possible with an integrated control of this type of braking system together with the friction brakes in order to achieve relevant deceleration values.

KEYWORDS: Electromagnetic braking, Electric taxi, Aircraft, Prototype, Regenerative braking.

ACKNOWLEDGEMENTS

This work would not have been possible without the help of several people. I would like to thank:

To my supervisor Prof. Horácio Fernandes, for all the support, guidance and patience during the last months. They were greatly appreciated.

To IPFN and his personnel for the support and practical advice, especially to Eng. João Fortunato for developing the dsPIC board that I used during my work and to Rui Dias for helping me developing the sensor board and the chopper board.

To my colleagues and friends Nuno Silva, João Teixeira, António Henriques, Anabela Reis, Pedro Casau, Carlos Henriques, Duarte Afonso, Guilherme Silva, José Rodrigues, Edmundo Ferreira, Tiago Fernandes, Pedro Fernandes for their unconditional support and friendship throughout the course. I'm also grateful to everyone who, in some way or another, has helped me get through these years.

My last thanks go to Diná and Marco for their unconditional love, and to my parents António and Teresa to whom I owe everything I have.

...Thank you all very much!

CONTENTS

RESUMO	II
ABSTRACT	IV
ACKNOWLEDGMENTS	VI
CONTENTS	VIII
LIST OF FIGURES	XII
LIST OF TABLES	XVI
LIST OF SYMBOLS	XVIII
LIST OF ACRONYMS	XX
1. INTRODUCTION.....	1
1.1 PURPOSE	1
1.2 PROBLEM DESCRIPTION	2
1.3 GOALS.....	2
1.4 LIMITATIONS	2
1.5 DISSERTATION STRUCTURE	2
2. BACKGROUND INFORMATION	3
2.1 AIRCRAFT ELECTRICAL POWER SYSTEMS OVERVIEW.....	3
2.1.1 INTRODUCTION	3
2.1.2 <i>HISTORICAL VIEW</i>	4
2.2 BRAKING SYSTEMS	8
2.2.1 INTRODUCTION	8
2.2.2 HYDRAULIC BRAKING SYSTEM.....	8
2.2.3 ELECTRIC BRAKING SYSTEM	9
2.2.4 APPROACH FOR AN ELECTROMAGNETIC BRAKING SYSTEM.....	10
2.3 ELECTRICAL MACHINES, POWER ELECTRONICS AND ENERGY STORAGE SYSTEMS	12
2.3.1 INTRODUCTION	12
2.3.2 ELECTRICAL MACHINES	12
2.3.3 POWER ELECTRONICS.....	14
2.3.4 ENERGY STORAGE SYSTEM.....	17

2.3.5	ENERGY DISSIPATION SYSTEMS.....	20
3.	DESIGN SOLUTION	21
3.1	INTRODUCTION	21
3.2	PRELIMINARY ANALYSIS.....	21
3.2.1	LANDING BRAKING POWER.....	21
3.2.2	LANDING POWER PROFILE	22
3.3	DESIGN REQUIREMENTS	22
3.3.1	BRAKING CAPABILITY.....	23
3.3.2	REGENERATION CAPABILITY.....	23
3.3.3	REQUIREMENTS.....	23
3.4	CONCEPTUAL DESIGN.....	24
3.4.1	ELECTRICAL MACHINES	24
3.4.2	ENERGY STORAGE SYSTEM.....	25
3.4.3	POWER ELECTRONICS.....	26
3.4.4	CONCEPT I	26
3.4.5	CONCEPT II	26
3.5	PRELIMINARY STUDY OF VIABILITY	27
3.6	DESIGN APPROACH - PROTOTYPE	27
3.6.1	VEHICLE	28
3.6.2	ELECTRICAL MACHINE	28
3.6.3	ENERGY STORAGE SYSTEM.....	28
4.	PROTOTYPE DESIGN	29
4.1	INTRODUCTION	29
4.2	MODELING AND SIMULATION SOFTWARE OVERVIEW.....	29
4.2.1	MATLAB/SIMULINK	29
4.2.2	BLOCK LIBRARY.....	30
4.2.3	SIMULATION PARAMETERS.....	30
4.3	PROTOTYPE DESIGN SUBSYSTEMS AND MODELS.....	31
4.3.1	VEHICLE SUBSYSTEM	31
4.3.2	POWER ELECTRONICS SUBSYSTEM	36
4.4	PROTOTYPE DESIGN RESULTS	42
4.4.1	TORQUE.....	42
4.4.2	POWER REGENERATION.....	43
4.4.3	DECELERATION	43

4.5	CONTROLLER	44
4.5.1	CONTROL STRATEGIE.....	44
4.5.2	MAIN CONTROLLER	45
4.5.3	BRAKING CONTROLLER.....	48
4.6	BRAKING CONTROL RESULTS	50
4.6.1	CURRENT CONTROLLER TUNING.....	50
4.6.2	DECELERATION CONTROLLER TUNING.....	53
4.6.3	BRAKING CONTROL	55
4.6.4	TRANSITION BETWEEN BRAKING MODES.....	57
5.	PHYSICAL PROTOTYPE - DESIGN AND TEST	59
5.1	PHYSICAL EQUIPMENT	59
5.1.1	VEHICLE	59
5.1.2	ELECTRIC MACHINE	60
5.1.3	BATTERY AND POWER RESISTOR	60
5.1.4	TRANSMISSION.....	61
5.2	SENSOR SYSTEM	61
5.2.1	CURRENT SENSOR	61
5.2.2	VOLTAGE SENSORS.....	64
5.2.3	5.2.3 ANGULAR SPEED SENSOR.....	65
5.2.4	5.2.4 BRAKE SWITCHES.....	66
5.2.5	5.2.5 SENSOR BOARD	66
5.3	CONTROL SYSTEM	67
5.3.1	MICROPROCESSOR BOARD	67
5.3.2	CHOPPER CIRCUIT	68
5.3.3	PROGRAMMING	69
5.4	PROTOTYPE TEST RESULTS	73
5.4.1	POWER	74
5.4.2	TORQUE.....	74
5.5	DISCUSSION AND LIMITATIONS	75
5.5.1	POWER	75
5.5.2	TORQUE.....	76
6.	CONCLUSIONS AND FUTURE WORK.....	77
6.1	CONCLUSIONS.....	77
6.2	FUTURE WORK	78

A: MATLAB SIMULINK MODELS.....	79
B: SENSOR AND CONTROL SYSTEM GRAPHICS.....	87
C: PROGRAMMING CODES	91
D: MANUFACTURED PIECES	98
BIBLIOGRAPHY.....	99

LIST OF FIGURES

FIGURE 2.1 - Historic Air Traffic Growth (In Trillions Of Passenger) [3]	4
FIGURE 2.2 - Commercial Aviation Electrical Power Systems And Infrastructures Market: Aircraft Electrical Power Generating Capacity By Aircraft Type [4]	5
FIGURE 2.3- CAD Representation of the Electric Motor Mounted In the Landing Gear [5]	6
FIGURE 2.4 - Aircraft Power Brake Control Valve System [9]	9
FIGURE 2.5 - Aircraft Electric Brake From Messier-Bugatti® [10]	9
FIGURE 2.6 - Parallel Regenerative Braking Graphic Representation	11
FIGURE 2.7 - Series Regenerative Braking Graphic Representation	11
FIGURE 2.8 - Three-Phase Bridge Rectifier Circuit	15
FIGURE 2.9 - Three-Phase Input Sinewaves and Resultant Dc Waveform Over Time	16
FIGURE 2.10 - Graphic Representation of Pulse Width Modulation with Different Duty Cycle VALUES (50% Duty Cycle On Top, And 25% Duty Cycle Down).....	16
FIGURE 2.11 – Typical Single Quadrant Chopper Circuit.....	17
FIGURE 2.12- Graphical Representation of Specific Energy and Specific Power by Type of Ess [14]	17
FIGURE 3.1 - Braking Power Profile during Landing (40ton Aircraft At 67m/S During 30sec)	22
FIGURE 3.2 - CAD Representation of a Possibility for the Electric Motor Mount in the Landing Gear	25
FIGURE 3.3 - Concept I Design.....	26
FIGURE 3.4 - Concept Ii Design.....	27
FIGURE 3.5 – Representation of the Rotor of a Lundell or Claw-Pole Alternator.....	28
FIGURE 4.1- Simulation models Schematic	31
FIGURE 4.2 - Vehicle Subsystem.....	32
FIGURE 4.3 - Forces Acting On a Vehicle [20]	32
FIGURE 4.4 - Vehicle Road Load Forces A Function Of Increasing Vehicle Speed (Slope = 0%)..	34
FIGURE 4.5 - Tire Model Variables	35
FIGURE 4.6 – Schematic of the Connections between the Different Equipments in the Power Electronics Subsystem.....	37
FIGURE 4.7 - Synchronous Machine Qd Frame Representation	38
FIGURE 4.8 - Clarke And Parke Transformations.....	38
FIGURE 4.9 - Electrical Model And Equations Of Synchronous Machine.....	39
FIGURE 4.10 – Method for Generating Pwm Pulses	40
FIGURE 4.11 - Typical Charge Characteristics	41
FIGURE 4.12 - Nominal Discharge Characteristic At Nominal Current.....	41

FIGURE 4.13 - Electromagnetic Torque Profile as the Vehicle Decelerates From 50km/H to 0km/H for Different Feeding Currents in Rotor (2,4A and 3,6A)	42
FIGURE 4.14 - Power Regeneration Profile as the Vehicle Decelerates From 50km/H to 0km/H for Different Feeding Currents in Rotor (2,4A and 3,6A)	43
FIGURE 4.15 - Vehicle Deceleration Profile as the Vehicle Decelerates From 50km/H to 0km/H for Different Feeding Currents in Rotor (2,4A and 3,6A)	43
FIGURE 4.16 - Overview of the Control Systems.....	44
FIGURE 4.17 - Main Controller Schematic.....	45
FIGURE 4.18 - Simplified Stateflow Control System.....	46
FIGURE 4.19 - Electromagnetic Braking Sub-State Detail	47
FIGURE 4.20- Control Logic Of Main Controller	48
FIGURE 4.21- PID Control Scheme	49
FIGURE 4.22- Ziegler-Nichols Open Loop Method: Reaction Curve With the Dead-Time “D” And the Rate “R” From the Process Step Response Represented [27]	50
FIGURE 4.23 - Current Regeneration in Open Loop during 10 Seconds with an Initial Velocity of 50km/h	51
FIGURE 4.24 - Current Regeneration with Pi Controller (P=0.12, I=0.75) During 10 Seconds with an Initial Velocity of 50km/h	51
FIGURE 4.25 - Current Regeneration with Pi Controller (P=0.15, I=0.2 and D=0.012) During 10 Seconds with an Initial Velocity of 50km/h.....	52
FIGURE 4.26- Vehicle Deceleration with PID Controller (P=I=D=1) as the Vehicle Decelerates From 50km/h.....	53
FIGURE 4.27 - Vehicle Deceleration with PI Controller (P=10, I=5) as the Vehicle Decelerates From 50km/h.....	54
FIGURE 4.28 - Vehicle Deceleration with PID Controller (P=25, I=20) as the Vehicle Decelerates From 50km/h.....	54
FIGURE 4.29 - Vehicle Deceleration as the Vehicle Decelerates from 50km/h to 0km/h in the ELECT_BRAKE_MODE1 Braking Mode	55
FIGURE 4.30 - Electromagnetic Torque as the Vehicle Decelerates from 50km/h to 0km/h in the ELECT_BRAKE_MODE1 Braking Mode	56
FIGURE 4.31 - Power Regeneration and Dissipation Profiles as the Vehicle Decelerates from 50km/h to 0km/h in the ELECT_BRAKE_MODE1 Braking Mode.....	56
FIGURE 4.32 - Vehicle Velocity as the vehicle decelerates from 50km/h to 0km/h in the ELECT_BRAKE_MODE1 Braking Mode	57
FIGURE 4.33 - Current Regeneration Response to the Transition between Different Braking Mode Solicitations.....	58
FIGURE 4.34 - Vehicle Deceleration Response to the Transition between Different Braking Mode Solicitations.....	58

FIGURE 5.1 - 24V, 80A Alternator.....	60
FIGURE 5.2 - 12V Battery and the Power Resistor	60
FIGURE 5.3 - Transmission	61
FIGURE 5.4 - High-Side and Low-Side Resistive Current Shunts	62
FIGURE 5.5 - Circuit of the Current Sensor.....	63
FIGURE 5.6 - Circuit of Voltage Sensor.....	64
FIGURE 5.7 - Circuit of Speed Sensor	65
FIGURE 5.8 - Motorcycle Handle Switches.....	66
FIGURE 5.9 - Top Side and Bottom Side Virtual Representation of the Sensors PCB	66
FIGURE 5.10 - Sensors PCB Top Side and Bottom Side	67
FIGURE 5.11 - Microprocessor Board.....	68
FIGURE 5.12 - Chopper Circuit Designed.....	68
FIGURE 5.13 - Chopper Board	69
FIGURE 5.14 - 10BIT, High-Speed ADC Functional Block Diagram [31]	70
FIGURE 5.15- UART Transmitter Block Diagram [31]	71
FIGURE 5.16 - PWM Output Timing	72
FIGURE 5.17 – Assembly to Test the Prototype	73
FIGURE 5.18 – Controller Assembly to Test the Prototype.....	73
FIGURE 5.19 – Measured Power Dissipated Vs Speed.....	74
FIGURE 5.20 – Measured Torque Vs Speed	74
FIGURE 5.21 - Power Dissipation (Duty Cycle =49%)	75
FIGURE 5.22 - Power Dissipation (Duty Cycle =99%)	75
FIGURE 5.23 - Electromagnetic Torque (Duty Cycle =49%).....	76
FIGURE 5.24 - Electromagnetic Torque (Duty Cycle =99%).....	76
FIGURE A.1 - Simulink Model Overview	79
FIGURE A.2 - Main Controller Stateflow	79
FIGURE A.3 - Vehicle Subsystem Models	80
FIGURE A.4 - Electromagnetic Braking System	80
FIGURE A.5 – ALTERNATOR AND BRIDGE RECTIFIER.....	81
FIGURE A.6 - Bridge Rectifier	81
FIGURE A.7 - Relay.....	82
FIGURE A.8 - Resistor and Measurements	82
FIGURE A.9 - Battery and Measurements	83
FIGURE A.10 - Braking Controller Block	83
FIGURE A.11 – Decel Field Controller.....	84
FIGURE A.12 - Decel Field Controller	84
FIGURE A.13 - PWM and Chopper.....	85
FIGURE A.14 - PWM Generator.....	85

FIGURE A.15 - Torque Actuator.....	85
FIGURE A.16 - Simulation Measurements and stop Simulation.....	86
FIGURE B.1 - Current Sensor Performance (Blue - Current, Green Output)	87
FIGURE B.2 - current ouput AC Analysis (F-3db =19,46Hz)	87
FIGURE B.3 – Angular Speed Sensor Performance (current in Yellow with 1 mA/V and Voltage Output in Blue).....	88
FIGURE B.4 - Chopper Circuit Measurements (Current in Purple with 1 A/V = 2.38A, Chopper Freq = 1khz, Duty cycle=99% and 24V Battery in Blue)	88
FIGURE B.5 - Chopper Circuit Measurements (Current in Purple with 1 A/V = 1.13A, Chopper Freq = 1khz, Duty Cycle=50% and 24V Battery in Blue)	89
FIGURE B.6 - Chopper Circuit Measurements (Current in Purple with 1 A/V = 527mA, Chopper Freq = 1khz, Duty Cycle=99% and 24V Battery in Blue)	89
FIGURE C.1 – Alternator Support Piece.....	98
FIGURE C.2 – Separation Disc for the Wheel’s Gear	98

LIST OF TABLES

TABLE 2.1- Main Characteristics of Common Power Switching Devices [13]	15
TABLE 2.2 - Characteristics of Commonly Used Rechargeable Batteries [15]	18
TABLE 3.1 - Electrical Machines Comparison	24
TABLE 3.2 - ESS Comparison.....	25
TABLE 3.3 –Scaling Between Aircraft And Prototype Designs	28
TABLE 4.1 - Vehicle Subsystem Main Characteristics.....	36
TABLE 4.2- alternator simulation parameters.....	39
TABLE 4.3- Bridge Rectifier Diodes Parameters	40
TABLE 4.4- Characteristics of the Chopper Circuit Devices.....	40
TABLE 4.5 - 36v lead-acid battery parameters.....	41
TABLE 4.6 - ziegler-nichols open loop method: formulas for the controller parameters [27] ...	50
TABLE 4.7 - current pi controller coefficients	52
TABLE 4.8 - Effects on the Closed-Loop Response of Adding to the Controller Terms K_p , K_i and K_d	53
TABLE 4.9 – Deceleration PID Controller Coefficients	55
TABLE 5.1 - Two-Wheeled Vehicle Characteristics.....	59
TABLE 5.2: Comparison of Current Sensing Methods [28].....	62
TABLE 5.3 - Advantages and Disadvantages of High-Side and Low-Side Current Measurement	63
TABLE 5.4 - Angular Speed Sensors Characteristics	65
TABLE A.1 - Model Overview.....	79
TABLE A.2 - Model Overview.....	80
TABLE A.3 - Electromagnetic Braking System	81
TABLE A.4 - Alternator And Bridge Rectifier	81
TABLE A.5 – Bridge Rectifier.....	81
TABLE A.6 - Relay.....	82
TABLE A.7 - Resistor and Measurements	82
TABLE A.8 - Battery and Measurements	83
TABLE A.9 - Braking Controller Block	83
TABLE A.10 - Deceleration Field Controller.....	84
TABLE A.11 – Current Field Controller	84
TABLE A.12 - PWM and Chopper.....	85
TABLE A.13 - PWM Generator.....	85
TABLE A.14 - Torque Actuator.....	86
TABLE A.15 - Simulation Measurements and Stop Simulation	86

LIST OF SYMBOLS

A	Frontal area of the vehicle, m ²	K _D	Differential gain
<i>a</i>	Acceleration, m/s ²	K _I	Integral gain
C	Capacity, F	K _P	Proportional gain
C _D	Aerodynamic drag coefficient	L	Inductance, H
d	Distance between capacitors plates	I _w	Wheels rotational inertia, kg.m ²
E	Energy, J	m	Mass, kg
F	Force, N	m _w	Wheel mass, kg
<i>F</i> _{AERO}	Aerodynamic Drag, N	P	Power, W
<i>F</i> _{BRAKE}	Friction Brakes Force, N	R	Resistance, Ω
f _c	Cutoff Frequency, Hz	r _e	Effective rolling radius, m
<i>F</i> _{EMBRAKE}	Electric motor braking/traction Force, N	r _w	radius of the wheel, m
<i>F</i> _G	Gravity Force (slope), N	t _c	time constant, s
f _r	Rolling resistance coefficient	u	tire deformation, m
<i>F</i> _{ROLL}	Rolling Resistance, N	v	Velocity, m/s
<i>F</i> _X	Represent the traction forces, N	V	Voltage
g	Gravity acceleration, 9,8 m/s ²	β	Road Grade, deg
I	Current, A	ρ	Air density, kg/m ³
K	Tire Slip	ω	Angular speed, rad/s

LIST OF ACRONYMS

AC – Alternate Current	ICE – Internal Combustion Engine
A/D - Analog-to-Digital	IM – Induction Motor
ADC - Analog-to-Digital Converter	I/O - Input/output
BBW – Brake-by-wire	IPFN - Instituto de Plasmas e Fusão Nuclear
BLDC – Brushless direct current	MEA – More Electric Aircraft
CG – Center of Gravity	MOSFET – Metal Oxide Semiconductor Field Effect Transistor
DC - Direct current	Op-amp - operational amplifier
DsPIC - Digital Signal Programmable Intelligent Computer	PCB - Printed Circuit Board
EM – Electromagnetic	PID – Proportional Integral Derivative
ESS – Energy Storage System	PWM - Pulse-Width Modulation
FBW – Fly-by-wire	S/H - Sample/Hold
FIFO - First-In-First-Out	SOC – State of Charge
FOD – Foreign objects debris	SRM – Switched Reluctance Motor
HEV – Hybrid Electric Vehicle	UART - Universal Asynchronous Receiver/Transmitter
IGBT – Insulated Gate Bipolar Transistor	

CHAPTER 1

INTRODUCTION

1.1 PURPOSE

An aircraft is composed of systems that convert fuel's energy to mechanical energy in order to perform work, which is the movement of people and cargo. Today, the fast-growing demand for air travel has outpaced the rate of improvement in the energy efficiency of aircraft systems. The increase in the total energy consumption and environmental impact of aviation demands a strategy to induce further technological and operational innovations to mitigate the increase in aircraft energy use and the environmental effects.

The integration of more electrical systems and the ability of energy regeneration onto the aircraft power system are some of the strategies and innovations recently studied. By replacing mechanical and hydraulic systems for electrical is possible to reduce operating costs, diminish weight and increase the aircraft's overall efficiency.

One of the electrical systems studied and already tested by Boeing Company [1] is the electric taxi system. This system consists on the integration of an electric motor on the nose landing gear which would allow the aircraft to taxi both backward and forward without the use of tugs or the engines. This is a very important feature that companies are looking forward to see implemented, especially if we remember that the ground taxi is traditionally the most inefficient operation of an aircraft and on typical short to medium-haul routes aircrafts spend a significant amount of time in such ground operations.

In this thesis the first approach to aircraft's "hybridization" is considered and new features are studied. Essentially, by making a parallelism with the automobile industry, is analyzed the possibility of using the wheel's electric motor concept as generator and its use for braking the aircraft. This would allow the regeneration of energy otherwise spent as heat in the brakes, and also successfully retard the aircraft's motion.

The emphasis of this thesis is placed in the project, simulation, construction and validation of a controller for braking energy recovery. In order to fulfill this objective was given special attention to the study of aircraft's braking systems, as well as electric motors, power converters and control strategies. To verify the viability of the concept was conducted a few tests in a two-wheeled vehicle.

1.2 PROBLEM DESCRIPTION

The design of an electromagnetic braking system for aircraft application implicates the complete dimensioning of the system considering the situations where it might be used.

The simulation of the system designed must be accurate, considering the vehicle dynamic and the electric equipment. The controller must regulate vehicle braking and manage the energy storage system. For last the physical construction and equipment must resemble the equipment simulation parameters.

1.3 GOALS

- Design of an electromagnetic braking system with energy recovery for an airplane.
- Simulation and development of the braking controller for a prototype vehicle.

1.4 LIMITATIONS

Given the fact that is impossible to have an airplane and the hardware for a full scale test, was developed a smaller scale project and the validation test was also made in a smaller vehicle. Afterward was made the correlation between the two scales for feasibility purposes.

1.5 DISSERTATION STRUCTURE

The thesis layout is made through the following short chapter's description:

- Chapter 2: Introduces the electric taxi concept and aircraft braking systems as well as background information about electrical machines and power electronics;
- Chapter 3: Presents the study of an electromagnetic braking system design both for an aircraft and for the developed prototype;
- Chapter 4: Displays the simulation results for the braking controller of the prototype design.
- Chapter 5: Shows the physical prototype project and results of a few tests made in it.
- Chapter 6: Concludes this project and presents future works.

The appendixes provide complementary information to the subjects discussed throughout this dissertation.

CHAPTER 2

BACKGROUND INFORMATION

2.1 AIRCRAFT ELECTRICAL POWER SYSTEMS OVERVIEW

2.1.1 INTRODUCTION

The increase of petrol consumption causes the problem of greenhouse effect and energy crises. The air transportation is responsible of burning large amounts of petrol and is a major source of air pollution, especially considering the expected air traffic growth (Figure 2.1). A strategy for energy economy is to use alternatives to petrol in order to reduce the consumption and emissions of greenhouse gas.

Research on alternative fuels has been ongoing for decades, but none has the energy density of aviation's fuel, which is essential since minimizing the gross weight of aircraft is critical for an efficient operation. Synthetic fuels have been demonstrated on aircraft and are mentioned as an alternative. However producing these fuels requires far more energy than common aviation fuel. Alternatives to fossil fuels are more practical with other forms of transportation; hence the airline industry must focus on increasing efficiency and finding ways of recycling energy which nowadays is being dissipated.

In this context the utilization of the electrical solutions in the non-propulsive aircraft systems has been put forward as a major medium-term improvement for aviation, just like the Hybrid electric Vehicle (HEV) for the automotive industries.

Advances in the areas of power electronics are providing the technology to improve efficiency and safety of aircraft systems operation. The aircraft industry is developing the More Electric Aircraft (MEA) with an ultimate goal of distributing only electrical power across the airframe [2].

With the MEA numerous advantages are achieved, such as optimizing the aircraft performance and decreasing operating and maintenance costs: gone would be the complex, heavy, maintenance-intensive, and (in combat) vulnerable hydraulic systems, with their flammable liquids operating at high temperature and pressure. Gone too would be the miles of tubing, the pumps and valves. Weight could be shifted from plumbing to passengers, fuel or mission payloads.

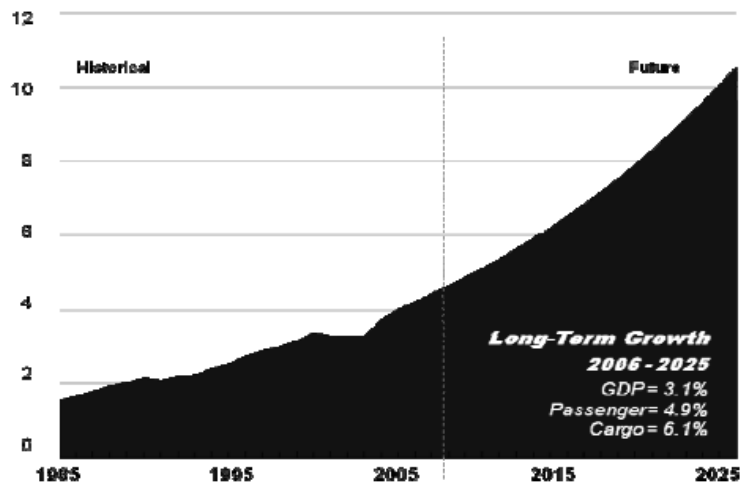


FIGURE 2.1 - Historic Air Traffic Growth (In Trillions Of Passenger) [3]

2.1.2 HISTORICAL VIEW

From the beginning of the aeronautic history airplanes have always become more and more electrical. In the 50's 115V AC was introduced in the power network of airplane to supply some power loads. In the 80's the first "Fly-by-Wire" (FBW) airplane was manufactured by Airbus in the A320 and later series. Boeing followed this design in 777 and later designs. In this design the electrical control linkages, combined with computers, replace the mechanical and hydraulic linkages between the control stick and the flight control surface. The design of FBW saves weight and improves the reliability and the use of computers makes the control easier and safer [2].

The revolution of FBW makes the electricity take a more important role. But in this design the actuators of the flight controls are still supplied by hydraulic system. As a consequence in most types of commercial airplanes there are several hydraulic circuits to transfer the energy from the pumps to the actuators of flight controls.

In the recent years with the Airbus 350, the Boeing 787, and the Airbus 380 adopting the More Electric Aircraft, several new technologies have emerged like electrohydrostatic actuators for the control surfaces or electric brakes [4]. Although other new features such as the electric taxi are reserved for the future.

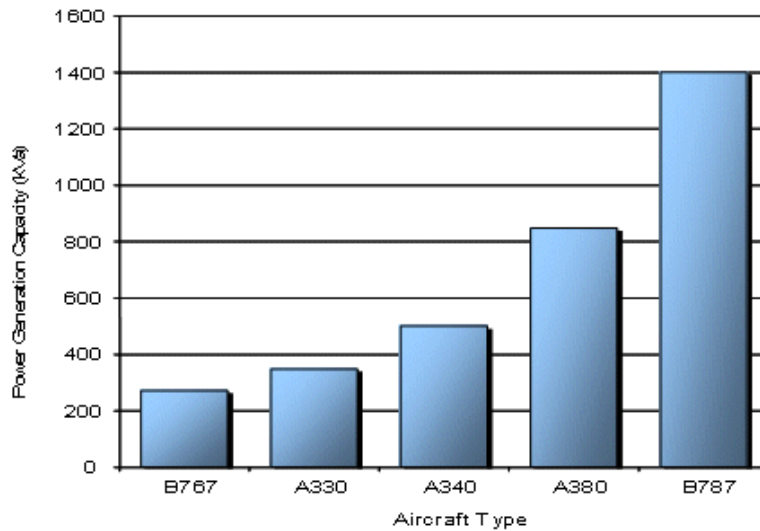


FIGURE 2.ERROR! BOOKMARK NOT DEFINED. - Commercial Aviation Electrical Power Systems and Infrastructures Market: Aircraft Electrical Power Generating Capacity by Aircraft Type [4]

2.1.2.1 ELECTRIC TAXI CONCEPT

On a typical short to medium-haul routes aircrafts spend a significant amount of time in ground operations, and these are often forgotten, especially if we keep in mind that one of the most inefficient operations of an aircraft is traditionally the ground taxi. For example a 737 will typically consume between 17 and 25 pounds/minute of fuel while idling.

In order to optimize this operation the engineers at Chorus Motors® developed a new AC induction motor and drive systems for the nose landing gear of an aircraft - Chorus WheelTug®. This system is very powerful and allows the aircraft to taxi both backward and forward without the use of tugs or engines [5]. This new technology was already tested but is not yet implemented in aviation.

The electric taxi WheelTug® system made for the 737NG is built around 2 multi-phase (18 phases) 5.6 kW AC-induction motors with integrated planetary gears to drive the wheels directly (these motors have 10 times more torque than normal tri-phase induction motors) [6] [7]. They work with 400-480 line to line AC voltage from the APU, generating a total of 15 HP to move the aircraft (confirmed to be more than enough by tow-test data).

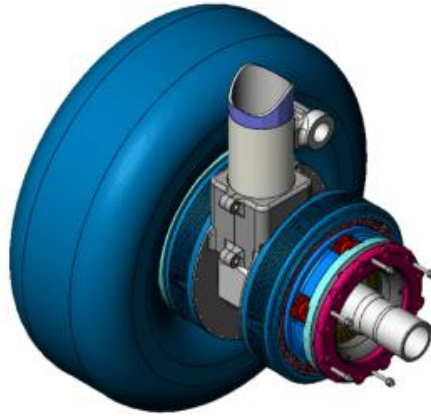


FIGURE 2.2- CAD Representation of the Electric Motor Mounted In the Landing Gear [5]

2.1.2.2 BENEFITS

With this system several benefits can be obtained in the following areas:

- Fuel Savings;
- Time Savings;
- FOD Protection;
- Brakes wear;
- Safety;
- Environmental savings;

FUEL SAVINGS

Taxiing at airports using the engines is forecasted to cost \$7Billion by 2012 only in fuel. With this technology is possible to largely cut the fuel consumption (about 13-21 lbs/min during taxi time - 737-800 data), reducing the airports fuel bill and minimizing the effects of unexpected ground delays.

TIME SAVINGS

With this system the pilot will be responsible for driving the aircraft while the engines are off. This means that the aircraft can immediately depart when tower approval is granted, without needing to wait for tugs and go through the tug attachment/detachment process.

Jet blast in the ramp (gate) area is a major cause of damage to aircraft and danger to ground personnel. These safety concerns result in numerous ground operations restrictions - impacting operational, insurance and scheduling costs.

FOD PROTECTION

When operating on the ground engines almost continually suck in dust and other debris: 85% of foreign object debris (FOD) can be found around the gate and taxiway areas. These objects frequently damage the structure, wheels and engines. With this system we can radically reduce foreign object damage by letting aircrafts to do ground operations with their engines off, allowing aircraft operators to cut their maintenance costs, improve efficiency, and reduce unscheduled out of service times.

BRAKES WEAR

Another area that will also benefit is the braking system because while taxiing, as the engines are off, there will be no need to use the brakes in order to counter the engine thrust. This will substantially reduce brake's wear and durability.

SAFETY

Engines in the ramp area create serious safety issues which require stringent procedural safety measures. For instance vehicles and personnel are generally prohibited in the area around aircraft, while the engines are in use. With this electric powered solution many of the ground-operation safety procedures could be relaxed, enabling faster, smoother and safer turnaround operations.

While in ground aircraft engines can also inhale items such as birds, baggage or tools which can be shredded and propelled out, becoming dangerous projectiles.

ENVIRONMENTAL SAVINGS

By eliminating one of the most inefficient part of every flight that is the ground taxi, it is possible to reduce carbon dioxide emissions by over 10%, and NOx emissions by over 20% (737-800 data) [8].

While eliminating the need for tugs, the emissions of these vehicles which are often significant polluters are also removed. Other important advantage is the almost inexistent noise in these operations when compared with the same operation with the engines on.

2.1.2.3 PROBLEMS

There are many problems that delay the implementation of this technology in aircrafts. Most of them concern the lack of space and preparation presented by in-service aircrafts landing gears for receiving this electric motor system. Though there are still other problems regarding for example the weight of the motor/drive assembly and the tires wear.

WEIGHT

One problem pointed to this technology is the increased weight put in the nose landing gear, not only because of the electric system weight but also because of the necessity for increasing the resistance of the nose landing gear structure in order to support the electric motor torque and weight.

TIRES

The placement will be done in the front landing gear and the exceeding weight of this propelling system might result in the tires traction to wear out more quickly. Also its performance over a wet/icy pavement might be an issue.

2.2 BRAKING SYSTEMS

2.2.1 INTRODUCTION

The purpose of the brakes is to retard or stop the vehicle in motion by converting the kinetic energy of the moving vehicle into rotational frictional torque. This energy will then change into heat and the brakes should be able to dissipate it and absorb the large braking torques encountered.

The typical brake for aviation is a carbon disk brake with hydraulic actuators, since it is an efficient method of transmitting the driver's foot-pedal force to individual brakes at each wheel. However the state-of-art for aviation are electric braking systems, which are standard carbon disc brakes actuated by electric motors.

2.2.2 HYDRAULIC BRAKING SYSTEM

All hydraulic brake systems operate on the same basic principle. When the operator moves a brake pedal, or other brake operating control, the movement is transmitted to a master cylinder or a power brake control valve from which fluid pressure is delivered through connecting lines to a brake assembly connected to a wheel or shaft whose movement is to be braked. The fluid pressure acting on the brake assembly pushes brake linings into contact with surfaces of a rotating disc. The resulting friction slows--and eventually stops--the continued rotation of the wheel or shaft to which the disc is connected. When the brake pedal or brake control is returned to the off position, brake operating pressure is relieved, the brake lining loses contact with the disc, and the wheel or shaft is free to rotate again [9].

Aircraft wheel's brake systems are dual in nature in a way that they are composed of two identical subsystems. They can be operated independently of each other to provide separate braking action for the landing gear on each side of the aircraft. Each subsystem is operated by a toe plate (brake pedal) that is hinge-mounted to the top of the aircraft rudder pedal. Since each brake pedal can be operated independently the brakes can be used for steering the aircraft.

A list of components, which can be found in varying combinations to make different wheel brake systems, includes the following: master cylinder (or a power brake control valve), wheel brake assemblies deboosters, parking brake valves, shuttle valves, accumulators, connecting lines, and bottles charged with compressed air. The minimum number of parts which could be used to perform the function of a simple wheel brake system are a master cylinder (or a power brake control valve), a wheel brake assembly, and connecting lines.

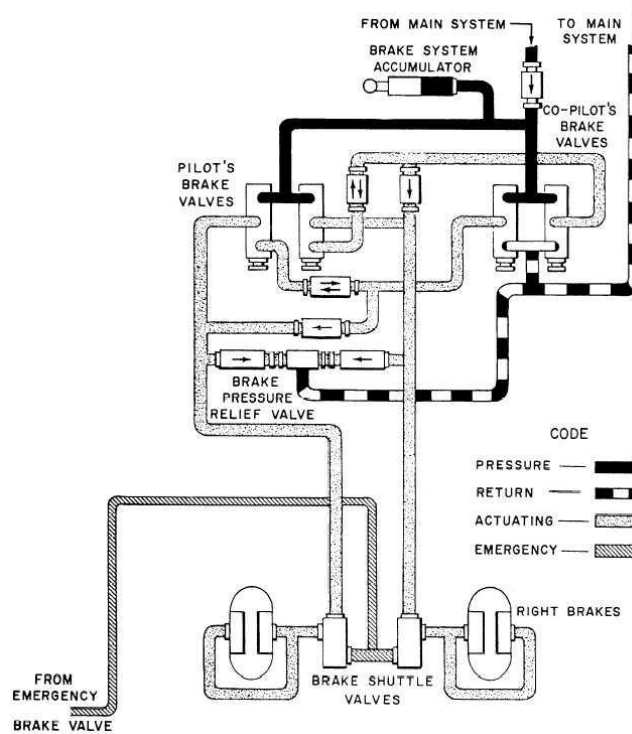


FIGURE 2.3 - Aircraft Power Brake Control Valve System [9]

2.2.3 ELECTRIC BRAKING SYSTEM

The electric brakes are the state-of-art of aircraft braking and this system, developed by Messier-Bugatti®, will supply the new 787-Dreamliner. In an electric braking system electronic control units and electrical wiring replace hydraulic lines and equipment, and electromechanical actuators replace hydraulic pistons. When the pilot steps on the brake pedal a computer sends information to a control box, which converts these electrical signals into an electromechanical command: the actuators on the brake ring, replacing the hydraulic pistons, press the carbon disks against each other as in a conventional hydraulic system.

This offers a host of advantages in terms of volume, weight, reliability, safety (by eliminating the risk of hydraulic fluid leaks and associated fire hazards), and operating/maintenance costs. Electric brake technology enhances the efficiency of braking in general and of each individual brake, through faster response simpler installation and easier diagnostics and maintenance.



FIGURE 2.4 - Aircraft Electric Brake From Messier-Bugatti® [10]

2.2.4 APPROACH FOR AN ELECTROMAGNETIC BRAKING SYSTEM

In almost all hybrid electric vehicles we can find some form of regenerative braking or dynamic braking, where the electric motor used to propel the vehicle is used as generator and with that successfully recover energy and retard the vehicle's motion.

Considering the hybrid electric vehicles and creating a parallelism with the Electric Taxi concept, the author proposes a system which would be mounted in the landing gear and where a dynamically functioning motor/generator coupled to the aircraft's wheels could be used not only to propel the aircraft in ground operations but also help to retard his movements while recovering energy.

With this system will be possible to reduce the brakes wear and recover some of the energy otherwise spent as heat in the brakes. This will be thoroughly specified in the Design Solution Chapter.

2.2.4.1 REGENERATIVE BRAKING

This is a key feature of electric and hybrid vehicles. The electric motors can be controlled to operate as generators to convert the kinetic energy of the vehicle into electrical energy that can be stored and reused. The regeneration occurs when the counter-electromotive force produced by the rotating system exceeds the supply voltage (such as a battery).

The braking capability is also an essential part of the design as the vehicle must be stopped in a certain recommended distance; however the braking torque required to stop a large aircraft is much larger than the torque that an electric motor can produce. Therefore the mechanical friction braking system must coexist with the electromagnetic braking.

Regenerative braking control strategies can be divided into two main categories, parallel and series braking strategies.

PARALLEL REGENERATIVE BRAKING

The parallel braking strategy always makes use of both regenerative braking and friction braking simultaneously. Figure 2.5 visualizes the strategy from which it can be seen that an arbitrary amount of regenerative braking (dependent on the component specification etc.) is used as basis. The total retardation demand, i.e. the sum of both brake contributions, is met by adding friction braking on top of the regenerative braking, regardless of the demand itself.

The advantages of this strategy are simple control and smooth operation because both brake-components scale linearly and there are no abrupt changes in the force distribution. However, compared to the series braking strategy, less energy will be captured because of the fact that some energy always will be lost to heat by the friction braking [11]

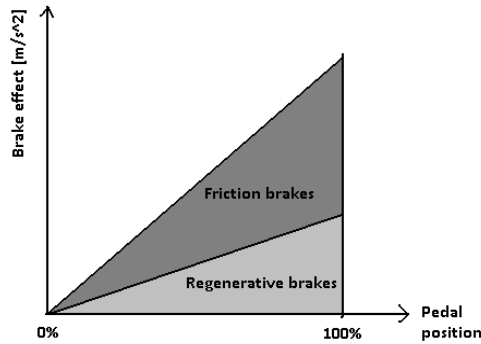


FIGURE 2.5 - Parallel Regenerative Braking Graphic Representation

SERIES REGENERATIVE BRAKING

Compared to the parallel strategy the series strategy uses exclusively regenerative braking up to a specified limit, which can be seen in Figure 2.6. The limit is normally specified as a “pedal position” which indirectly can be translated into a certain braking torque.

By only using regenerative braking up to a certain level of retardation, all of the kinetic energy (without compensation for the non-ideal efficiency) can be harnessed during mild retardations. If the retardation level is increased above the preset level, the friction brakes will be activated and energy is once again lost directly into heat.

The obvious advantage over the parallel strategy is that 100 % regenerative braking is possible up to a certain level of retardation; hence more energy can be harnessed. However the force distribution control between the two brake-components will be more advanced and there is an increased risk of erratic brake operation during transitions [11].

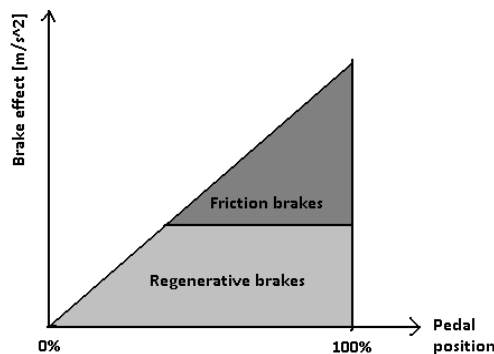


FIGURE 2.6 - Series Regenerative Braking Graphic Representation

2.2.4.2 DYNAMIC BRAKING

The electromotive force generated by the machine, acting as a generator, driven by the mechanical system forces current in the reverse direction through the armature. Thus a torque is produced to oppose rotation and the load decelerates as its energy is dissipated, mostly in the external resistor, but to some extent also in core and copper losses of the machine. Summarizing, this concept is very similar to Regenerative Braking but instead of using the electricity to charge a battery, the energy is burned in a high-wattage resistor wasting it as heat.

2.3 ELECTRICAL MACHINES, POWER ELECTRONICS AND ENERGY STORAGE SYSTEMS

2.3.1 INTRODUCTION

The following section will describe the basic components and operation of electric motors, power electronics and energy storage systems that can be used for vehicles electromagnetic braking.

2.3.2 ELECTRICAL MACHINES

The basics of electrical machines take advantage of the interaction between an electric current and a magnetic field. This is called the “Lorenz force” and is the basis for torque production. All electrical machines have a stator and a rotor with a gap in between but the component design can either be plates or cylinders. The most common type is the cylindrical version and the magnetic field is either produced by a permanently magnetized material or alternatively with the use of electromagnets [12].

When currents are drawn through the motor windings in a certain direction, relative to the polarity of the adjacent permanent magnet, and in the other direction near magnets with the reversed polarity, torque will be produced. This can be done in many ways and with many types of rotor and stator configuration, along with different magnetization methods, but the basic idea is the same.

For the purpose of the electromagnetic braking system there are several features that the electric motor should meet, some of the most important are:

- Small and lightweight
- High and controllable torque
- Good regeneration capability
- High efficiency
- Good reliability
- Low cost

Having into account the previous requirements and considering that the electrical machine will be used both as generator and motor in the vehicle, in the following section we can find a short description of the main options for the electrical machine selection.

2.3.2.1 PERMANENT MAGNET DC MOTOR

DC motor design generates an oscillating current in a wound rotor with a permanent magnet stator. A rotor consists of one or more coils of wire wound around a core on a shaft; an electrical power source is connected to the rotor coil through the commutator and its brushes, causing current to flow in it. The commutator causes the current in the coils to be switched as the rotor turns, so that the rotor never stops (like a compass needle does) as long as power is applied and is sufficient for the motor to overcome the shaft torque load and internal losses.

Controlling the brushed DC motor can be easily achieved by controlling the supply voltage to the motor, which proportionally controls the rotational speed of the motor. The need for brushes to press against the commutator is one of the main limitations since this creates friction and the brushes wear out rapidly.

2.3.2.2 PERMANENT MAGNET BRUSHLESS DC

BLDC motors are a type of synchronous motor. This means the magnetic field generated by the stator and the magnetic field generated by the rotor rotates at the same frequency. BLDC motors do not experience the “slip” that is normally seen in induction motors.

BLDC motors are typically 85-90% efficient or more and come in single-phase, 2-phase and 3-phase configurations. Corresponding to its type, the stator has the same number of windings. Out of these, 3-phase motors are the most popular and widely used. The rotor is made of permanent magnet and can vary from two to eight pole pairs with alternate North (N) and South (S) poles.

Unlike a brushed DC motor, the commutation of a BLDC motor is controlled electronically. To rotate the BLDC motor, the stator windings should be energized in a sequence. It is important to know the rotor position in order to understand which winding will be energized, following the energizing sequence. Rotor position is sensed using Hall Effect sensors embedded into the stator.

2.3.2.3 AC INDUCTION MOTOR

Electrical induction machines (IM), sometimes called asynchronous machines (ASM), are a very mature and robust technology that is used in a very wide range of applications. The main reason why the induction machine is so popular is the simple design and the low cost (no brushes or permanent magnets).

The stator contains three windings that are arranged so that a positive current produces a magnetic field (flux) in each coil 120 degrees apart. If these coils are then fed with a three phase alternating current, the resultant magnetic field rotates proportional to the frequency of the current. This induces an electromagnetic field and current in the rotor windings (which usually are short circuited at the ends creating a cage-like structure). This induced current in the rotor produces a force which turns the rotor and ‘chases’ the rotating magnetic field in the stator caused by the alternating current, causing the so mentioned ‘slip’.

2.3.2.4 AC SYNCHRONOUS MOTOR

Synchronous machines are commonly used as generators especially for large power systems, such as turbine generators and hydroelectric generators, they can also be used as motors, but they are usually built in very large sizes. The armature of a conventional synchronous machine is almost invariably in the stator and is usually a three phase winding. The rotor field winding is usually excited by dc current. So, a synchronous motor is like an induction motor except the rotor is excited by a DC field. Slip rings and brushes are used to conduct current to rotor. The rotor poles connect to each other and move at the same speed hence the name synchronous motor.

2.3.2.5 SWITCHED RELUCTANCE MOTOR

Reluctance machines are based on a very robust rotor structure without magnets or windings; therefore it is very high speed and temperature stable. The peak torque capacity of a reluctance machine is limited due to the ease of flux saturation of the stator. Additionally the power management is quite complex which can easily lead to noise, vibration and erratic torque delivery. However the SRM still are a good choice in some vehicle traction applications due to the wide power range and the high temperature stability.

The basic operation of a switched reluctance motor is quite simple. The iron stator and rotor are magnetized by a current through the coil on the stator. If the rotor is out of line with the magnetic field of the stator, a torque will be produced to rotate the rotor and minimize the air gap (reluctance) between the two to make the magnetic field symmetrical. When the rotor is aligned with the stator, the current is switched off and its momentum is allowed to carry the rotor to a new position where the current can be reapplied.

2.3.3 POWER ELECTRONICS

Power electronics is the technology associated with the efficient conversion, control and conditioning of electric power from its available input into the desired electrical output [13].

Electrical motors are most likely to use AC current or multiphase DC current. For that to be possible, some kind of energy conversion device has to be placed in between the ESS and the electrical machine, let's call it the motor controller. Additionally it is required that this device can manage the power output from the machine, i.e. the power consumption from the ESS; otherwise the vehicle will have no throttle and speed control.

Modern power electronics use semiconductors in switching mode which leads to lower energy losses, smaller dimensions and a decrease in cost compared to linear regulators. For each application parameters such as current capacity, voltage capacity, switching frequencies, efficiency and so on has to be considered for each component choice. The most common types of semiconductors in power electronics are:

- Diodes
- IGBT transistors
- MOSFET transistors

Common diodes, i.e. a device that flows current in one direction and blocks current in the other direction, more or less function in the same way. Power metal oxide silicon field effect transistors (MOSFET's) and insulated gate bipolar transistors (IGBT's) are two competing alternatives when it comes to transistors. In the Table 2.1 are summarized the characteristics of these technologies. The main difference is in the current. When a MOSFET changes state from on to off the resistance is quite high and the losses are proportional to the square of the current. The IGBT on the other hand shows a similar behavior to a simple bipolar junction transistor where losses during state change is a product of the smallest on-voltage and the very low on-resistance.

Transistor Type	Max. Voltage (V)	Max. Current (A)	Max. Freq. (kHz)	Cost
Two-stageDarlington	1400	800	20	Low
Thyristor	3000	2000	1	Low
MOSFET	1000	100	10000	High
IGBT	1200	400	100	High

TABLE 2.1- Main Characteristics of Common Power Switching Devices [13]

2.3.3.1 THREE-PHASE INVERTER

The Three-Phase inverter is mainly used to power AC motors. Some of these “DC-AC converters” are unidirectional and some are bidirectional. In the case of traction motor drive, it is important that the motor can spin in both ways as otherwise the vehicle won’t be able to reverse.

DC to AC conversion can be made in a number of ways of varying complexity. Some motors work better with pure sinusoidal waveforms compared to trapezoidal waveforms. However the circuit is the same and consists of six power switching devices (power transistors) with feedback diodes arranged in a three phase bridge. The current to the motor is controlled by pulse width modulation (PWM) using a microprocessor (DSPic) which is designed specifically for real time computing and motor control. It can convert analog feedback signals back into digital signals for processing and then convert these digital signals back to analog signals for output to the system

2.3.3.2 THREE PHASE BRIDGE RECTIFIER

A three-phase bridge contains six diodes to provide full-wave rectification (two diodes for each line of the three phases). Figure 2.7 shows the electrical diagram for a three-phase bridge rectifier.

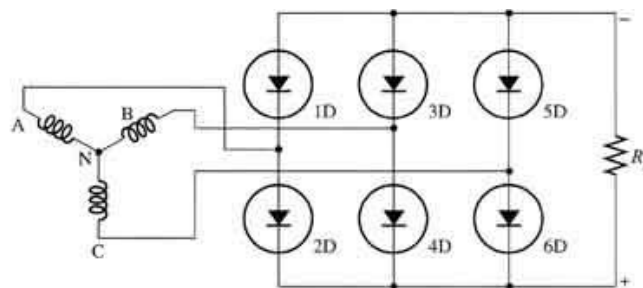


FIGURE 2.7 - Three-Phase Bridge Rectifier Circuit

Phase A of the three-phase voltage source is connected to the point where the cathode of diode 1D is connected to the anode of diode 2D. Phase B is connected to the point where the cathode of diode 3D is connected to the anode of diode 4D, and phase C is connected to the point where the cathode of diode 5D is connected to the anode of diode 6D. The anodes of diodes 1D, 3D, and 5D are connected together to provide a common point for the dc negative terminal of the output power. The cathodes of diodes 2D, 4D, and 6D are connected to provide a common point for the dc positive terminal of the output power.

The waveforms of the three-phase sine waves that supply the bridge, and the six half-waves of the output pulsing dc voltage can be seen in Figure 2.8. Since the output waveforms of the half-waves overlap, they provide a low ripple percentage. In this circuit, the output ripple is six times the input frequency. Since the ripple percentage is low, the output dc voltage is usable without much filtering.

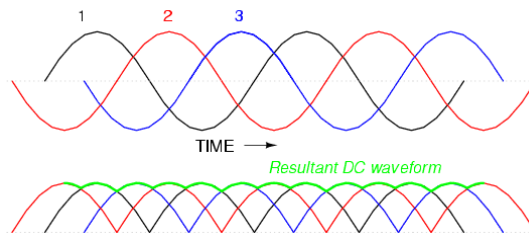


FIGURE 2.8 - Three-Phase Input Sinewaves and Resultant Dc Waveform Over Time

2.3.3.3 PULSE WIDTH MODULATION (PWM)

Pulse-width modulation (PWM) is a modulation technique for generating variable width pulses to represent the amplitude of an input analog signal or wave. It is a very efficient way of providing intermediate amounts of electrical power between fully on and fully off. As it applies to motor control is a way of delivering energy through a succession of pulses rather than a continuously varying (analog) signal. By increasing or decreasing pulse width the controller regulates energy flow to the motor shaft. The motor's inductance acts like a filter, storing energy during the “on” cycle while releasing it at a rate corresponding to the input or reference signal.

The underlying principle in the whole process is that the average power delivered is directly proportional to the modulation duty cycle. The term duty cycle describes the proportion of on time to the regular interval or period of time; a low duty cycle corresponds to low power, because the power is off for most of the time. Duty cycle is expressed in percent, 100% being fully - Figure 2.9.

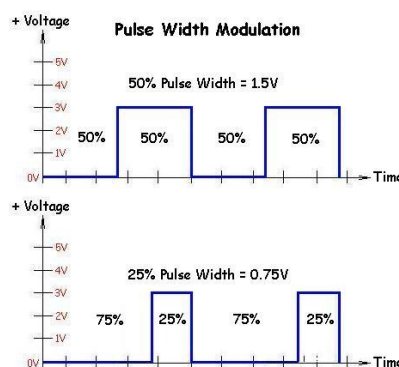


FIGURE 2.9 - Graphic Representation of Pulse Width Modulation with Different Duty Cycle Values (50% Duty Cycle On Top, And 25% Duty Cycle Down)

2.3.3.4 CHOPPER CIRCUIT

A chopper circuit is used to refer to numerous types of electronic switching devices and circuits. Essentially a chopper is an electronic switch that is used to interrupt a signal, when actuated by a control signal.

There are many types of chopper circuits depending on the application. If it is necessary to control both positive and negative voltage and current, a four quadrant chopper circuit is required. If it is only necessary to control positive voltage and current, is enough a single quadrant chopper circuit - Figure 2.10.

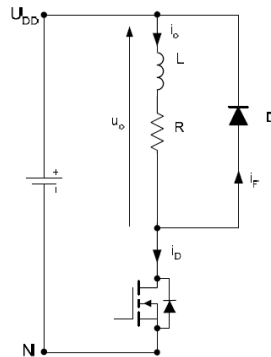


FIGURE 2.10 – Typical Single Quadrant Chopper Circuit

2.3.4 ENERGY STORAGE SYSTEM

Energy storage systems are responsible for accumulating energy when the electric motor is generating, or supply energy in case of motoring. In a vehicle volume and mass are limiting factors and, as we know, a physically large vehicle with high mass will consume more energy than a light and nimble alternative. To minimize the addition of mass and volume together with the entry of a secondary energy source, energy and power density are therefore important factors. The most important factors to have into account when choosing an ESS are:

- Energy to mass density;
- Energy to volume density;
- Power to mass density;
- Power to volume density;
- Cost;

The following image (Figure 2.11) represents several ESS's power to mass density and energy to mass density.

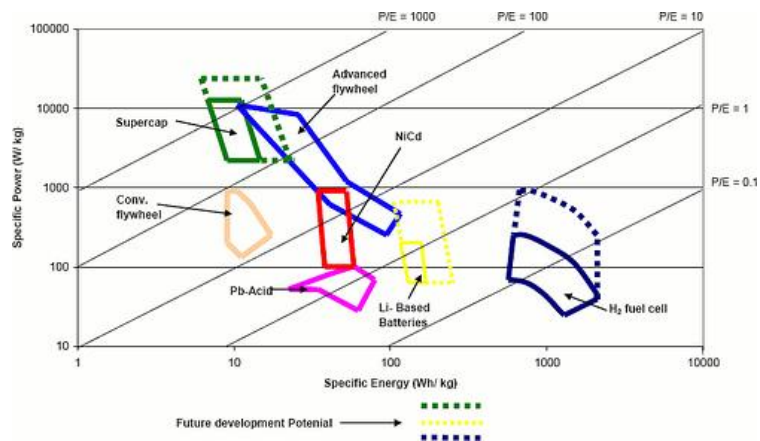


FIGURE 2.11- Graphical Representation of Specific Energy and Specific Power by Type of Ess [14]

2.3.4.1 BATTERIES

A battery is a device that converts chemical energy directly to electrical energy. The accumulator is built of one or more voltaic cells. Each cell consist of two half cells connected in series by a conductive electrolyte. One half cell acts as positive electrode (anode) and the other one is the negative electrode (cathode). The power of a battery comes from a reduction-oxidation (redox) reaction between the two electrodes. The reduction occurs at the cathode and oxidation at the anode. The electrodes do not touch each other but are electrically connected by a liquid or solid electrolyte.

Though batteries can store substantial amounts of energy they are not capable of releasing this energy quickly, and therefore have low power densities. Batteries store energy chemically and are limited by the time it takes for a chemical reaction to produce electricity. This reaction time, along with the internal resistance of the cell, lowers the power density of batteries.

The four battery types that are more usually found are nickel cadmium (NiCd), nickel metal hydride (NiMH), lithium ion (Li-ion) and Lead-acid, the following table summarizes the technical specifications of them all (table 2.2).

	Nickel-cadmium	Nickel-metal-hydride	Lead-acid sealed	Lithium-ion cobalt	Lithium-ion manganese	Lithium-ion phosphate
Gravimetric Energy Density (Wh/kg)	45-80	60-120	30-50	150 - 190	100 - 135	90 - 120
Internal Resistance in mΩ	100 to 200 ¹ 6V pack	200 to 300 ¹ 6V pack	<100 ¹ 12V pack	150 - 300 ¹ pack 100 -130 per cell	25 – 75 ² per cell	25 – 50 ² per cell
Cycle Life (to 80% of initial capacity)	1500 ²	300 to 500 ^{3,4}	200 to 300 ³	300 - 500 ³	Better than 300 – 500 ⁴	>1000 lab conditions
Fast Charge Time	1h typical	2 to 4h	8 to 16h	1.5 - 3h	1h or less	1h or less
Overcharge Tolerance	moderate	low	high	Low. Cannot tolerate trickle charge.		
Self-discharge / Month (room temperature)	20% ⁵	30% ⁵	5%	<10% ⁶		
Cell Voltage Nominal Average	1.25V ⁷	1.25V ⁷	2V	3.6V 3.7V ⁸	Nominal 3.6V Average 3.8V ⁸	3.3V
Load Current peak best result	20C 1C	5C 0.5C or lower	5C ⁹ 0.2C	<3C 1C or lower	>30C 10C or lower	>30C 10C or lower
Operating Temperature ¹⁰ (discharge only)	-40 to 60°C	-20 to 60°C	-20 to 60°C	-20 to 60°C		
Maintenance Requirement	30 to 60 days	60 to 90 days	3 to 6 months ¹¹	not required		
Safety	Thermally stable, fuse recommended	Thermally stable, fuse recommended	Thermally stable	Protection circuit mandatory; stable to 150°C	Protection circuit recommended; stable to 250°C	Protection circuit recommended; stable to 250°C
Commercial use since	1950	1990	1970	1991	1996	2006
Toxicity	Highly toxic, harmful to environment	Relatively low toxicity, should be recycled	Toxic lead and acids, harmful to environment	Low toxicity, can be disposed in small quantities		

TABLE 2.2 - Characteristics of Commonly Used Rechargeable Batteries [15]

2.3.4.2 ULTRA CAPACITORS

Ultra capacitors consist of two, hence “double layer”, active carbon electrodes which are immersed into an electrolyte. Separated by a membrane that allows transport of charged ions, the two electrodes are prevented to get electrical contact. The electrolyte supplies and conducts the ions from one electrode to the other, if an electrical charge is applied between the two. In the double layer capacitor the “dielectric”, i.e. the membrane, is very thin (nanometers). That combined with a very large surface area of the electrodes results in extremely high capacitances while maintaining normal sizes.

However, double layer capacitors can only withstand a low voltage (around 2 to 3V). So in the same way as batteries, high voltage ultra capacitors have to be built by serial connection of many ultra capacitors. The energy of a capacitor is calculated using equation 2.1.

$$E = \frac{1}{2} CV^2 \quad (2.1)$$

Where C is the capacitance in farads and V is the voltage. The capacitance is proportional to the plate surface area of the conducting plates and inversely proportional to the distance d between the plates which in modern ultracapacitors are extremely small leading to a higher energy density when compared to normal capacitors.

The double-layer capacitor offers a number of distinct performance advantages over the battery, namely an increased power density, very high lifetime both in regards to cycles (millions or more compared to 200–1000 for most commercially available rechargeable batteries) and the calendar. The design is also very robust and resistant to environmental changes. The drawbacks however are still the limited energy density and high self-discharge rate, when compared to batteries.

2.3.4.3 INERTIAL

Storage of energy in a flywheel works by acceleration of a rotor to a very high speed and storing the energy in the system as inertial energy. An accelerating torque causes the flywheel to increase its speed and store energy, while a decelerating torque causes the flywheel to reduce its speed and regenerate energy.

Since the industrial revolution flywheels have been used in most rotating engines and machines for very short time energy storage. One good example is the smoothing of pressure pulses in an ICE, minimizing engine speed oscillations during operation.

The amount of energy that can be stored in a flywheel is governed by two main variables, the inertia of the rotor (J) and the rotor rotational speed (ω). The kinetic energy of a rotating mass is described in equation 2.2.

$$E = \frac{1}{2} J\omega^2 \quad (2.2)$$

A great feature of the kinetic energy storage with the help of flywheels is the quick charging and discharging. In the case of a flywheel-electrical storage system where a motor/generator is connected to the flywheel the rate of charge/discharge is only limited by the electrical machine itself.

The main limitations of flywheel energy storage are the relative high self-discharge coupled with the full cycle efficiency being highly dependent on the rate of discharge plus the speed limitation of the rotor (risk of overloading), and the cost of peripheral equipment needed for harnessing and storage of energy in the flywheel.

2.3.5 ENERGY DISSIPATION SYSTEMS

The potential amount of energy that can be saved by using regenerative braking is dependent on the nature of the energy storage system and particularly on how much braking is performed. Therefore to slow down or to quickly stop a motor an energy dissipation system is added to enable faster braking and lower the wear and tear of friction braking components.

2.3.5.1 RESISTIVE LOAD BANK

A resistive load bank provides equivalent loading for both generators and prime movers. This means that for each kilowatt of load applied to the generator by the load bank, an equal amount of load is applied to the prime mover by the generator. A resistive load bank, therefore, removes energy from the complete system: load bank from generator—generator from prime mover.

The “load” of a resistive load bank is created by the conversion of electrical energy to heat via high-current resistors. This heat must be dissipated from the load bank, either by air or liquid. The most common type uses wire resistance, usually with fan cooling, and this type is often portable and moved from generator to generator for test purposes.

CHAPTER 3

DESIGN SOLUTION

3.1 INTRODUCTION

From the study of electric vehicles and the solutions employed by them to increase efficiency there was one feature that stood out to be a possibility for aircraft application: regenerative braking. Considering that the electric taxi concept is a tested solution and expectantly a reality in the years to come, a study for the best design solution to implement regenerative braking in airplanes will be made in the following chapter.

Regenerative braking is widely used in hybrid electric vehicles and significantly contributes to increase the overall efficiency. In order to study the possibility of using regenerative braking in aircrafts, a preliminary analysis of viability is made and a conceptual design is created. Afterward a small scale design is also developed in order to prove the aircraft's concept.

3.2 PRELIMINARY ANALYSIS

3.2.1 LANDING BRAKING POWER

A fast travelling aircraft contains significant kinetic energy. When an aircraft lands the kinetic energy is dissipated as waste heat. For example during the landing of an aircraft with 40ton and a touching speed $v=67\text{m/s}$, the average energy is about 900MJ given by equation 3.1. Considering a landing period $\Delta t = 30\text{s}$ a total of 3MW of power (P) is dissipated (equation 3.2).

$$E = \frac{1}{2}mv^2 \quad (3.1)$$

$$P = \frac{\Delta E}{\Delta t} \quad (3.2)$$

At Heathrow Airport a landing happens at every two minutes. This gives a constant (average) power source of 750kW. For big aircrafts such as the A380 the landing weight can be up to 386 tones, which gives an almost 10 times higher power. Convert and recover partially this power would be very important to reduce braking losses.

3.2.2 LANDING POWER PROFILE

Assuming that the braking force F is constant, which gives a constant deceleration 'a', the braking power is given by equation 3.3.

$$P = F.v = F.(v_0 - a.t) \quad (3.3)$$

This decreases with time. For the previous data the deceleration is $a=2.2 \text{ m/s}^2$ and the braking force is given by equation 3.4.

$$F = m.a \quad (3.4)$$

As a result the instantaneous braking power is represented in Figure 3.1. The shaded area shows a lower speed region where the electromagnetic braking might be more important (less power generated).

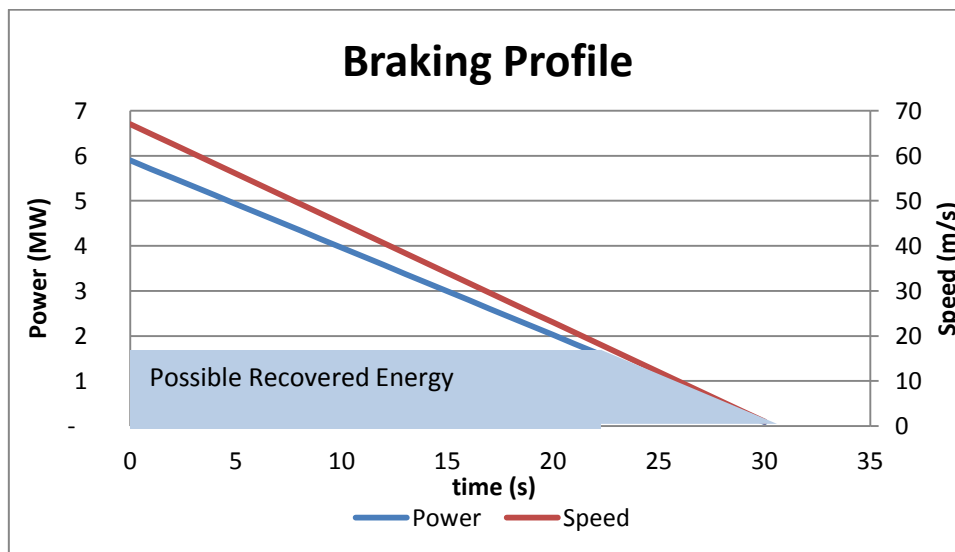


FIGURE 3.1 - Braking Power Profile during Landing (40ton Aircraft At 67m/S During 30sec)

3.3 DESIGN REQUIREMENTS

Considering the design of a regenerative/dynamic braking system for an aircraft there are several requirements from different areas that should be analyzed, such as cost and weight. However the most important features involve the:

- Braking Capability;
- Regeneration Capability;

3.3.1 BRAKING CAPABILITY

The preliminary analysis shows that the power dissipated while braking a mid-size aircraft is incredibly huge, due to the aircraft weight and landing speed. In order to have the same braking capability with a Regenerative/Dynamic braking system, this same amount of power has to be generated and here resides the first limitation for the electromagnetic braking system.

Motors/Generators that are capable of delivering such amounts of power (in the order of MW/hundreds of kW) are very large and weight hundreds of kilograms. This is something completely impossible to include in an aircraft. Therefore it is easy to conclude that the electromagnetic braking system would never be able to independently stop the aircraft during landing.

Consequently, for the design phase, the braking torque of the motors/generators won't be a primary requirement as the friction brakes will always be required. However the braking torque should be controllable.

3.3.2 REGENERATION CAPABILITY

As stated before there is a huge amount of power involved in braking an aircraft. Consequently is important that the electric motor selected can become a good generator when used for braking in order to deliver as much energy as possible. The amount of energy generated should also be controllable.

The energy storage/dissipation system should be able to receive large amounts of power for a short period of time. The electrical machine must have the ability to be used as motor and push the aircraft. The complete system should be efficient and as light and inexpensive as possible, guarantying a high level of reliability.

3.3.3 REQUIREMENTS

The main requisites for this system are:

- Small and lightweight – Should be small enough to fit the landing gear of an aircraft and light to not force too much the structure.
- Good regeneration capability – The machine must have the ability of retrieving as much energy as possible when working as generator and the ESS must be dimensioned to receive it.
- Controllable braking torque – Easy to control braking torque and possibility to be turned off.
- Good efficiency
- High reliability – Low probability of failures and no effect on the aircraft performance in case of a system failure.
- Low cost

3.4 CONCEPTUAL DESIGN

Initially in the conceptual design phase it was made the selection of the elements that will be part of the system, such as the electrical machines, energy storage systems and power electronics. Subsequently designs were generated and evaluated iteratively based on the project definition, with the goal of choosing the best design. Once a concept is chosen, a preliminary study of viability is made.

3.4.1 ELECTRICAL MACHINES

The selection of the electrical machine was made based on the design requirements. In table 3.1 is represented a qualitative analysis of the different machines performance in fulfilling the requirements.

	Induction Machine	Permanent Magnet Machine	Synchronous Machine	Switched Reluctance Machine
Small and lightweight	-	✓	-	-
Good regeneration capability	-	-	✓	-
Controllable braking torque	-	-	✓	-
High efficiency	-	✓	-	✓
Good reliability	✓	-	✓	✓
Low cost	✓	-	✓	✓

TABLE 3.1 - Electrical Machines Comparison

Permanent magnet machines give the impression that might be the best solution due to the high power to weight ratio and high efficiencies that the magnets guarantee. However magnets are very expensive and make the machine less reliable than the others since the magnets may unglue with heat or demagnetize. Also is not easy to control the power (force) and they have a limited working depth because the magnetic field produced by the magnets is fixed and cannot be turned off (releasing load). All things considered permanent magnet machines have more failure modes. This is why the new electric vehicles concepts are opting to use non-permanent magnet motors.

Between the other machines the Synchronous machine stood out as a very good solution due to the fact that possesses an electromagnet in his rotor. This means that the strength can be readily controllable and is possible to release the load. It is able to carry out high loads and it is the best generator (energy regeneration). In case of failure a dead motor leaves the wheel free. The new AMG SLS E-CELL uses 4 AC Synchronous motors with a combined peak power of 400kW [16].

Like stated in the section 2.1.3 of this thesis, the electric taxi WheelTug© system made for the 737NG is built around 2 multi-phase (18 phases) AC-induction motors that have 10 times more torque than normal tri-phase induction motors. They work with 400-480 line to line AC voltage from the APU, to a total of 15 HP to move the aircraft [6] [7] (confirmed to be more than enough by tow-test data).

The low power of the WheelTug[®] system compared for instance with the power of the AMG E-Cell electric motors besides the huge different of mass between the two vehicles can be justified with the speed requirements and slopes. The AMG is supposed to be able to face difficult slopes and achieve velocities of more than 200Km/h in a short period of time, while the aircraft runs in plain ground and with a speed of 50km/h, which can be reached after more than a minute or so. Torque is a primary concern for this type of application, while velocity and acceleration are not.

If the time given for braking a vehicle was the same given to accelerate, a 20kW AC Synchronous Machine with a considerable gear ratio (5 to 10) would be enough. However that's not true and braking is most of the times much more sudden, when compared to accelerations. So a more powerful machine should be added.

All things considered is possible to estimate that one AC Synchronous Motor with about 200kW peak power and with a considerable gear ratio of 5 to 10 (in order to have more torque) should be able to successfully move and slow down a commercial size aircraft (like 737NG) in taxi procedures, regenerating energy. Possibly this machine has to be custom made in order to be compact and lightweight and also fit the landing gear (Figure 3.2).

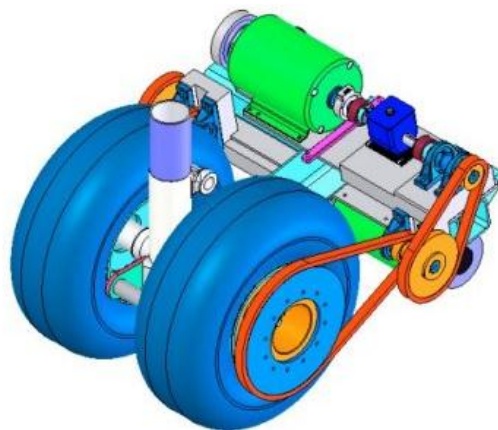


FIGURE 3.2 - CAD Representation of a Possibility for the Electric Motor Mount in the Landing Gear

3.4.2 ENERGY STORAGE SYSTEM

In order to regenerate energy it is required to have some sort of energy storage system on board. Aircrafts already possess low voltage batteries on board (typically of 24VDC) which are used to power systems for emergency situations that shouldn't be used for taxiing purposes. Therefore a new ESS should be integrated just for the ground operations. In the table 3.1 is represented a qualitative analysis of the different ESS performance in fulfilling the requirements.

	Lithium Batteries	Super capacitors	Lead- Acid Batteries	Inertial
Specific Power (W/Kg)	100	2000	50	500
Specific Energy (Wh/Kg)	100	10	50	10
Cost	-	-	✓	✓

TABLE 3.2 - ESS Comparison

These values are approximated and based on the Figure 2.11 in Chapter 2. From the analysis of table 3.2 is easy to verify that lithium batteries are the best and more balanced energy storage system available. These batteries have long lasting life-cycles and for instance the new Lithium-Titanate Batteries can be fast recharged withstanding huge loads. A battery pack of 270V with energy content of about 10kWh should be more than enough considering the amount of braking energy regenerated and that typical taxi operations don't exceed 30 minutes.

3.4.3 POWER ELECTRONICS

Concerning the power electronics it will be necessary a Chopper Circuit for the rotor in order to control electromagnet field (especially in "generator mode" during braking). Furthermore it is also necessary to use a three phase Inverter in order to convert the DC voltage from the batteries to AC when in "motor mode". The switching device utilized in both these pieces of equipment should be IGBT due to the high voltage and current that these devices can withstand (Table 2.1). They must also have freewheeling diodes in order to allow the conversion of the AC to DC when generating energy.

3.4.4 CONCEPT I

The first concept design consists of placing the electric motor only in the nose landing gear Figure 3.3.

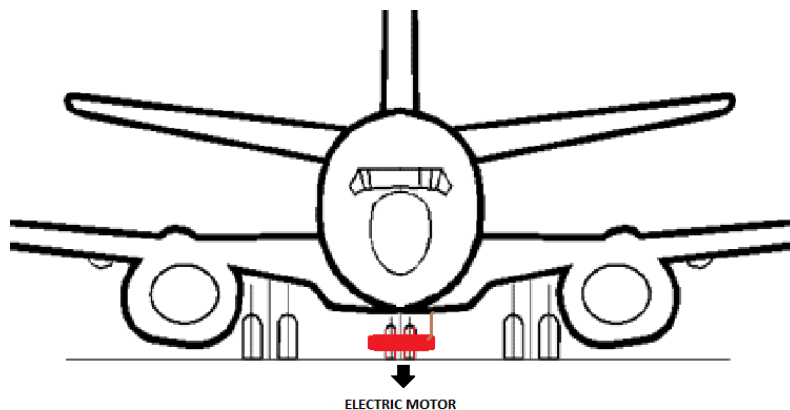


FIGURE 3.3 - Concept I Design

Having in mind the electric motor, energy storage system and power electronics selection, it is possible to estimate that the overall system will weigh more than the double of the Chorus WheelTug© System (which weighs about 100kg [17]) especially due to the ESS that is proposed to be added.

However the brakes wear will be reduced and fuel consumption will be improved. The batteries added might also be used to power other systems in case of emergency.

3.4.5 CONCEPT II

This design concept consists of placing electric motors in both main landing gear and nose landing gear Figure 3.4.

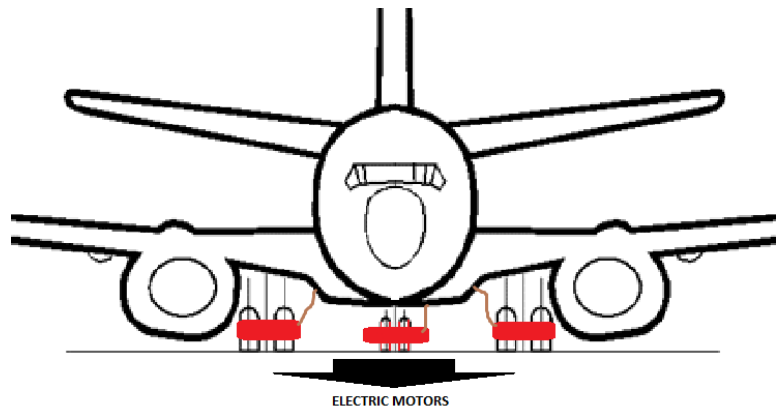


FIGURE 3.4 - Concept II Design

This design provides an increasing braking and regeneration capability when compared with the first concept. However main landing gears already have the friction brakes, so there won't be much room to place the system and, besides that, the heat produced by the friction brakes (when solicited) might harm the apparatus. Furthermore, this concept substantially increases the weight and cost of the system.

3.5 PRELIMINARY STUDY OF VIABILITY

From the analysis of the previous designs the Concept I stood out as the best study solution. Overall this design appears to be viable to apply in an aircraft, since it improves the existent electric taxi concept adding it new features by allowing reducing the wear of the brakes and regenerating energy otherwise spent as heat during ground operations.

The complete system is estimated to weigh about 300kg (more or less the weight of 4 passenger) and cost more than 2\$M [17]. All the benefits mentioned in section 2.1.3.1 of this thesis are also applicable to the chosen solution and the investment will quickly be amortized through the big reductions expected in operating costs.

However it is not wise to develop this design further since the applicability of the electromagnetic braking control is still unknown. Therefore a prototype was simulated and developed with characteristics similar to this design concept.

3.6 DESIGN APPROACH - PROTOTYPE

In order to prove the design concept of a regenerative/dynamic braking system for an aircraft it was decided to develop simulations and create a physical prototype of the controller. However that would be impossible to develop for an aircraft due to the lack of the necessary equipment.

Therefore the simulations had to be developed for a small scale prototype, designed to a scale of about 1/100 in order to obtain values which might be comparable with the prototype developed. Later on, based on this prototype results were taken conclusions about the viability of the concept for an aircraft scale design.

Only with a feasible prototype solution, specific aircraft simulations and tests should be made as future work. However, as it would be expected, a few adaptations to the original aircraft design concept had to be made in order to apply it to the scaled prototype design. In table 3.3 is possible to see the scaling between designs.

Aircraft Design	Prototype Design
20Ton aircraft	200Kg Motorcycle
200kW Synchronous Machine	2kW Claw-Pole Alternator
Lithium Battery 270VDC	Lead Acid Battery 36VDC

TABLE 3.3 –Scaling Between Aircraft And Prototype Designs

3.6.1 VEHICLE

The vehicle chosen had to be lightweight in order to work with low power. Consequently a motorcycle was taken as the test vehicle. The fact that this is a 2-wheeled vehicle helped to improve the similarity with an aircraft landing gear.

3.6.2 ELECTRICAL MACHINE

Concerning the synchronous machine was selected an automotive alternator (also known as Lundell Machine and Claw-Pole alternator). This alternator is similar to standard wound rotor synchronous machines in functionality, having just a different structure. It has only one exciting coil in the rotor to generate a magnetic field with a higher number of pole-pairs. Two rings with 6 slanted poles are pressed on the shaft against the core and form the magnetic circuit of the rotor. This type of machine is not usually used for applications where it has to be used as motor and generator, consisting by itself in an innovative solution of this project.



FIGURE 3.5 – Representation of the Rotor of a Lundell or Claw-Pole Alternator

3.6.3 ENERGY STORAGE SYSTEM

The batteries in the prototype are of Lead-acid and complete a total of 36VDC. These were the only type of batteries available at the time of developing this thesis, but were enough since they were only used to power rotor's electromagnet.

CHAPTER 4

PROTOTYPE DESIGN

4.1 INTRODUCTION

The objective of this chapter is to establish the design configuration of the controller and to demonstrate the ability of the system to function as described in the initial project definition. In order to accomplish this objective the following areas were modeled and simulated in the MATLAB/Simulink environment:

- Complete 2-wheeled vehicle dynamic for braking study;
- Excitation control strategies for Synchronous motor;
- Electromagnetic Braking controller;
- Energy storage system and energy dissipation system management;

4.2 MODELING AND SIMULATION SOFTWARE OVERVIEW

The simulation of the braking system design was developed in Simulink environment. The models created in Matlab are displayed in Appendix A, along with the physical constants of the system.

4.2.1 MATLAB/SIMULINK

MATLAB is a general purpose mathematical utility program which provides editing, plotting, debugging, and graphics capabilities, as well as access to an extensive and sophisticated library of powerful computational algorithms, and is becoming widely used throughout the engineering community. Simulink is a software package designed to run within MATLAB. Simulink can be used for modeling, simulating, and analyzing dynamic system, whose performance is described with sets of differential equations. The package has a graphical user interface for building the dynamic system model from a comprehensive library of built-in or user-defined, functional blocks.

The main advantages and reasons for using MATLAB/Simulink in this project are:

- Rapid development of the product;
- Access to sophisticated reliable mathematical models and solution algorithms;
- Assistance in output control, particularly with regards to graphics and results.

4.2.2 BLOCK LIBRARY

From the Simulink Library the blocks used were mainly from two toolboxes – SimDriveline and SimPowerSystems.

The first toolbox (SimDriveline) enables structural modeling, i.e. to model the physical components and their interconnections; providing an efficient and easy mean to construct driveline models such as the drive shaft within the Simulink environment. These tools include components such as gears, torque actuators, clutches, ICE, vehicle and tire models by specialized blocks.

The second toolbox (SimPowerSystems) contains blocs of electrical power machines, power electronics and other electrical equipment. SimPowerSystems have no direct compatibility with SimDriveline, so electrical machines were connected through torque actuators from the library of SimDriveline. The drawback of joining these two different program atmospheres is that the computation time increases and takes a longer time to get results [18].

4.2.3 SIMULATION PARAMETERS

For the modeling and simulation of all these systems there is an important issue that needs to be carefully considerate. The difficulty lies in getting a good balance between accuracy and simplicity. The models should be accurate enough for the application, and at the same time not too complicated since that often results in slower simulations.

For this application the models must be fast enough to be easily used when developing control strategies. Many articles deal with static models that are built up from maps and static relationships between parameters in the model. These models are comforting since they give fast simulations, but for the author's intents a dynamic model that can fully describe the electric motor and drive shaft variations, that occur while braking, is needed.

The simulation parameters affect the detail and accuracy of the models used. Because there are both mechanical and electrical dynamics, a variable-step stiff system solver was required. The solver uses a fundamental simulation time-step of 0.1ms because it adequately samples the simplified electrical subsystem models and does not excessively oversamples the mechanical subsystems.

4.3 PROTOTYPE DESIGN SUBSYSTEMS AND MODELS

The following schematic represents the systems developed with all the inputs and outputs (Figure 4.1):

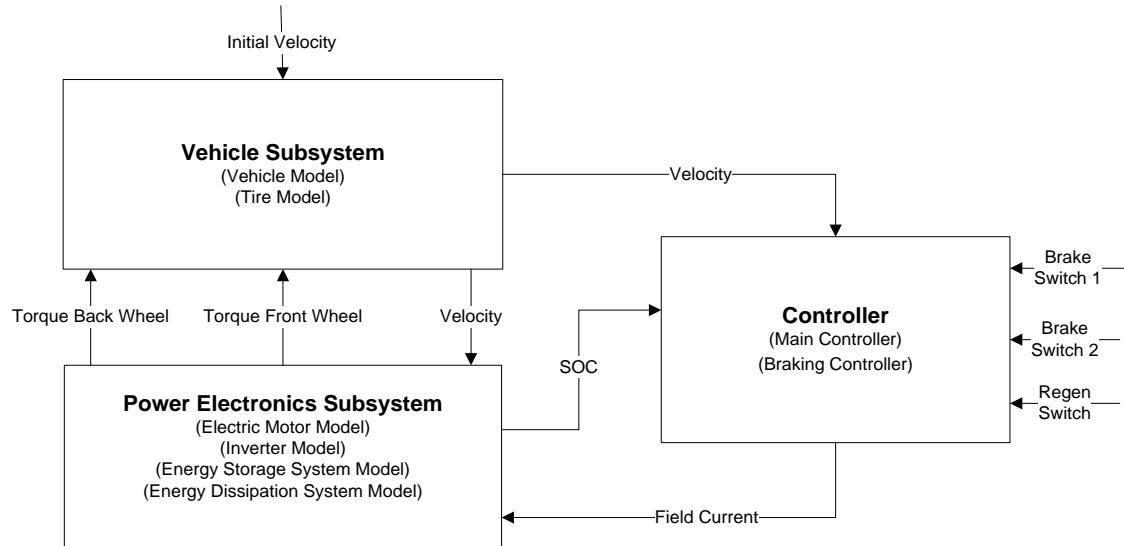


FIGURE 4.1- SIMULATION MODELS SCHEMATIC

In the vehicle Subsystem block was implemented the longitudinal dynamic of a 2-wheeled vehicle with tires, it yields the vehicle velocity and receives braking torque. The Power Electronics Subsystem contains the model of an electrical machine (alternator) with suitable power electronics control and Energy Storage/Dissipation Systems. The field controller receives the braking command from three switches and controls the braking torque through the regulation of the rotor's excitation current (Figure 4.1).

4.3.1 VEHICLE SUBSYSTEM

For this simulation it was important to implement an accurate two-wheeled vehicle model, that is why the vehicle is modeled considering parameters such as the rolling resistance and aerodynamic drag (which account for 95% of driveline losses) [19]. The other frictional forces are associated with friction in rotating driveline components that are difficult to model and for that reason were discarded.

A tire model was also included in order to obtain a better estimate of the vehicle contact with road while braking. The following figure represents the Vehicle Subsystem Block with all the inputs and outputs (Figure 4.2).

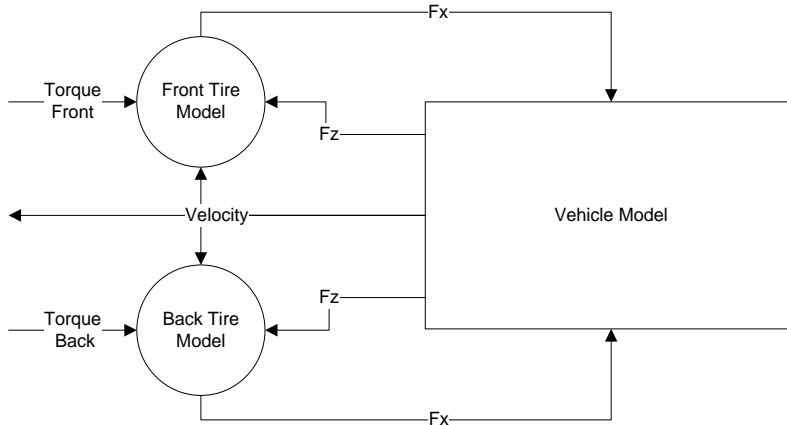


FIGURE 4.2 - Vehicle Subsystem

4.3.1.1 VEHICLE MODEL

In order to simulate the reaction of a vehicle when braking with an electric motor it is sufficient to consider only the longitudinal motion. The following figure is representative of the horizontal and vertical forces acting on a vehicle (Figure 4.3):

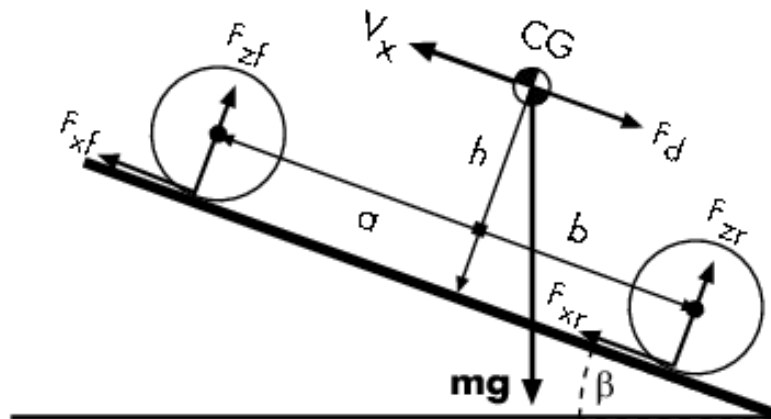


FIGURE 4.3 - Forces Acting On a Vehicle [20]

The Model input signals are the front and rear longitudinal forces F_{xf} , F_{xr} applied at the front and rear wheel contact points, as well as the incline angle β . The output signals are the vehicle velocity v_x and the front and rear vertical load forces F_{zf} , F_{zr} .

LONGITUDINAL FORCES

Once the other frictional forces have been neglected, the longitudinal Vehicle Dynamics is described by equation 4.1

$$m\dot{v} = F_x + F_{AERO} + F_{ROLL} + F_G + F_{BRAKE} + F_{EMBRAKE} \quad (4.1)$$

All these forces included in the vehicle model will be shortly summarized in the following section, except the brake force (friction brakes) and the Electric Motor force which will both be external to the vehicle subsystem.

Traction Force

The traction force F_x required to drive a vehicle normally comes from a combustion engine or electric motors. However, once the objective of this simulation was to study the braking, no accelerating sources, such as combustion engines, were implemented and the electric motor is only used as generator.

The strategy followed was to set the Vehicle Model with an initial speed and then study the dynamic of the various subsystems in order to effectively brake the vehicle.

Gravity Force

The equation 4.2 represents the longitudinal force gravity places on the vehicle as a function of road slope β .

$$F_G = -m.g.\sin \beta \quad (4.2)$$

Aerodynamic Force

As a result of the air stream interacting with the vehicle, six components of forces and moments are imposed. These components are drag and rolling moment in the longitudinal direction, sideforce and pitching moment in the lateral direction, and lift and yawing moment in the vertical direction. Among them, and considering only the longitudinal motion for the simulation purposes, drag is the largest and most important aerodynamic force encountered by vehicles at higher speeds. It acts on the vehicle body in the direction of vehicle motion, i.e., x direction. Aerodynamic drag is a function of vehicle's velocity (v) and it can be characterized by equation 4.3.

$$F_{AERO} = -\frac{1}{2} \cdot \rho \cdot v^2 \cdot C_D \cdot A \cdot \text{sgn}(v) \quad (4.3)$$

The parameter A (frontal area) and C_D (Drag Coefficient), were extracted from the references [21] from which was found that $A=0.8 \text{ m}^2$ and C_D is equal to 0.7.

ρ is the air density, which can be can be estimated for the prevailing pressure and temperature conditions by equation 4.4.

$$\rho = 1.2 \left(\frac{P_R}{101325} \cdot \frac{288}{273 + T_R} \right) \quad (4.4)$$

Under standard simulation conditions (Temperature $T_R=15^\circ\text{C}$ and Pressure $p_R=101325 \text{ Pa}$) the air density (ρ) is equal to 1.2 kg/m^3 .

Rolling Resistance

Considering the vehicle as a whole the total rolling resistance is the sum of the resistance from all the wheels (two). For theoretically correct calculations the dynamic weight of the vehicle, including the effects of acceleration, trailer towing forces and the vertical component of air resistance should be used. However the implementation of such parameters is rather complex and is not very important to have this level of precision. Therefore the author decided to utilize a simplified rolling resistance formula, in the reference [21] it can be found that the Rolling Resistance for two-wheeled vehicles is approximately constant and it can be considered equal to 1% of the vehicle's weight per wheel. Hence the rolling resistance can be expressed as the equation 4.5.

$$F_{ROLL} = (F_{ROLL_Front} + F_{ROLL_Back}) = -fr.m.g.sgn(v) \quad (4.5)$$

Where $fr=0.02$.

The combined effect of the rolling resistance and aerodynamic drag in a vehicle is usually denominated as Road Load and the following graphic shows the variation of the road load with velocity.

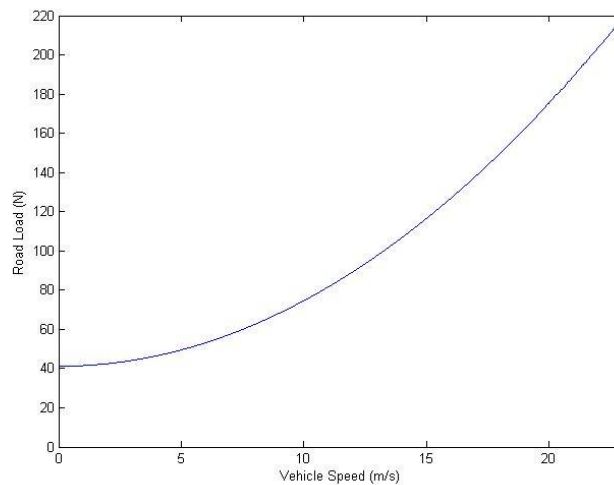


FIGURE 4.4 - Vehicle Road Load Forces A Function Of Increasing Vehicle Speed (Slope = 0%).

The constant part of the graphic Figure 4.4 corresponds to the rolling resistance while the aerodynamic drag is responsible for the quadratic evolution of the road load.

VERTICAL FORCES

According to all the previous forces and the CG location is possible to determine the amount of vertical force acting over the front and rear wheel. The CG position was estimated from historical data and estimated that the distance between the front axle and the CG is $b=0.9$, the distance between the rear axle and the CG is $c=0.5$ and the distance between the ground and the CG is $h=0.5$ (Figure 4.3). The equations employed were the following (4.6 and 4.7):

$$F_{zf} = \frac{h.(F_{AERO} - m\dot{v} - F_{ROLL} - F_G) + c.mg.\cos \beta}{b + c} \quad (4.6)$$

$$F_{zr} = \frac{-h.(F_{AERO} - m\dot{v} - F_{ROLL} - F_G) + b.mg.\cos \beta}{b + c} \quad (4.7)$$

These values will be very important for the tire model which requires the vertical load in each wheel.

4.3.1.2 TIRE MODEL

The tire model was based in a Simulink block from the Simdriveline toolbox. It requires the vertical load F_z and the vehicle longitudinal velocity V as Simulink input signals. The model provides the tire angular velocity Ω and the longitudinal force F_x on the vehicle as output signals. It also has a physical driveline connection simulating the driveshaft to which is transferred the wheel's torque and angular velocity; to this driveshaft was connected the wheel's inertia.



FIGURE 4.5 - Tire Model Variables

The tire model is rather complex and considers several parameters like deformation and slip in order to accurately define the tire dynamics. Some of these attributes can be mathematically described through the following equations.

SLIP

If the tire was a rigid solid and did not slip, it would roll and translate as $v_x = r_E \cdot \omega$. In reality even a very rigid tire slips and a tire develops a longitudinal force F_x only in response to that slip. Consequently slip (K) can be defined as the ratio between the linear speed and the $r_E \cdot \omega$ relation (equation 4.8). For a locked, sliding tire, $K = -1$. For perfect rolling $K = 0$.

$$K = -1 + \frac{r_E \cdot \omega}{v_x} \quad (4.8)$$

Where:

K is the slip considered equal to approximately -0.1, r_E is the effective rolling radius, ω is the angular speed of the tire and v_x is the linear speed.

DEFORMATION

The tire is made of flexible material and because of that it deforms, the contact point turns at a slightly different angular velocity ω' from the wheel. The tire deformation u directly measures the difference of wheel and contact point slip and satisfies equation 4.9.

$$\frac{du}{dt} = r_E (\omega' - \omega) \quad (4.9)$$

$\frac{du}{dt}$ is the variation of the tire deformation is, r_E is the effective rolling radius, ω is the angular speed of the tire and ω' is the angular speed of tire in the contact point with road.

INERTIA

The tire block does not include the wheel's inertia, because of that the author added an inertia block to the wheel's driveline connection. It is assumed that a wheel and a tire are a single object with the same center of mass at a rotating axis and that the mass is symmetrically distributed.

$$I_W = m_W \cdot R_W^2 \quad (4.10)$$

Assuming that the mass of a 17 inch wheel ($R_W=0.2159$ m) including the tire and brake rotors is $m_W=15$ kg. Inertia of $0.7 \text{ kg}\cdot\text{m}^2$ was obtained for each Wheel from equation 4.10.

4.3.1.3 VEHICLE SUBSYSTEM CHARACTERISTICS

In table 4.1 are reunited the values of the constant parameters utilized in the simulation models of the vehicle and tires.

PART	PARAMETERS	VALUES
VEHICLE	MASS	210kg
	HORIZONTAL DISTANCE FROM CG TO FRONT AXLE	0.9m
	HORIZONTAL DISTANCE FROM CG TO REAR AXLE	0.5m
	CG HEIGHT FROM GROUND	0.5m
	FRONTAL AREA	0.8m^2
	DRAG COEFFICIENT	0.7
TIRE	WHEEL RADIUS	0.2159m
	INERTIA	$0.7\text{kg}\cdot\text{m}^2$
	SLIP	10%

TABLE 4.1 - Vehicle Subsystem Main Characteristics

4.3.2 POWER ELECTRONICS SUBSYSTEM

The power electronics subsystem consists of four major components: Alternator, Battery, Bridge Rectifier and Resistor. The bridge rectifier is connected to the alternator and converts the three phase alternating current into DC current. The battery is used to store the energy used to power the electric motor, while the resistor is used for the dynamic braking. A controlled relay will switch between these devices. A schematic of the power electronics system is shown in Figure 4.6. The power electronics system was modeled using Matlab/Simulink blocks for the electrical machine, bridge rectifier, ESS and resistor.

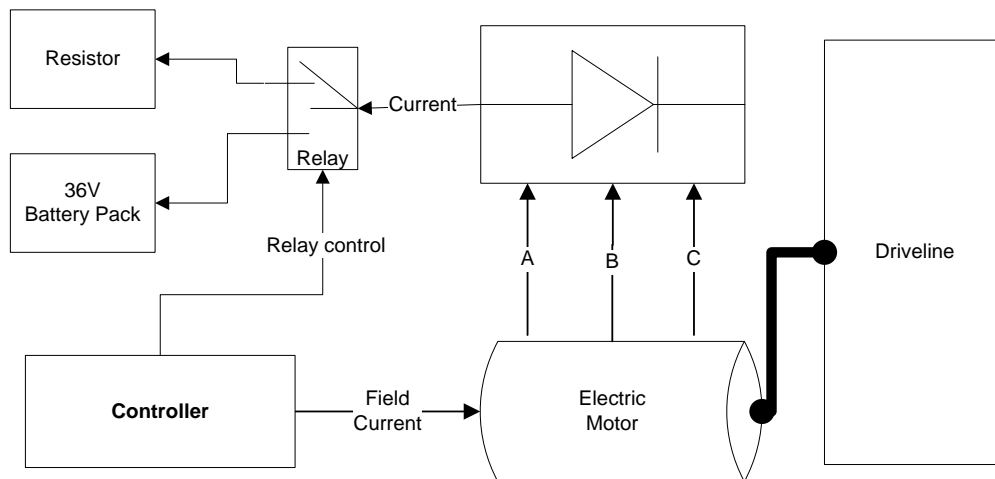


FIGURE 4.6 – Schematic of the Connections between the Different Equipments in the Power Electronics Subsystem

4.3.2.1 ELECTRIC MACHINE MODEL

There are no mathematical models of an alternator; so far the only way to reasonably simulate a claw pole alternator is by using finite elements analysis. Some authors that are able to model it in Simulink use look-up-tables with experimental data and/or use very simplified approximations (considering constant output voltage and disregarding the excitation current). Neither of these solutions was a possibility for this project.

Considering this, the most accurate way found to model the automotive alternator was utilizing a Synchronous Machine block from the SimPowerSystems toolbox because of the structural similarity. This block operates in generator or motor modes. The operating method is dictated by the sign of the mechanical power (positive for generator mode, negative for motor mode). The electrical part of the machine is represented by a sixth-order state-space model. The inputs are the rotor voltage and the rotor angular velocity. The outputs of this model are the three AC currents.

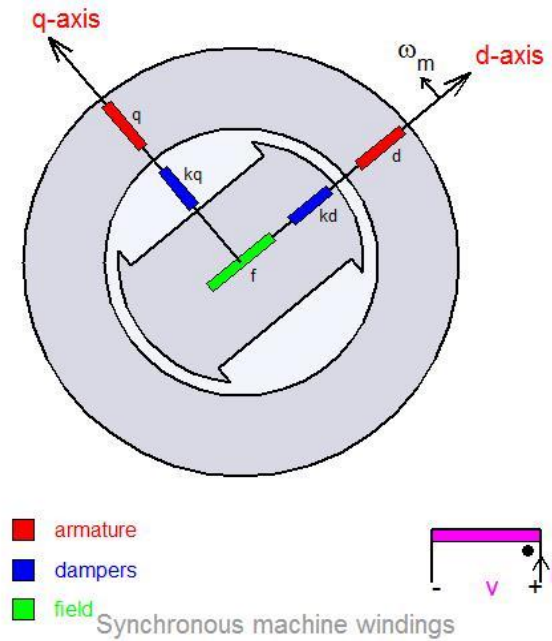


FIGURE 4.7 - Synchronous Machine Qd Frame Representation

The model takes into account the dynamics of the stator, field, and damper windings (Figure 4.7). The equivalent circuit is represented in the rotor reference frame (qd frame). All rotor parameters and electrical quantities are viewed from the stator. The qd frame is obtained through Clarke and Park transformations of the original abc frame of reference - Figure 4.8.

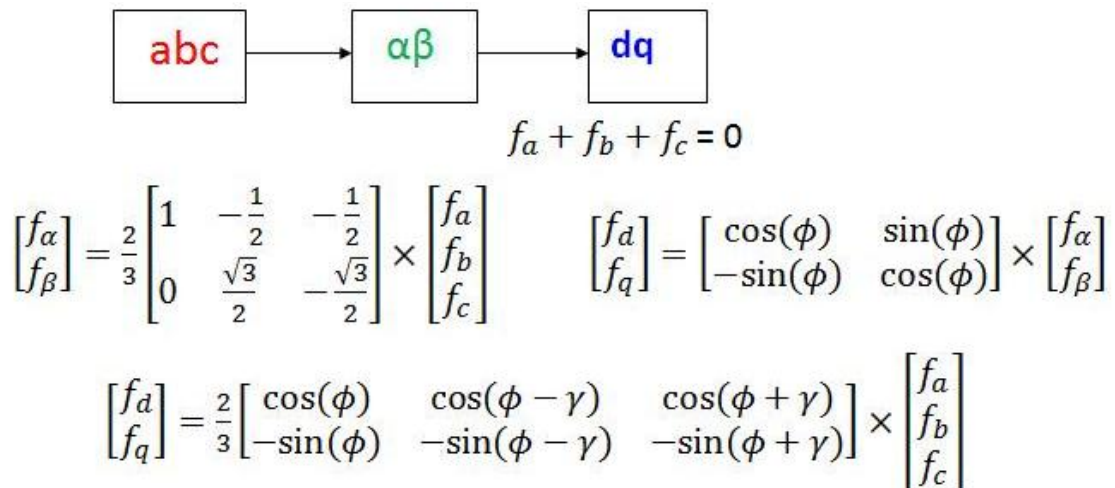
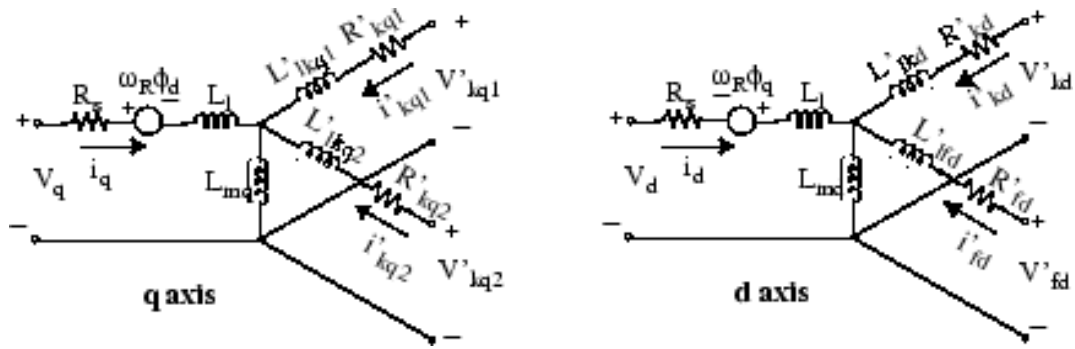


FIGURE 4.8 - Clarke and Parke Transformations

The electrical model of the Synchronous Machine is given by the following equivalent circuit in the dq frame - Figure 4.9.



$$\begin{aligned}
 V_d &= R_s i_d + \frac{d}{dt} \phi_d - \omega_R \phi_q & \phi_d &= L_d i_d + L_{md} (i'_{fd} + i'_{kd}) \\
 V_q &= R_s i_q + \frac{d}{dt} \phi_q + \omega_R \phi_d & \phi_q &= L_q i_q + L_{mq} i'_{kq} \\
 V'_{fd} &= R'_{fd} i'_{fd} + \frac{d}{dt} \phi'_{fd} & \phi'_{fd} &= L'_{fd} i'_{fd} + L_{md} (i_d + i'_{kd}) \\
 V'_{kd} &= R'_{kd} i'_{kd} + \frac{d}{dt} \phi'_{kd} & \phi'_{kd} &= L'_{kd} i'_{kd} + L_{md} (i_d + i'_{fd}) \\
 V'_{kq1} &= R'_{kq1} i'_{kq1} + \frac{d}{dt} \phi'_{kq1} & \phi'_{kq1} &= L'_{kq1} i'_{kq1} + L_{mq} i_q \\
 V'_{kq2} &= R'_{kq2} i'_{kq2} + \frac{d}{dt} \phi'_{kq2} & \phi'_{kq2} &= L'_{kq2} i'_{kq2} + L_{mq} i_q
 \end{aligned}$$

FIGURE 4.9 - Electrical Model And Equations Of Synchronous Machine

With the appropriate values for the main parameters of the Synchronous machine, the author tried to obtain a good approximation to an alternator - table 4.2. The values of both Stator and Rotor were obtained through experimental measurements and also from literature [22].

PART	PARAMETERS	VALUES
ALTERNATOR	POLE PAIRS (p)	6
	NOMINAL POWER (Pn)	2kW
	NOMINAL VOLTAGE (Vn)	36V
STATOR	STATOR RESISTANCE (Rs)	0.05Ω
	STATOR LEAKAGE INDUCTANCE (Ll)	250μH
	STATOR D-AXIS MAGNETIZING INDUCTANCE (Lmd)	3.5mH
	STATOR Q-AXIS MAGNETIZING INDUCTANCE (Lmq)	3.5mH
ROTOR	FIELD RESISTANCE (Rfd)	10Ω
	FIELD LEAKAGE INDUCTANCE (Llfd)	1.5H

TABLE 4.2- Alternator Simulation Parameters

4.3.2.2 POWER ELECTRONICS MODEL

Concerning Power electronics two systems were made, a three phase bridge rectifier and a shoper circuit. In both of them were utilized blocks from SimPowerSystems toolbox.

BRIDGE RECTIFIER

The bridge rectifier was designed according with Figure 2.7 using Shottski diodes with the following characteristics (table 4.3):

PARAMETERS	VALUES
RESISTANCE R_{ON}	0.01 Ω
INDUCTANCE L_{ON}	0H
FORWARD VOLTAGE V_f	0.35V

TABLE 4.3- Bridge Rectifier Diodes Parameters

CHOPPER

The chopper circuit was designed in agreement with Figure 2.10 where the diode utilized has a forward voltage of 0.7V and the MOSFET had the parameters of IRFP4310ZPBF [23] which was used in the physical prototype. In table 4.4 are summarized all the characteristics of these devices.

PART	PARAMETERS	VALUES
DIODE	FORWARD VOLTAGE V_f	0.7V
	RESISTANCE R_{ON}	0.01 Ω
	INDUCTANCE L_{ON}	0H
MOSFET	RESISTANCE R_{ON}	0.0048 Ω
	INTERNAL DIODE FORWARD VOLTAGE V_f	1.3V
	INTERNAL DIODE RESISTANCE R_{ON}	0.01 Ω
	INTERNAL DIODE INDUCTANCE L_{ON}	0H

TABLE 4.4- Characteristics of the Chopper Circuit Devices

PWM GENERATOR

The PWM Generator is responsible to fire forced-commutated devices (in this case a MOSFET). This generator creates the pulses by comparing a sawtooth carrier waveform to a reference modulating signal that defines the duty cycle.

The modulating signal (duty cycle) is limited between -1 and 1 and is given by the controller. The carrier has unit gain and a frequency of 1 kHz. The Figure 4.10 shows how the pulses are produced by the PWM Generator.

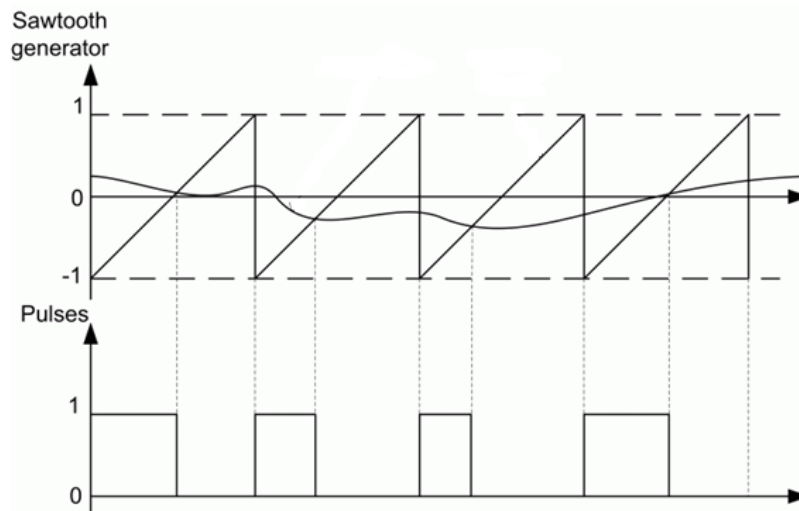


FIGURE 4.10 – Method for Generating Pwm Pulses

4.3.2.3 ENERGY STORAGE SYSTEM MODEL

For the ESS model was utilized a Battery block from the SimPowerSystems toolbox which implements a generic dynamic model parameterized to represent different types of rechargeable batteries. In this simulation are used the parameters of a 36V lead-acid battery since it was the type of batteries available for testing the prototype - table 4.5.

PARAMETERS	VALUES
NOMINAL VOLTAGE	36V
RATED CAPACITY	36Ah
INTERNAL RESISTANCE	0.01Ω
NOMINAL DISCHARGE CURRENT	7.2A
FULLY CHARGED VOLTAGE	39.2V

TABLE 4.5 - 36V Lead-Acid Battery Parameters

The battery charging is made according with the characteristic of Figure 4.11.

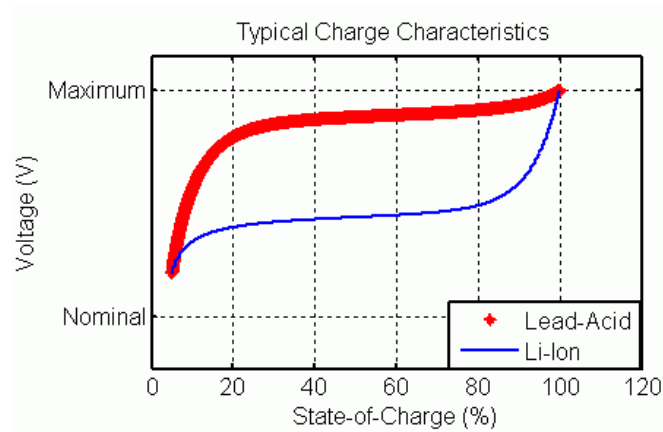


FIGURE 4.11 - Typical Charge Characteristics

The discharge characteristic at nominal current is also plotted in Figure 4.12.

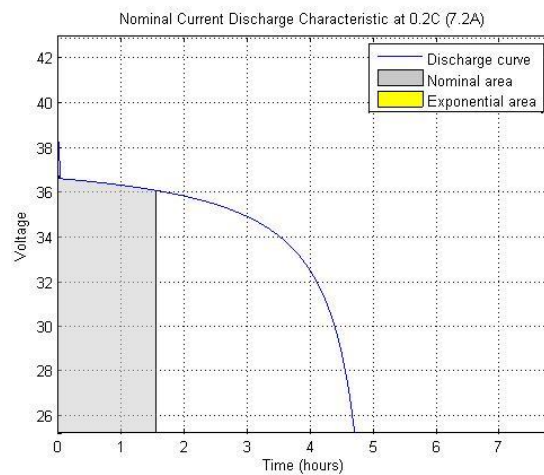


FIGURE 4.12 - Nominal Discharge Characteristic At Nominal Current

4.4 PROTOTYPE DESIGN RESULTS

With the models implemented several simulations were conducted in order to verify the regeneration and braking capability of this system (open loop). In these simulations the load was a battery pack for regenerative braking.

Were conducted two simulations with a battery pack of 36v and 24v respectively since these are the voltages at which the alternator was dimensioned. The rotor was fed with the same batteries which corresponded to currents of approximately 2.4A and 3.6A.

It was also included a gear ratio of 5.3 between the vehicle's wheel and the alternator's rotor. The vehicle was set with an initial speed of 50km/h (around 600 rpm in the wheel and 3000 rpm in the rotor).

4.4.1 TORQUE

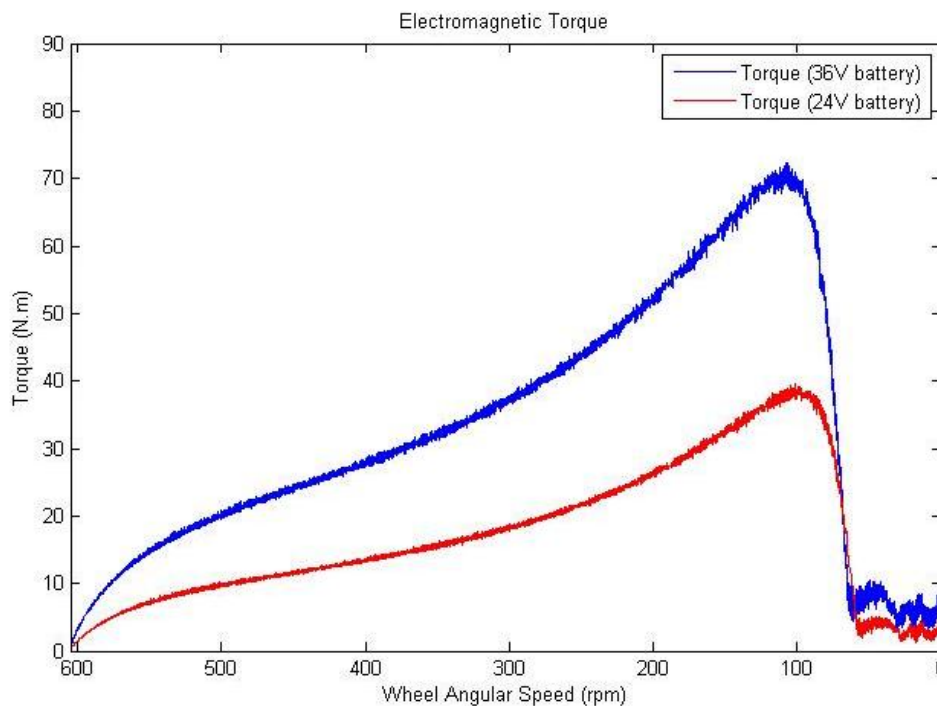


FIGURE 4.13 - Electromagnetic Torque Profile as the Vehicle Decelerates From 50km/H to 0km/H for Different Feeding Currents in Rotor (2,4A and 3,6A)

The torque profile (Figure 4.13) is typical for an electric motor, reaching higher values at low rotations, but presenting low torque at higher speeds. The low and oscillatory torque near the end is resultant from the incapacity of the battery to receive the energy. Apparently this is a good approximation suitable for testing the braking control.

4.4.2 POWER REGENERATION

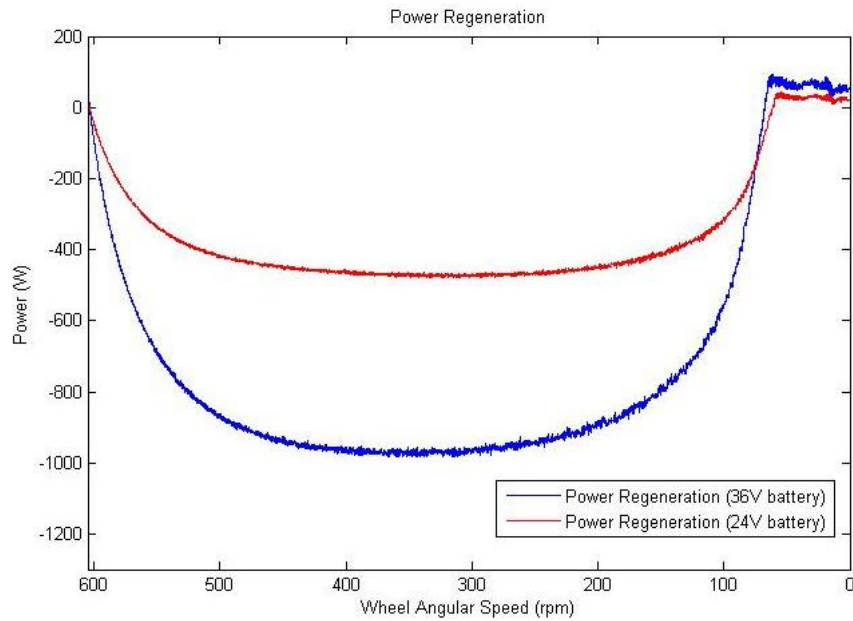


FIGURE 4.14 - Power Regeneration Profile as the Vehicle Decelerates From 50km/H to 0km/H for Different Feeding Currents in Rotor (2,4A AND 3,6A)

The power regeneration profiles are similar to each other as it would be expected (Figure 4.14), and correspond to typical power outputs of alternators. Notice also that near the end the regeneration drops rapidly, until it starts to expend more energy than it regenerates (this energy is expended in feeding the rotor).

4.4.3 DECELERATION

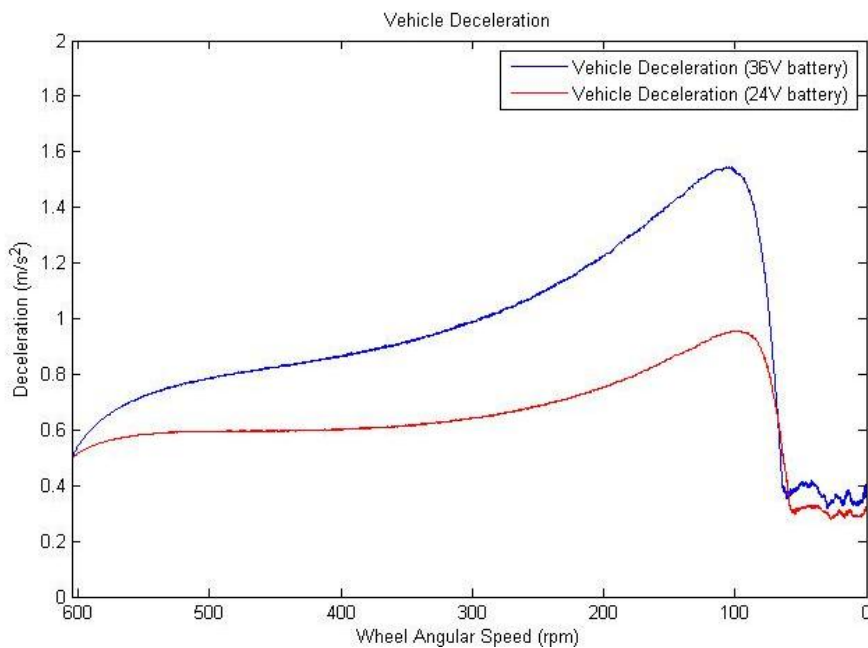


FIGURE 4.15 - Vehicle Deceleration Profile as the Vehicle Decelerates From 50km/H to 0km/H for Different Feeding Currents in Rotor (2,4A AND 3,6A)

In Figure 4.15 is possible to verify that the vehicle's deceleration is uncontrolled, especially near the end when the maximum value is obtained. This occurs because the rotor current is steady not compensating the high torque produced by the alternator at low rotations.

The maximum deceleration value obtained is about 1.8m/s^2 which is very low when comparing to other vehicles standards. For instance the maximum "comfortable" deceleration values for cars, buses and trucks are between 2m/s^2 and 2.5m/s^2 , and emergency braking typically reach 5m/s^2 [24].

Notice that when the vehicle is below 100rpm (approximately) the deceleration drops quickly. This is the point where the rotation does not generate enough emf to recharge the batteries. Switch to a resistive load at this point would greatly benefit the braking performance of the vehicle.

4.5 CONTROLLER

4.5.1 CONTROL STRATEGIE

There are two different controllers used for this system. The main controller that is responsible to choose the deceleration or current reference and where to dump the energy – ESS (regenerative braking) or resistors (dynamic braking). The braking controller has the purpose of controlling the amount of current necessary to feed the excitation winding in order to follow the references supplied by the main controller.

The controller has three input buttons that control the deceleration or current reference value. These signals along with the angular speed of the wheel (rotor) and the state of charge (SOC) of the battery are used as inputs.

An overview of these systems is shown in Figure 4.16.

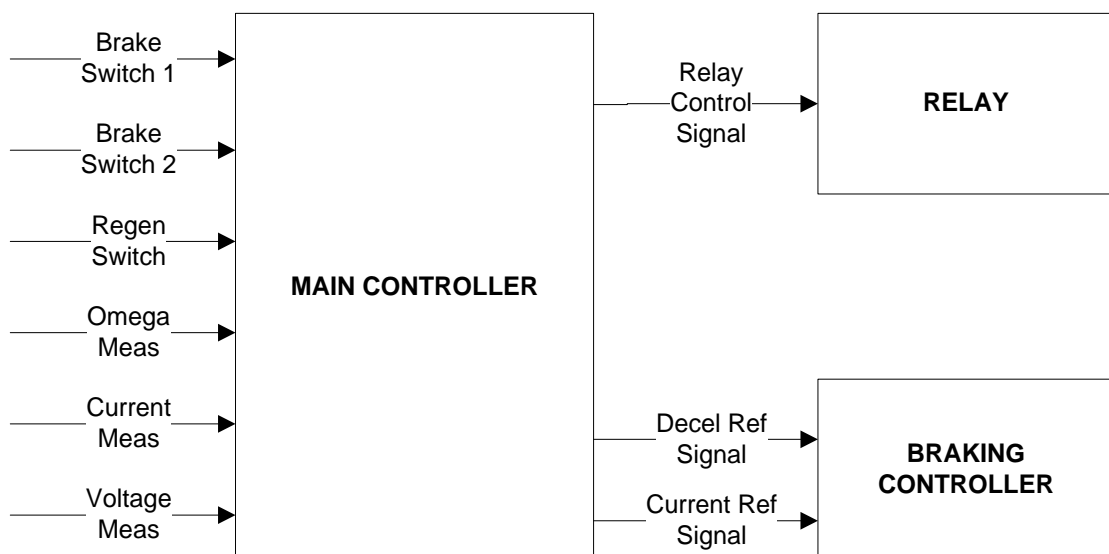


FIGURE 4.16 - Overview of the Control Systems

4.5.2 MAIN CONTROLLER

The purpose of this system was to define the amount of the vehicle's deceleration/current and also responsible to select the load (ESS or resistor). To develop this control system, an interactive design and simulation program called Stateflow was used within Matlab/Simulink. Stateflow is a graphical design and development tool for simulating complex reactive systems based on finite state machine theory [25].

The Stateflow chart contains six input ports and two output ports. The six input ports are listed as follows:

- Brake Switch 1;
- Brake Switch 2;
- Regeneration Switch;
- Voltage generated;
- Current generated;
- Rotational velocity of the electric motor;

Figure 4.17 shows an overview of the inputs and outputs of the control system.

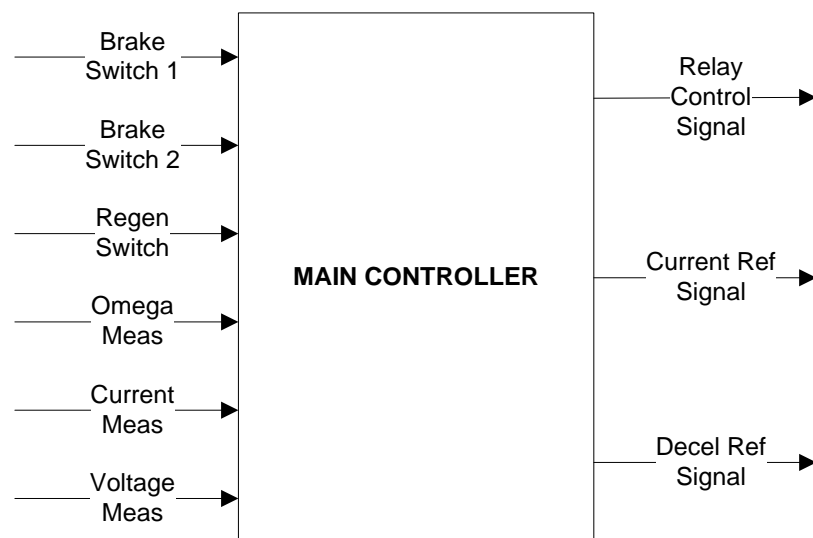


FIGURE 4.17 - Main Controller Schematic

The two outputs are listed below:

- Deceleration reference value;
- Current reference value;
- Relay control signal;

Besides the inputs and outputs there were also two threshold constants used within the Stateflow control chart. They are listed as follows:

- Maximum state of charge (SOC).
- Minimum regeneration speed

4.5.2.1 STATEFLOW

The Stateflow control chart consists of two major states: the 'BRAKE_OFF' state and the 'BRAKE_ON' state (Figure 4.18). The 'BRAKE_ON' state is only active when the brakes are applied and the angular velocity of the electric motor is not zero. During all other events, the control system is in the 'Off' state giving output of zero for the deceleration signal.

Furthermore the 'BRAKE_ON' state consists of three different sub-states running in parallel. The friction brake sub-states (forward and backward) and the electromagnetic brake sub-state.

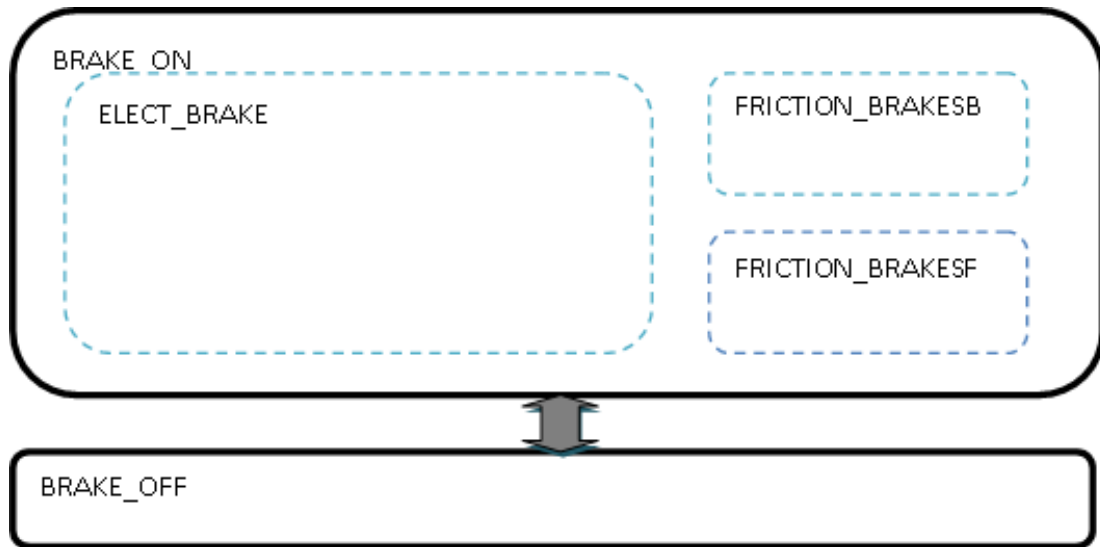


FIGURE 4.18 - Simplified Stateflow Control System

The friction brakes sub-states are equal and controlled externally by independent commanding signals. When activated sets a certain amount of pressure on the friction clutch, that effectively reduces the vehicle's speed.

The electromagnetic brake sub-state is the most important sub-state and contains five different states that can transit among each other depending on the input conditions to the Stateflow control system (Figure 4.19)

The five states are as follows:

- ELECT_BRAKE_MODEOFF
- ELECT_BRAKE_MODE1
- ELECT_BRAKE_MODE2
- REGEN
- RESISTOR

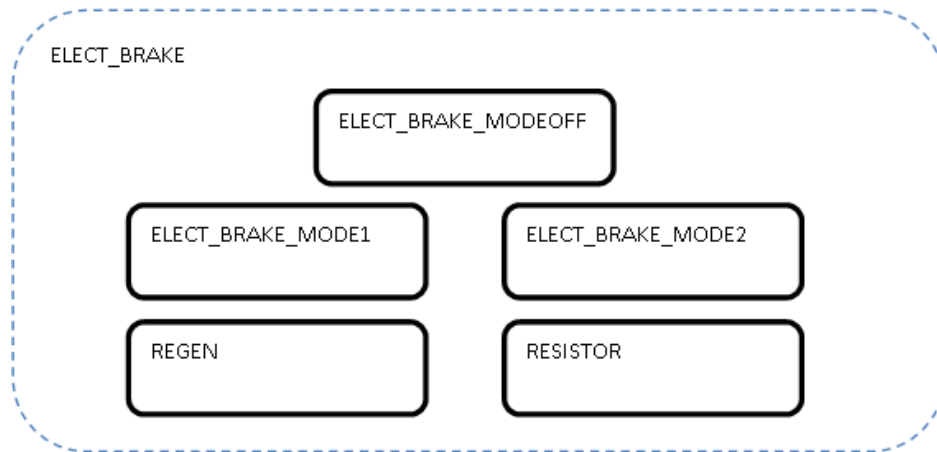


FIGURE 4.19 - Electromagnetic Braking Sub-State Detail

ELECT_BRAKE_MODEOFF STATE

This is the primary state and is responsible to initialize both the deceleration signal and relay signals to zero.

ELECT_BRAKE_MODE1 STATE

This state is set when the velocity is different of zero and Brake_switch1 is active. It sets the deceleration to 1 m/s^2 , which corresponds to a soft braking. The relay signal is set to regenerate connecting the battery.

ELECT_BRAKE_MODE2 STATE

This state requires the previous state to be active (ELECT_BRAKE_MODE1) and Brake_switch2 also set on. It is very similar to the ELECT_BRAKE_MODE1 state but sets the vehicle's deceleration to 2 m/s^2 , which corresponds to a tougher braking (but still "comfortable"). The relay signal is also set to regenerate connecting the battery.

REGEN STATE

The REGEN STATE is also active through a button (Regen_switch) and sets the relay signal to connect the battery. It is present to force a certain amount of energy regeneration to the battery by setting a current reference value of 5 Amperes.

RESISTOR STATE

All the previous states were different regenerative braking modes and the relay signal was connected the ESS. This state is the dynamic braking mode which sets the relay signal to connect the power resistors. The deceleration value is the same set in the previous state of the Stateflow.

Differently from the other states this one is not activated from switches. It requires OMEGA of the rotor to be lower than 50 rad/s or the SOC of the ESS higher than 95%. The OMEGA condition exists because at low rotation values the BEMF generated is not enough to successfully produce a relevant braking torque; the SOC condition is there mainly to protect the ESS's health.

A simple overview control schematic is shown in Figure 4.20. Notice that there are modes with priority over others in case of more than one active. For instance the ELEC_BRAKE_MODE1 have priority over the REGEN mode.

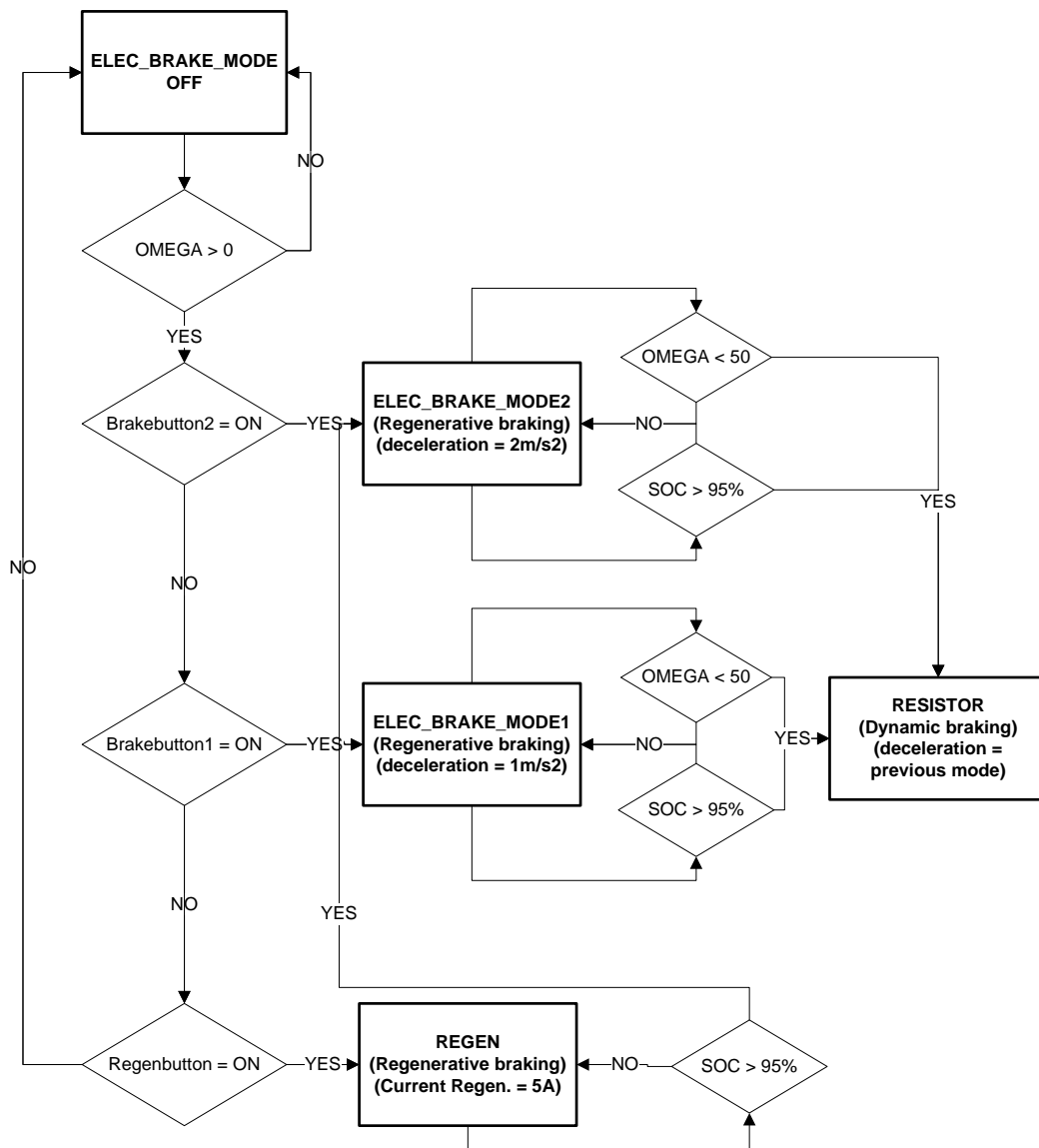


FIGURE 4.20- Control Logic Of Main Controller

4.5.3 BRAKING CONTROLLER

The braking controller regulates the amount of current necessary to feed the excitation winding in order to have a certain braking torque that would meet the desired deceleration/current of the vehicle or the desired amount of current regeneration. In order to develop this braking controller a PID was implemented.

PID controller (proportional-integral-derivative controller) is the most commonly used feedback controller. A PID controller calculates an "error" value as the difference between a measured process variable and a desired set point. The controller attempts to minimize the error by adjusting the process control inputs.

The PID controller calculation (algorithm) involves three separate parameters, and is accordingly sometimes called three-term control: the proportional, the integral and derivative values, denoted K_p , K_i and K_d . The proportional value determines the reaction to the current error, the integral value determines the reaction based on the sum of recent errors, and the derivative value determines the reaction based on the rate at which the error has been changing. By tuning the three constants in the PID controller algorithm, the controller can provide control action designed for specific process requirements.

The following equations (4.11, 4.12 and 4.13) represent the PID implemented, where e is the error, u is the output and K_p , K_i and K_d represent the proportional, integral and differential gains [26].

$$u = K_p \cdot e + K_i \int e \cdot dt + K_d \cdot \frac{de}{dt} + bias \quad (4.11)$$

Differentiating both sides of the equation gives:

$$du = K_p \cdot d(e) + K_i \cdot e + K_d \cdot \frac{d(de)}{dt} \quad (4.12)$$

Using difference to approximate the differential we get the discrete PID equation where T_s is the sampling period.

$$u(k) = u(k-1) + K_p \cdot [e(k) - e(k-1)] + K_i \cdot T_s \cdot e(k) + \frac{K_d}{T_s} \cdot [e(k) - 2e(k-1) + e(k-2)] \quad (4.13)$$

An overview of the PID control scheme is shown in Figure 4.21. The PID will receive the error between the reference and the measured value, computing the necessary duty cycle for the chopper circuit. The sampling period is set equal to the PWM period - 1kHz.

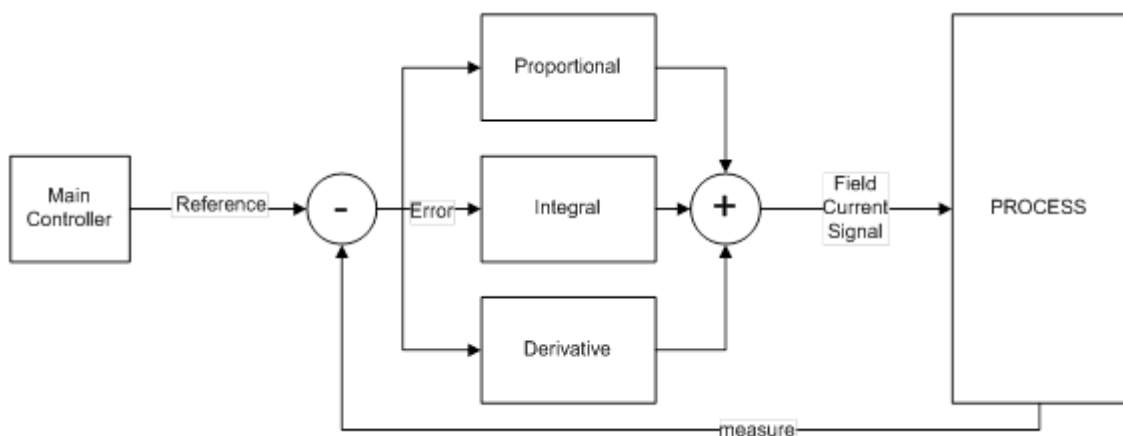


FIGURE 4.21- PID Control Scheme

4.6 BRAKING CONTROL RESULTS

4.6.1 CURRENT CONTROLLER TUNING

The regeneration current controller is used for the REGEN mode. The PID controller was also tuned by trial and error; however in this case the first approach for the PID gains were found using the Ziegler Nichols open loop method.

The Ziegler-Nichols open loop method is based on the process step response of the uncontrolled process. The PID parameters are calculated from the response in the output after a step in the control variable (Figure 4.22). So using table 4.6, it is possible to obtain a first insight for the controller gains by measuring the dead-time (D), the rate/slope (R) and the amplitude of the step (X).

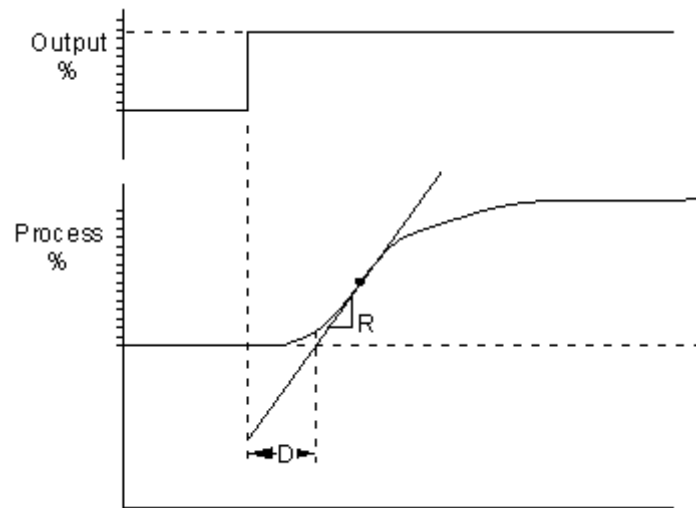


FIGURE 4.22- Ziegler-Nichols Open Loop Method: Reaction Curve With the Dead-Time “D” And the Rate “R” From the Process Step Response Represented [27]

	K_p	K_i	K_d
P	X/DR	—	—
PI	$0.9X/DR$	$0.3/D$	—
PID	$1.2X/DR$	$0.5/D$	$0.5D$

TABLE 4.6 - Ziegler-Nichols Open Loop Method: Formulas for the Controller Parameters [27]

Using the 36v system simulation parameters and setting the vehicle’s initial velocity to 50km/h, the open loop response to a step was taken - Figure 4.23.

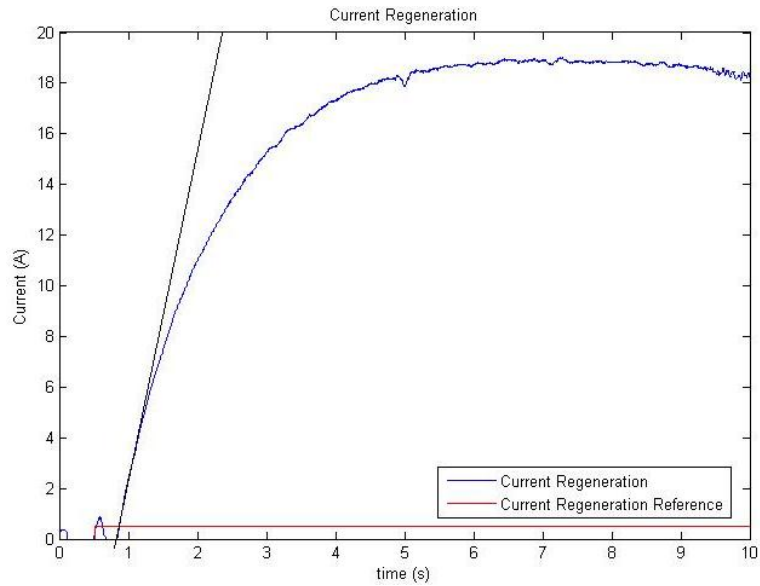


FIGURE 4.23 - Current Regeneration in Open Loop during 10 Seconds with an Initial Velocity of 50km/h

The step in the control variable should be about 10% of the operation step, so a step of 0.5 amperes was used, which resulted in $X=0.5$ A. Also from the response in Figure 4.23 is possible to read off that the dead-time is $D=0.4$ seconds.

R can be calculated from the slope of the response. From Figure 4.23 can be found that the inclination is about 20A in about 2 seconds which results in a slope $R=10$ A/s. Therefore, using the PI equations from table 4.6 is obtained that:

- $K_p \approx 0.12$
- $K_i \approx 0.75$

These values were used in the PI controller which resulted in the following graphic for a step of 5 amperes - Figure 4.24.

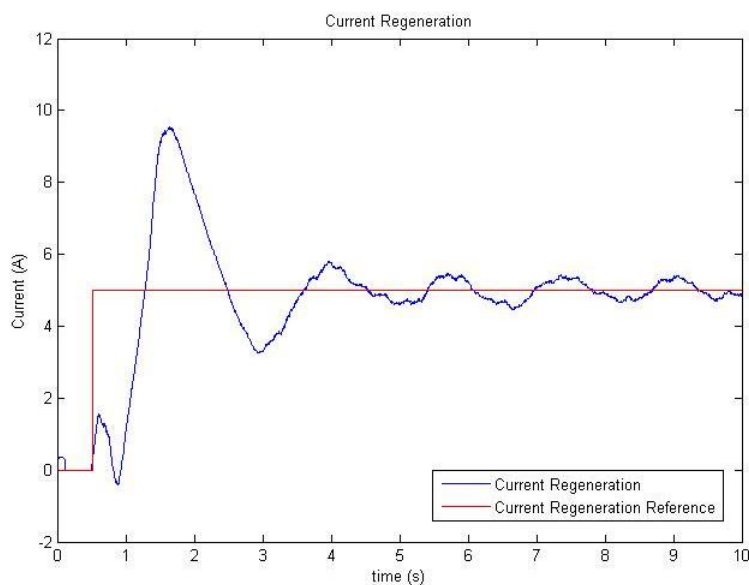


FIGURE 4.24 - Current Regeneration with Pi Controller ($K_p=0.12$, $K_i=0.75$) during 10 Seconds with an Initial Velocity of 50km/h

The stability of the control system is on the limit of being acceptable, with the system already following the reference. However it is still very oscillatory with a great overshoot, but this is to be expected with this tuning method since it only gives a raw first approach.

To correct the overshoot and the oscillations the integral gain was significantly reduced to 0.2 in to decrease the impulsive response. A small derivative effect of 0.012 was also added. The results obtained are represented in Figure 4.25.

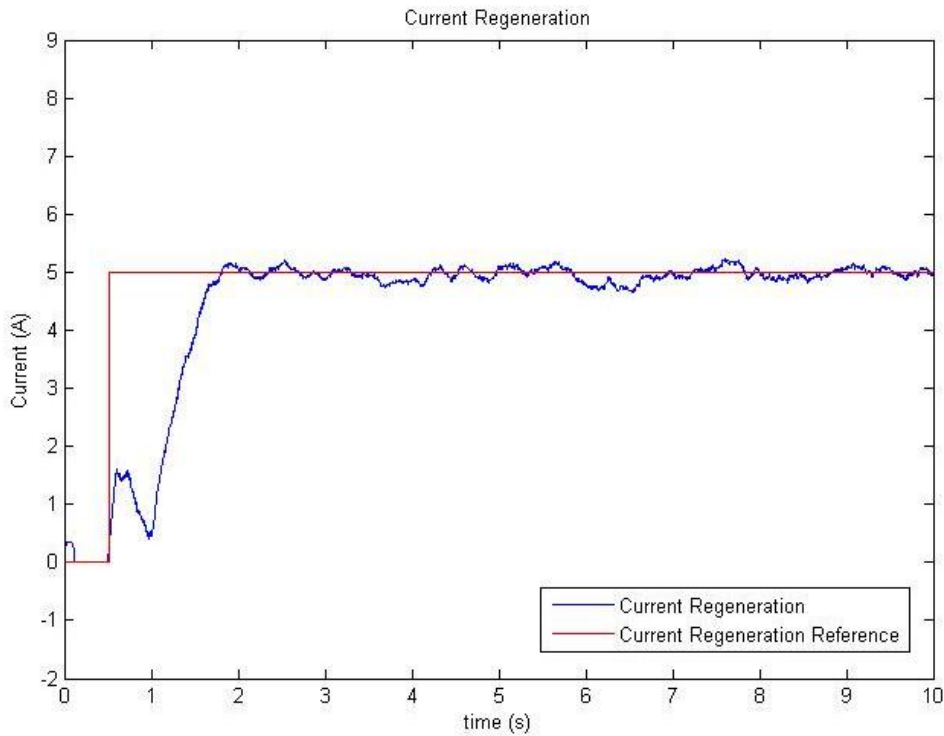


FIGURE 4.25 - Current Regeneration with Pi Controller ($K_p=0.15$, $K_i=0.2$ and $K_d=0.012$) During 10 Seconds with an Initial Velocity of 50km/h

In Figure 4.25 is possible to verify that with this PID controller the system is reaching the reference very fast (in about 1.5 seconds) without overshoot and with minimal oscillations. The coefficients for this controller can be seen in table 4.7.

COEFFICIENTS	VALUES
PROPORTIONAL	0.15
INTEGRAL	0.2
DERIVATIVE	0.012

TABLE 4.7 - Current PI Controller Coefficients

4.6.2 DECELERATION CONTROLLER TUNING

The results obtained in chapter 4.4 showed that the deceleration imposed by ELEC_BRAKE_MODE1 (1m/s^2) is only achieved when the vehicle slows down to the 300 rpm so the Ziegler-Nichols method was ignored. Also, the system is particularly complex in order to create a transfer function. Consequently the PID controller was tuned by trial and error, considering only as reference the effects of adding the different gains (table 4.8).

CL RESPONSE	RISE TIME	OVERSHOOT	SETTLING TIME	S-S ERROR
K_p	Decrease	Increase	Small Change	Decrease
K_i	Decrease	Increase	Increase	Eliminate
K_d	Small Change	Decrease	Decrease	Small Change

TABLE 4.8 - Effects on the Closed-Loop Response of Adding to the Controller Terms K_p , K_i and K_d

In order to regulate the PID values and try to make the vehicle follow a certain deceleration, several simulations in ELEC_BRAKE_MODE1 were conducted. It was implemented only regenerative braking and the rotor was fed with a 36v battery. The vehicle was set with an initial velocity of 50km/h.

The first test was conducted with the proportional, integral and differential gains all equal to one. The results can be seen in Figure 4.26.

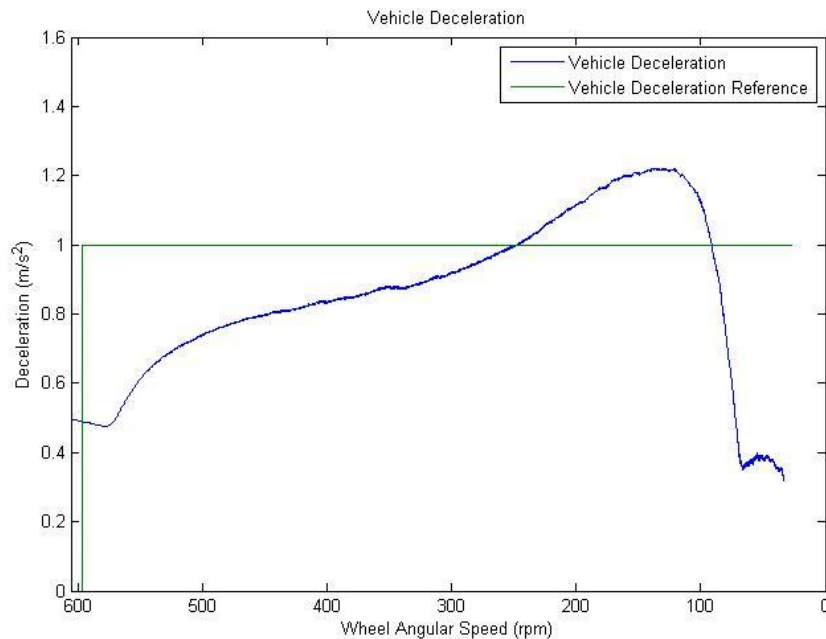


FIGURE 4.26- Vehicle Deceleration with PID Controller ($K_p=K_i=K_d=1$) as the Vehicle Decelerates From 50km/h

The vehicle does not follow the deceleration reference value. The low deceleration value at the end corresponds to the moment when the battery is not recharging anymore due to the low rotation.

In order to fix the error in the deceleration both proportional and integral gains were raised (proportional = 10 and integral =5). The derivative gain was set to zero.

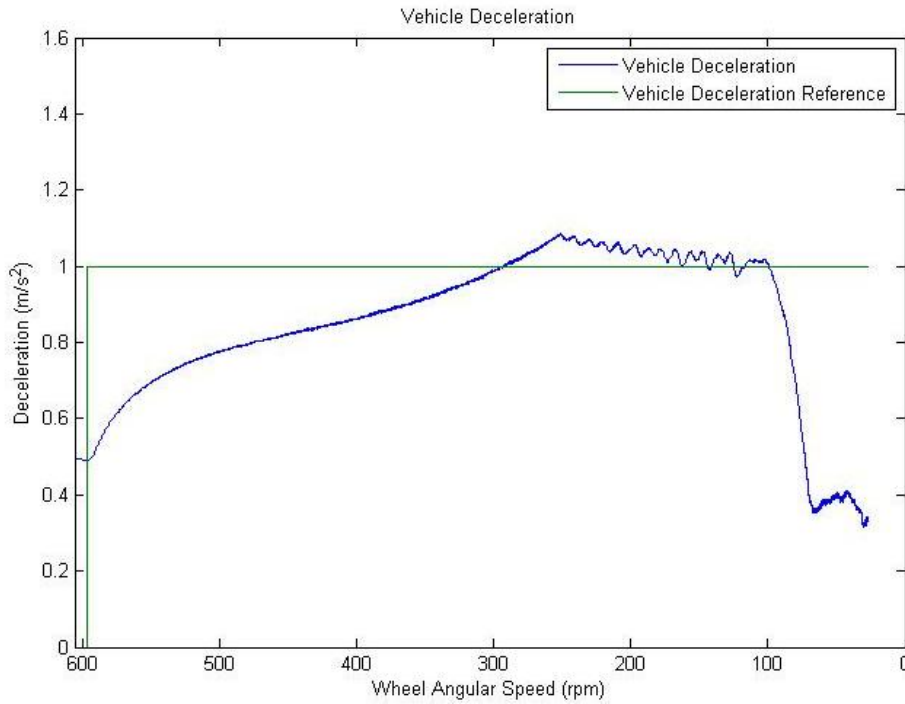


FIGURE 4.27 - Vehicle Deceleration with PI Controller ($K_P=10$, $K_I=5$) as the Vehicle Decelerates From 50km/h

With the controller of Figure 4.27 the system already tends to follow the reference. The last step was to reduce both settling time and rise time by increasing the proportional and integral gains. The result is shown in Figure 4.28.

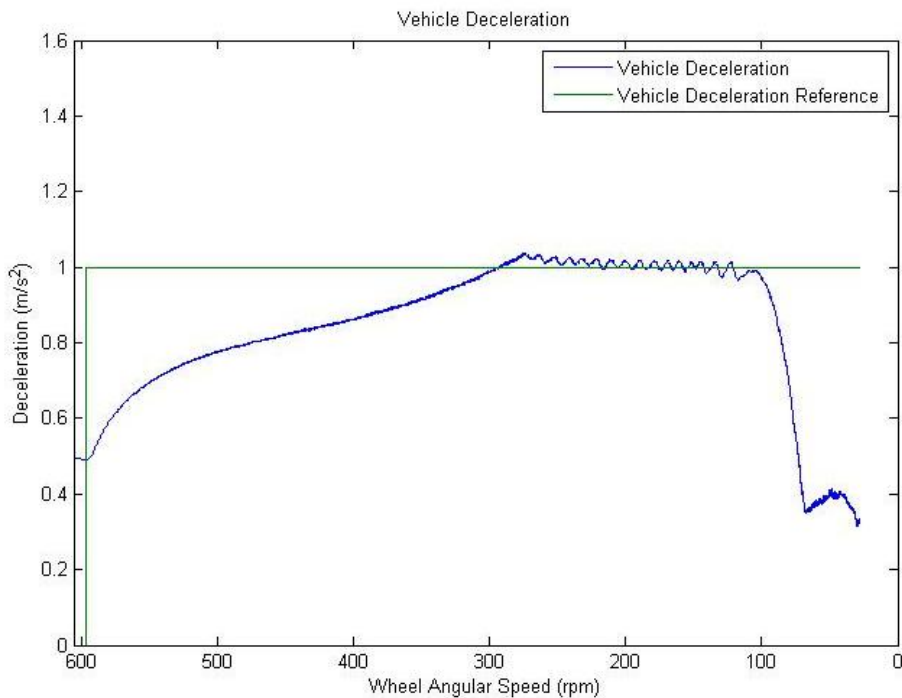


FIGURE 4.28 - Vehicle Deceleration with PID Controller ($K_P=25$, $K_I=20$) as the Vehicle Decelerates From 50km/h

With this PI controller the system (Figure 4.28) is responding much faster considering that only at 300 rpm the alternator generates enough torque to produce the reference deceleration. With this controller the deceleration was successfully managed, following the reference provided. The coefficients for this controller can be seen in table 4.9.

COEFFICIENTS	VALUES
PROPORTIONAL	25
INTEGRAL	20
DERIVATIVE	0

TABLE 4.9 – Deceleration PID Controller Coefficients

4.6.3 BRAKING CONTROL

In this section the author will present the results obtained with the complete system operational, controlling the vehicle deceleration in the ELECT_BRAKE_MODE1 braking mode. The load was commuting between a 36V battery pack and a 2Ω resistor and the rotor was fed with the 36v battery pack. The vehicle was set with an initial velocity of 50km/h and the braking signal was actuated half a second after the simulation beginning.

4.6.3.1 DECELERATION

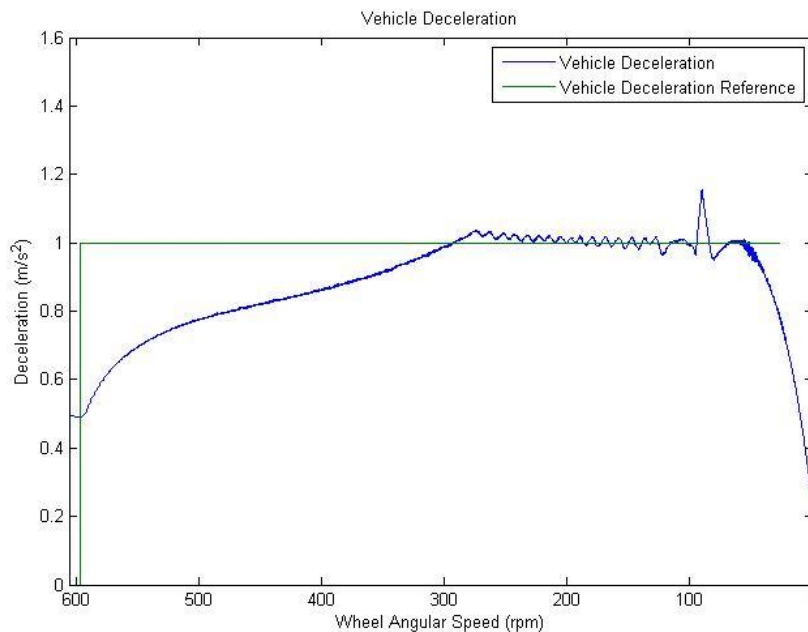


FIGURE 4.29 - Vehicle Deceleration as the Vehicle Decelerates from 50KM/H TO 0KM/h in the ELECT_BRAKE_MODE1 Braking Mode

The deceleration profile (Figure 4.29) is similar to what has been seen in the previous sections where the deceleration is successfully following the reference. The introduction of the resistor at the 100 rpm moment produces a short spike in the deceleration profile (a variation to the reference of less than 20%). However this spike is almost instantly attenuated by the controller, retrieving the vehicle to the original deceleration reference.

4.6.3.2 TORQUE

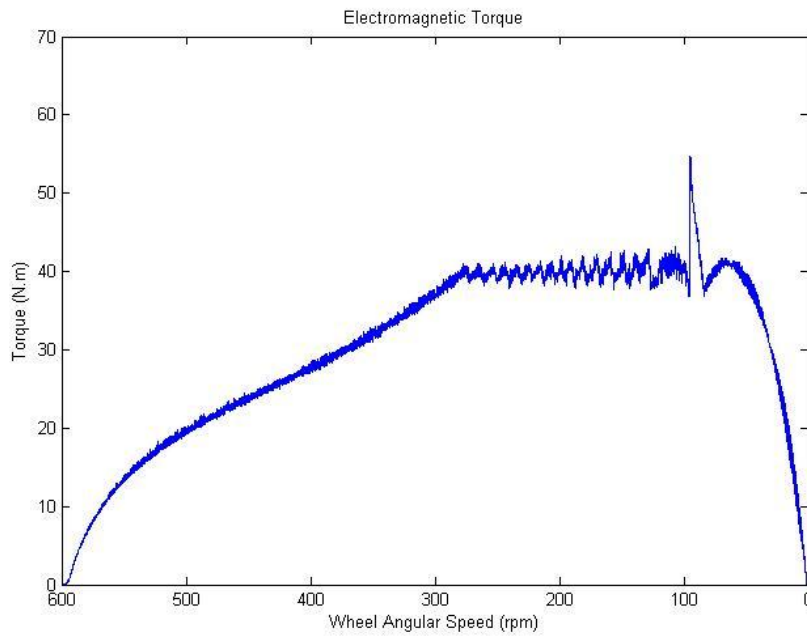


FIGURE 4.30 - Electromagnetic Torque as the Vehicle Decelerates from 50KM/h to 0KM/h in the ELECT_BRAKE_MODE1 Braking Mode

4.6.3.3 POWER REGENERATION AND DISSIPATION

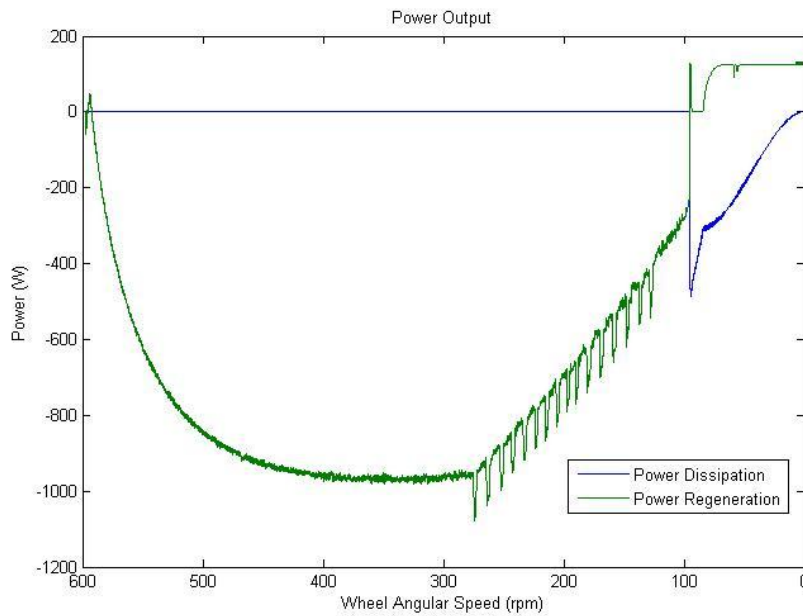


FIGURE 4.31 - Power Regeneration and Dissipation Profiles as the Vehicle Decelerates from 50KM/h to 0KM/h in the ELECT_BRAKE_MODE1 Braking Mode

In the previous graphic (Figure 4.31) is possible to see the moment where the load transition occurs at 100 rpm. Notice also that a maximum of 1000W is regenerated during this simulation. At the end is possible to notice that the power regeneration is positive, this is the energy that is continuously being removed from the battery to feed the rotor.

4.6.3.4 VEHICLE VELOCITY

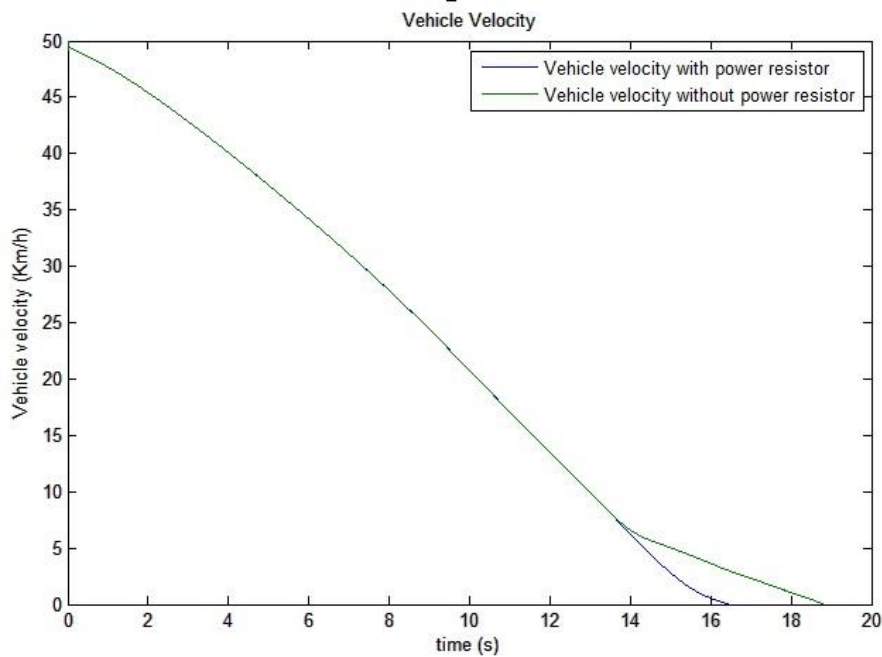


FIGURE 4.32 - Vehicle Velocity as the vehicle decelerates from 50KM/H TO 0KM/h in the ELECT_BRAKE_MODE1 Braking Mode

In Figure 4.32 is possible to verify the vehicle Velocity over time (in km/h). As we can see by the linearity of the graphic the previous variations in the deceleration don't reflect in any discrepancy in the movement of the vehicle.

In the last part is possible to see that apparently the resistor is a good asset for the design, since significantly improve the braking capability of the vehicle by reducing the braking time to about 50% (from 100 rpm to 0 took about 5 seconds to stop the vehicle only with the battery and half of the time with the resistor)

The other braking mode (ELECT_BRAKE_MODE2) is different just in the deceleration reference value. However the electromagnetic braking system can't achieve the deceleration value imposed by this state independently ($2m/s^2$), requiring for example the help of the friction brakes. However for the previous mode presented (which demand less torque) the results obtained are enough to confirm that the braking system control is operational.

4.6.4 TRANSITION BETWEEN BRAKING MODES

In this segment the vehicle is braking in REGEN mode and at the 325rpm the ELECT_BRAKE_MODE1 is activated. All the parameters (Battery voltage, Resistor and Vehicle Initial Speed) are configured just like the previous simulations.

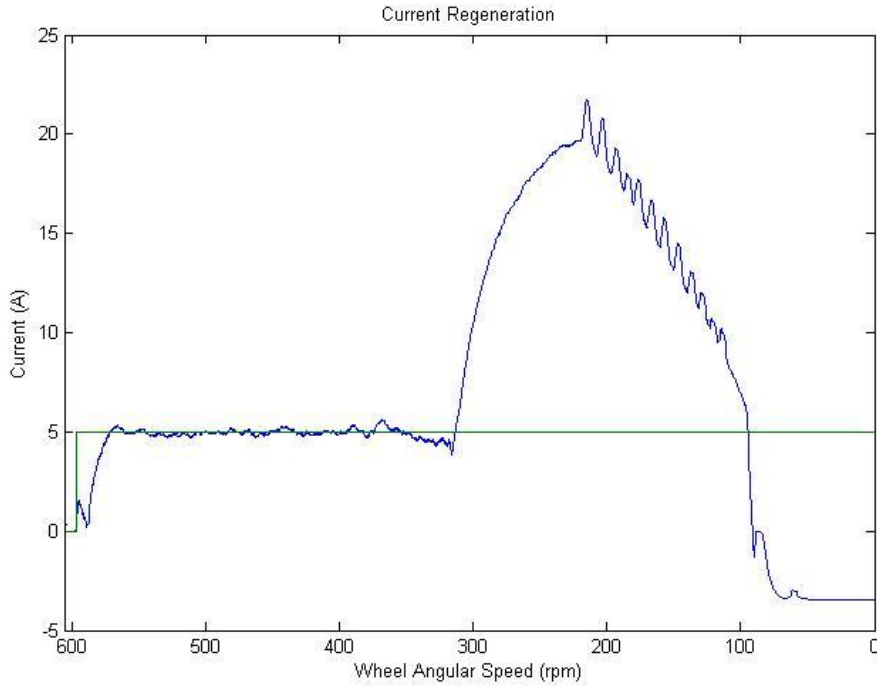


FIGURE 4.33 - Current Regeneration Response to the Transition between Different Braking Mode Solicitations

The system responds immediately to the solicitation of the braking modes (Figure 4.33 and Figure 4.34). On the first part (REGEN mode) is possible to verify that the current regenerated is controlled. Later the ELECT_BRAKE_MODE1 is activated and the current regenerated substantially increase and the vehicle deceleration is controlled. There is no rough transitory between the braking modes in both current and deceleration.

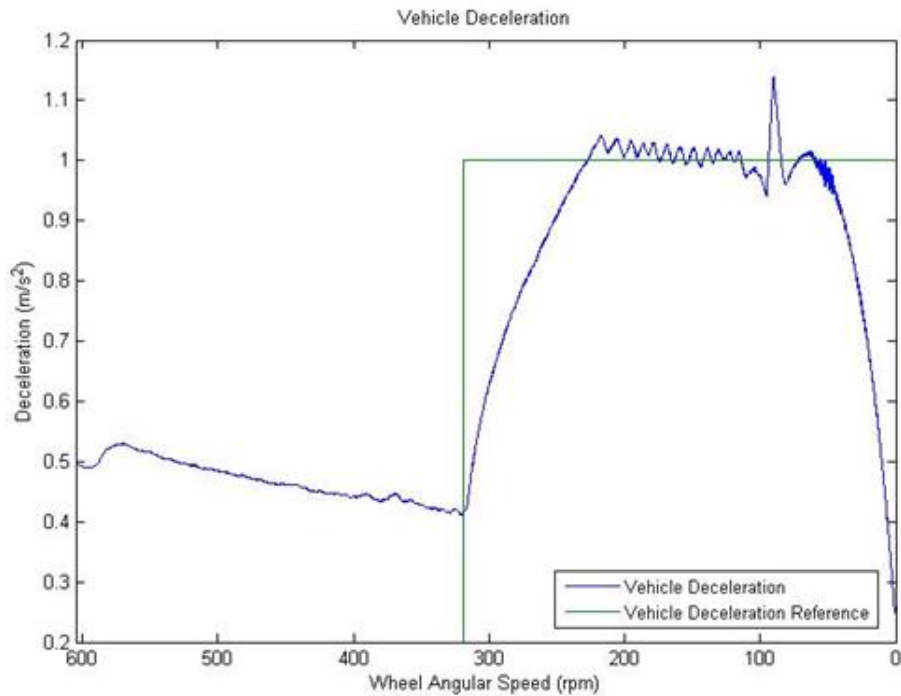


FIGURE 4.34 - Vehicle Deceleration Response to the Transition between Different Braking Mode Solicitations

CHAPTER 5

PHYSICAL PROTOTYPE - DESIGN AND TEST

5.1 PHYSICAL EQUIPMENT

5.1.1 VEHICLE

The vehicle used was a motorcycle AD 125 MY09. The main characteristics of the vehicle were used on the simulation and can be found in table 4.1 (Chapter 4). In table 5.1 are represented a few other characteristics of this vehicle. This specific motorcycle was chosen because it was the one where the integration of the electric motor would be easier.

Characteristics	Value
Engine Bore/stroke	48,8 x 57 single cylinder four-cycle
Displacement	124,5 cc
Max power	9,7kW at 8500 rpm
Max torque	10,9 Nm at 6500 rpm
Gear	CVT with automatic clutch
Front brake	260 mm disc brake
Rear brake	240 mm disc brake

TABLE 5.1 - Two-Wheeled Vehicle Characteristics

Still some adaptations had to be made, such as the resizing and bending of the exhaust tube. It was also necessary to fabricate some pieces that were important for example to support and fix the electric motor to the vehicle. In annex C can be found the drawings of all the pieces designed in Solidworks 2010.

5.1.2 ELECTRIC MACHINE

The electric machine used for the practical tests was a Bosch 28V, 80A alternator with reference 6033GB3054, typically utilized in trucks (Figure 5.1). The parameters of this alternator are similar to the ones used in the simulation, which can be found in table 4.2.



FIGURE 5.1 - 24V, 80A Alternator

5.1.3 BATTERY AND POWER RESISTOR

The battery pack used was composed by three 12V 36Ah Lead Acid batteries connected in series in order to have a 36V battery set. It was used to power the rotor coil and store energy during regenerative braking. The resistor has low impedance (approximately 0.1Ω) and can endure the maximum current that the alternator is able to provide - 80A. In Figure 5.2 is represented the resistor and one of the batteries.

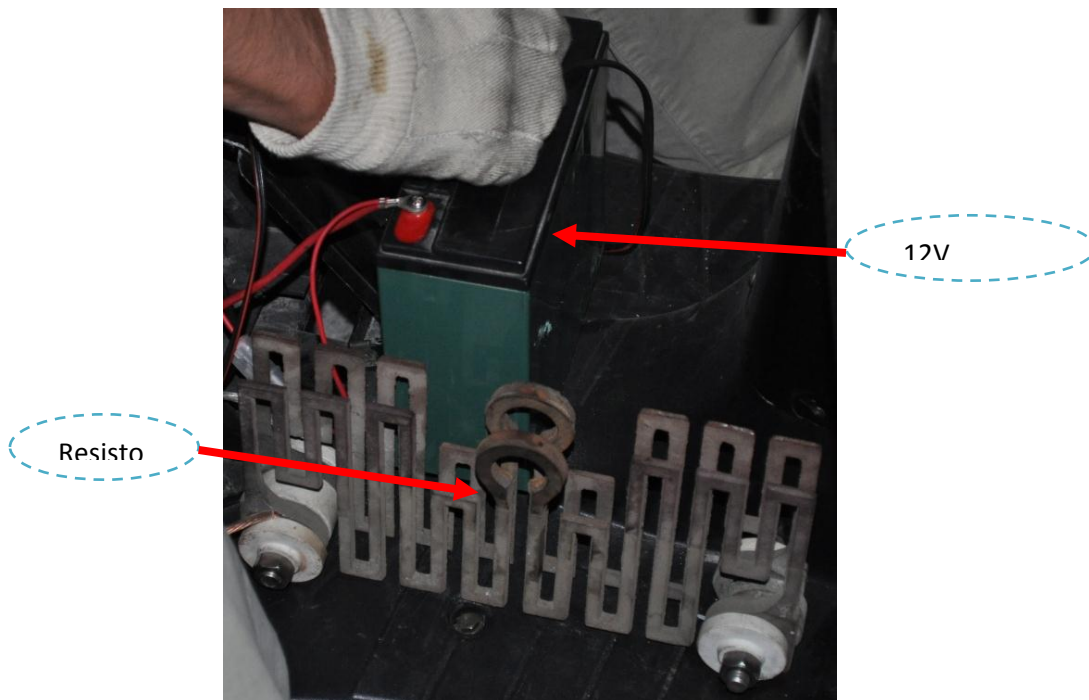


FIGURE 5.2 - 12V Battery and the Power Resistor

5.1.4 TRANSMISSION

The connection between the alternator and the wheel was made through a metal chain. This chain connected a gear in the alternator's rotor with 8 teeth to a gear in the vehicle's wheel with 42 teeth. The ratio of the gears is 5.3 – equation 5.1.

$$\text{Gear Ratio} = \frac{\text{Wheel Gear}}{\text{Alternator Gear}} = \frac{42}{8} = 5.3 \quad (5.1)$$

In Figure 5.3 is possible to see the gear in the wheel and the chain connected to the alternator.



FIGURE 5.3 - Transmission

5.2 SENSOR SYSTEM

Sensors are a critical component in a motor control system and they are normally used to sense the current, position, speed and direction of the rotating motor. In most motor control systems, several sensors are used to provide feedback information on the motor. These sensors are used in the control loop and to improve the reliability by detecting fault conditions that may damage the motor.

5.2.1 CURRENT SENSOR

There are several solutions for measuring the current, however for motor control applications the three most common current sensors are:

- Shunt Resistors
- Hall Effect Sensors
- Current Transformers

A summary of the advantages and disadvantages of each one of the previous current sensors is provided in Table 5.2.

Current Sensing Method	Shunt Resistor	Hall Effect	Current Sensing Transformer
Accuracy	Good	Good	Medium
Accuracy vs. Temperature	Good	Poor	Good
Cost	Low	High	Medium
Isolation	No	Yes	Yes
High Current-Measuring Capability	Poor	Good	Good
DC Offset Problem	Yes	No	No
Saturation/Hysteresis Problem	No	Yes	Yes
Power Consumption	High	Low	Low
Intrusive Measurement	Yes	No	No
AC/DC Measurements	Both	Both	Only AC

TABLE 5.2: Comparison of Current Sensing Methods [28]

Consulting the Table 5.2 in order to choose the best method to sense the battery current (bi-directional), the Shunt resistor stands out as the most suitable solution, mainly because it provides accurate measurements at a significantly low cost.

5.2.1.1 SHUNT RESISTOR

The shunt current resistor was made from a piece of steel wire with about 10cm and with an impedance of 2.5mΩ, this value was selected considering that the current range is approximately [-40A, 40A]. The consequent maximum power dissipation will be of 4W (equation 5.2).

$$P_{diss} = R_{shunt} \cdot I^2 \quad (5.2)$$

The shunt measurement can be made either in the High-Side or the Low-Side of the system - Figure 5.4 - A high-side analysis has the resistor connected in series with the power source, while the low-side analysis locates the resistor between the load and the ground current return path.

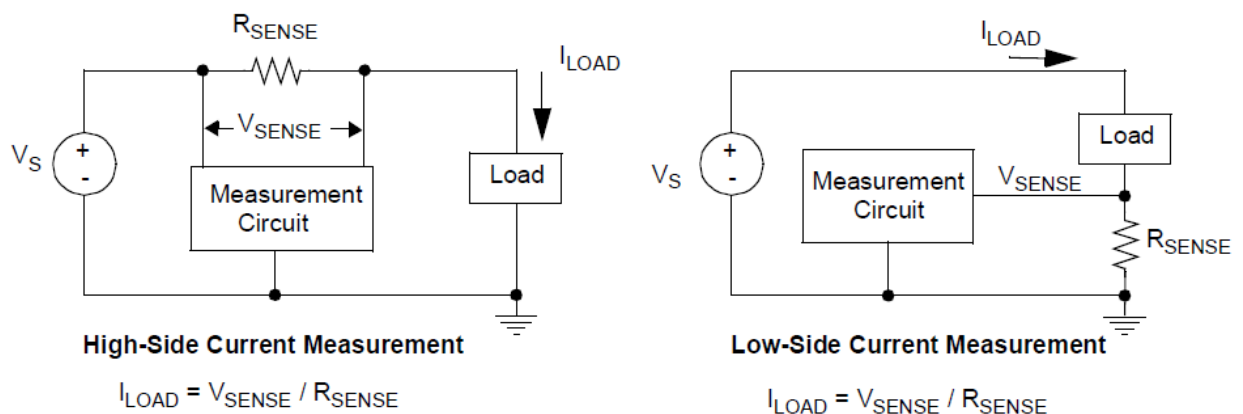


FIGURE 5.4 - High-Side and Low-Side Resistive Current Shunts

The following table - Table 5.3 -summarizes the main advantages and disadvantages of using a High-side or a Low-side current measurement.

High-Side		Low-Side	
Advantages	Disadvantages	Advantages	Disadvantages
Current sensor connected directly to the power source can be used to detect any downstream failure.	Requires very careful resistor matching in order to obtain an acceptable common-mode rejection ratio (CMMR).	Requires only one low voltage Operational Amplifier.	More susceptible to EMI noise.
Won't create an extra ground disturbance that comes with a low side current sensing design.	Must withstand very high, and often dynamic, common-mode voltages.	Inexpensive and precise.	The shunt resistor disrupts the ground path.

TABLE 5.3 - Advantages and Disadvantages of High-Side and Low-Side Current Measurement

Having the previous table into account (Table 5.3), and because our application can tolerate the extra disturbance in the ground path, we decided to use a low-side measurement, which involves a more simplified circuitry and cheaper components.

5.2.1.2 5.2.1.2 MEASUREMENT CIRCUIT

The circuitry developed to measure the voltage drop in the shunt resistor combines an EMI filter, a differential amplifier, a low-pass filter and offset - Figure 5.5.

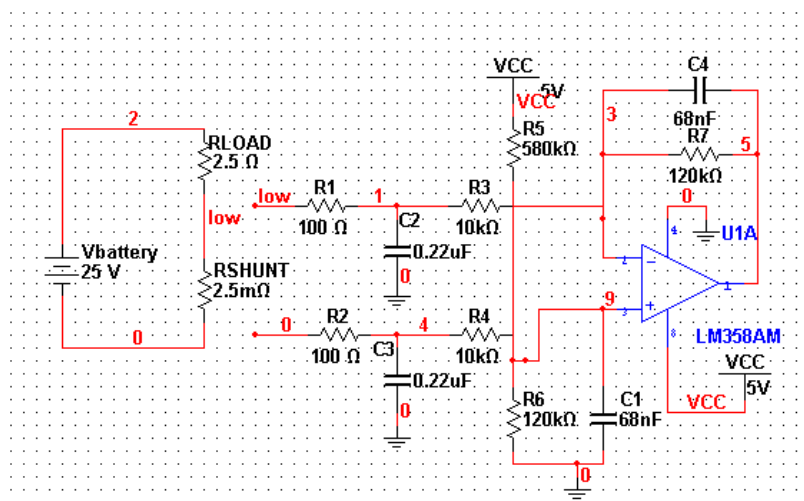


FIGURE 5.5 - Circuit of the Current Sensor

The EMI filter is regulated to cut high frequencies (about 50kHz) in order to reduce the noise. In order to accurately model the filter response, the gain of the circuit and the offset, several calculations and SPICE simulations were made to proper dimension the components of the shunt measurement circuit

The dimensioning of the resistors and capacitors had to be made together in order to obtain agreeable values of frequency, gain and offset. Having these in mind the following equations were used (5.3, 5.4, 5.5 and 5.6).

$$F_{-3dB} = \left(\frac{1}{(2\pi \cdot C_4 \cdot R_7)} \right) \quad (5.3)$$

$$Gain = \left(\frac{-R_7}{(R_1 + R_3)} \right) \quad (5.4)$$

$$Offset = \left(\frac{R_6 // R_4}{(R_5 + R_6 // R_4)} \right) \cdot V_{CC} \quad (5.5)$$

$$V_{OUT} = \left[\left(I_{Load} \cdot R_{sense} \right) \cdot \left(\frac{R_7}{(R_1 + R_3)} \right) + \left(\left(\frac{R_6 // R_4}{(R_5 + R_6 // R_4)} \right) \cdot V_{CC} \right) \right] \quad (5.6)$$

Which, for the following elements - $R_1=R_2=100\Omega$, $R_3=R_4=10k\Omega$, $C_2=C_3=220nF$, $R_5=R_7=120k\Omega$, $R_6=580k\Omega$, $C_1=C_4=68nF$ - resulted in a cutoff frequency of 20Hz, a gain of 12 and an offset of approximately 1.25 V.

The gain allows having a precision of 30mV/A, the offset permit the measurement of currents between +40A and -80A since the op-amp Im358 used has an output range between [0V, 3.8V]. The cutoff frequency is enough to obtain a stable signal. In annex B can be found the graphics showing the performance of the sensor.

5.2.2 VOLTAGE SENSORS

The voltage sensor consists of a voltage divider dimensioned to 36V. This means having $\left(\frac{R_1}{R_2} \right) = 7$ which can be obtained with $R_1=33k\Omega$ and $R_2=4.7k\Omega$. It was also added an RC low-pass filter with $F_c=1Hz$ in order to have stable measurements. The circuit is represented in the following Figure 5.6.

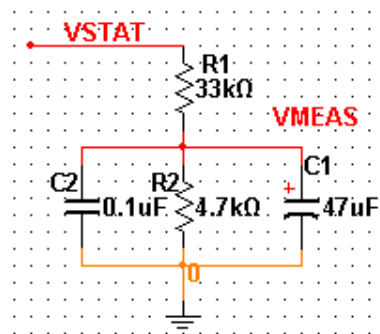


FIGURE 5.6 - Circuit of Voltage Sensor

5.2.3 5.2.3 ANGULAR SPEED SENSOR

The angular speed of the motor shaft is required as a feedback for the electromagnetic braking control of the vehicle. The available possibilities for the angular speed sensor are displayed in table 5.4, where the main advantages and disadvantages are also presented.

OPTICAL	MAGNETIC	
Encoder Disc	Hall Effect	Hall Effect Gear tooth
->Good Precision (Depends only on the disc pattern and quality of the photodiode). ->Low cost. ->Difficult to mount onto vehicle.	->Low cost. ->Requires magnet. ->Low Precision (Depends on the number of magnets placed on the rotary system).	->Good precision (Depends only on the number of teeth of the rotary system). ->Internal magnet. ->Easy mounting onto vehicle.

TABLE 5.4 - Angular Speed Sensors Characteristics

Based on the table 5.4 an Hall Effect tachometer (also known as gear tooth sensor) with the reference ATS642LSHTN-I2-T [29] was chosen to measure the speed of the rotor. The main criterion for this selection was the simplified mounting of this sensor in the vehicle (fixed to the alternator sensing the cooling fan blades).

This Hall Effect gear tooth sensor incorporates a dual element Hall effect IC and signal processing. This element senses the variation in the flux of the air gap between the passing ferrous gear tooth and the magnet switching in response to the differential magnetic signals created.

This two wire gear tooth sensor has a current output of 7mA and 14mA as low and hi signal, so an electronic circuit was developed in order to convert this output into TTL voltage levels (Figure 5.7) [29].

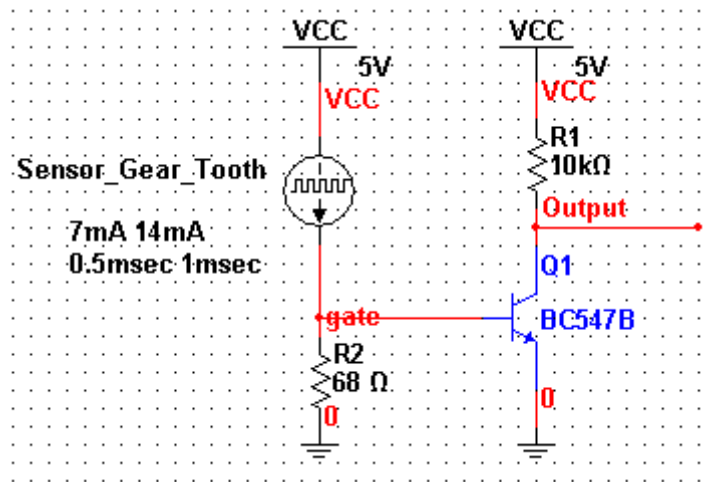


FIGURE 5.7 - Circuit of Speed Sensor

This circuit basically consists in opening and closing the transistor, for that V_{BE} must be higher or lower than 0,7V respectively. So by dimensioning the R_2 resistor equal to 68Ω we obtain that $V_{BE} = 0,476V$ (transistor closed) when the output is 7mA, and that $V_{BE} = 0,952V$ (transistor opened) when the output is 14mA. In annex B can be found the graphics showing the performance of this sensor.

5.2.4 5.2.4 BRAKE SWITCHES

The brake control switches used were in the motorcycle handle. All the switches are press buttons which means that they require to be continuously pressed in order to be active.

One brake switch was already implemented in the handle brake, but as we require two braking states a second switch (microswitch) was added to the hand brake. The Regen switch is a button on the side of the motorcycle handle (Figure 5.8).



FIGURE 5.8 - Motorcycle Handle Switches

5.2.5 5.2.5 SENSOR BOARD

All the previous measurement circuitry and signal conditioning was developed in a small double layer PCB with the elements soldered on one side and the routing on the other. The PCB connects to the analog I/O's of the microcontroller board to transmit the signals, share the ground and VDD. These connections are made through the connectors on the lateral part of the board. The PCB was projected in the NI Multisim/Ultiboard environment. A 3D representation of the top layer and the bottom layer of the board as it was designed can be observed in Figure 5.9.

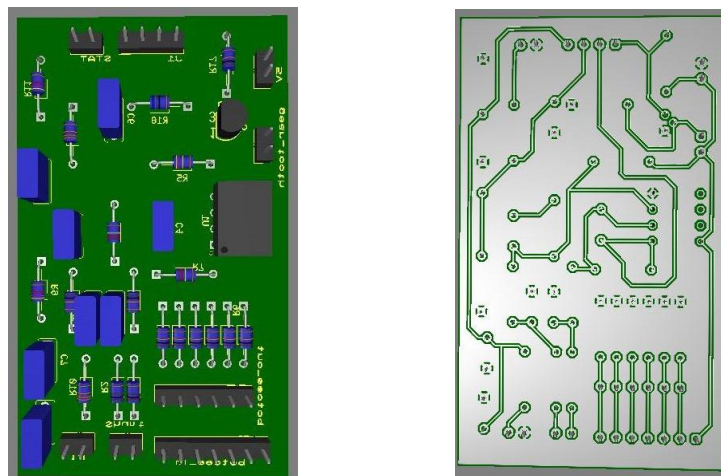


FIGURE 5.9 - Top Side and Bottom Side Virtual Representation of the Sensors PCB

A photograph of the developed sensors PCB board is shown in the following image (Figure 5.10).

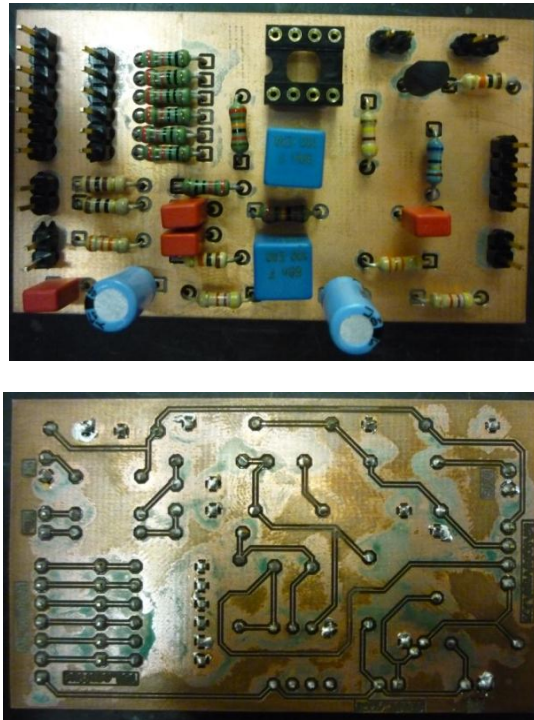


FIGURE 5.10 - Sensors PCB Top Side and Bottom Side

5.3 CONTROL SYSTEM

Concerning the equipment required to perform the real-time control of braking, several specifications had to be met, such as:

- Seven analog input channels for data acquisition;
- Two analog output channels - one PWM;
- Communication module for sending the results.

5.3.1 MICROPROCESSOR BOARD

The Microprocessor board (Figure 5.11) was developed by IPFN and is thoroughly used in several projects of the institute. The board is powered by a 12 volt source and contains voltage regulators to 5 volt in order to supply the microcontroller and all the sensors. The I/O's, grounds and VDDs leave the board through a 96 pin DIN 41612. The microcontroller chosen was the dsPIC30F4011 [30] [31], due to its easiness of use, versatility and low-cost. This microcontroller belongs to the dsPIC16 family of Microchip.

In terms of speed, the microcontroller uses an external crystal oscillator with an oscillation frequency of 7.3728 MHz. Is possible to multiply this value by sixteen due to a PLL, obtaining this way a clock frequency of 117.9648 MHz (FOSC). This value is within the working limits of the microcontroller (maximum clock frequency of 120 MHz). Since each instruction needs 4 clock cycles, the instruction frequency (FCY) is 29.4912 MHz. This instruction frequency allows the use of most frequent baud rates for communication with no error.

The microcontroller has an ADC module with one 10-bits ADC and 16 analog inputs. It also possesses an UART module responsible for asynchronous serial communication in full-duplex. This communication can be made at the standard baud rates 9600, 19200, 38400, 115200 and 460800 by RS23211 and also 921600 and 1843200 by optic fiber. Due to the low transmission rates necessary for this project (115200), the communication was established by RS232 connecting the D9 port on the board with the USB port of a computer through an adapter (serial/USB).

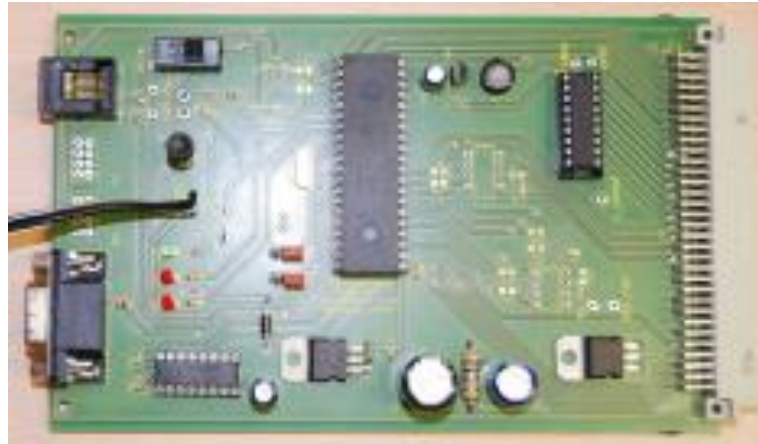


FIGURE 5.11 - Microprocessor Board

5.3.2 CHOPPER CIRCUIT

The Chopper circuit was developed just as represented in Figure 5.12. It was first simulated in Multisim and afterwards the PCB was created. Figure 5.13 correspond to the circuit in CCAM Software before the printing.

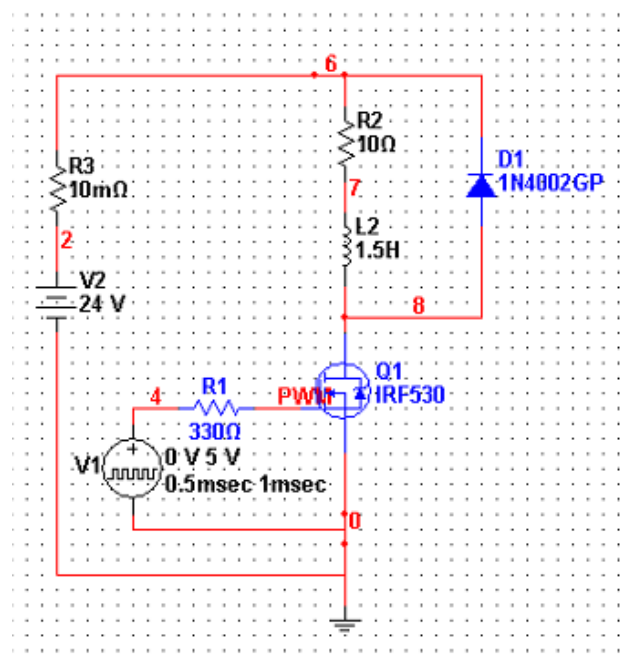


FIGURE 5.12 - Chopper Circuit Designed

The components have characteristics similar to the ones used in the simulation chapter – Diode and MOSFET [IRFP4310ZPBF [23]]. The resistor placed in the MOSFET’s gate is there to limit the current drawn from the dsPIC and with it create enough voltage to drive this device. In this case, considering that the maximum current that can be drawn from the dsPIC is 20mA, was used a 330Ω resistor which will draw 15mA (at 5V).

The PWM frequency should be selected so that it does not create too much current ripple in the rotor winding, since current ripple results in heating of the motor. By knowing the terminal inductance L and the terminal resistance R of the motor we can calculate the time constant of the rotor (equation 5.7).

$$t_c = \left(\frac{2\pi \cdot L}{R} \right) \quad (5.7)$$

With the time constant calculated and approximately equal to 1s, the PWM frequency was set (much) higher – 1kHz.

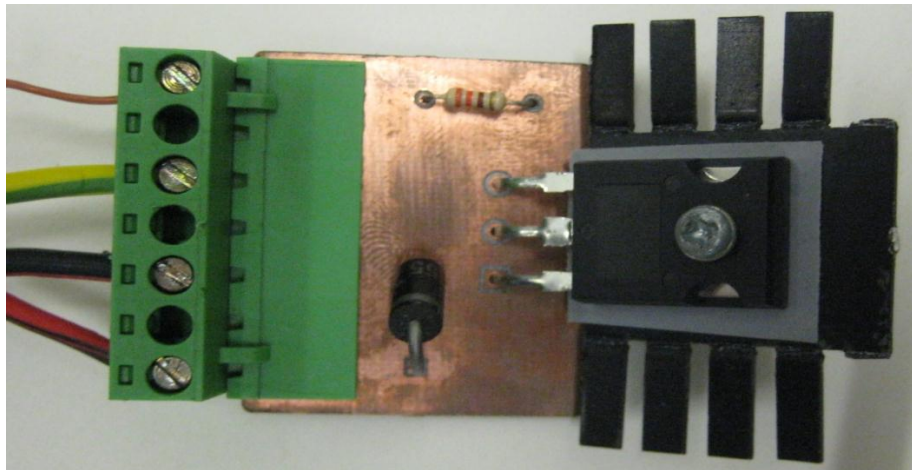


FIGURE 5.13 - Chopper Board

5.3.3 PROGRAMMING

The microprocessor programming is a significant part of this project. The microprocessor can be either programmed in C or assembly. The language chosen was C due to its simplicity and MPLAB C30 [32] was used to compile the code. It is the microcontroller that is going to be responsible for the signals acquisition, the braking calculation and the communication with an external device to send the results.

This way the programming can be divided in three distinct parts: the configuration of the A/D module, the PWM and the configuration of the UART module. Besides microcontroller programming, some microcontroller configuration bits needed to be changed. This consisted on choosing the external crystal oscillator to be PLL16 as the clock source, in order to achieve maximum processing speed and perfect serial communication. The watchdog timer was also disabled since it performs a reset to the microcontroller when it is inactive for some time which is not desired.

5.3.3.2 UART MODULE

The UART is an asynchronous full-duplex serial communication system. This module was used because it allowed an efficient way for sending the data to a peripheral device, like a computer, by RS232. The UART module main features are the following:

- Full-duplex, 8 or 9-bit data communication;
- Even, Odd or No Parity options (for 8-bit data);
- One or two Stop bits;
- 4-deep FIFO18 transmit data buffer;
- 4-deep FIFO receive data buffer;
- Fully integrated Baud Rate Generator with 16-bit prescaler;
- Baud rates range from 38 bps to 1.875 Mbps at a 30 MHz instruction rate;
- Parity, Framing and Buffer Overrun error detection;
- Support for Interrupt only on Address Detect (9th bit = 1);
- Separate Transmit and Receive Interrupts;
- Loopback mode for diagnostic support;

Note that the microcontroller has two independents UART modules. However in the adaptations made to the development board in order to receive the dspic30f4011 the UART1 pin became unusable. Either way it was not important as only one UART was required and used - UART2 - which was the one connected to the D9 connector on the board.

The block responsible for receiving data is completely independent from the block responsible for transmitting data, sharing only the clock generated by the baud rate generator. In this project it was only necessary to use the UART transmitter block - Figure 5.15.

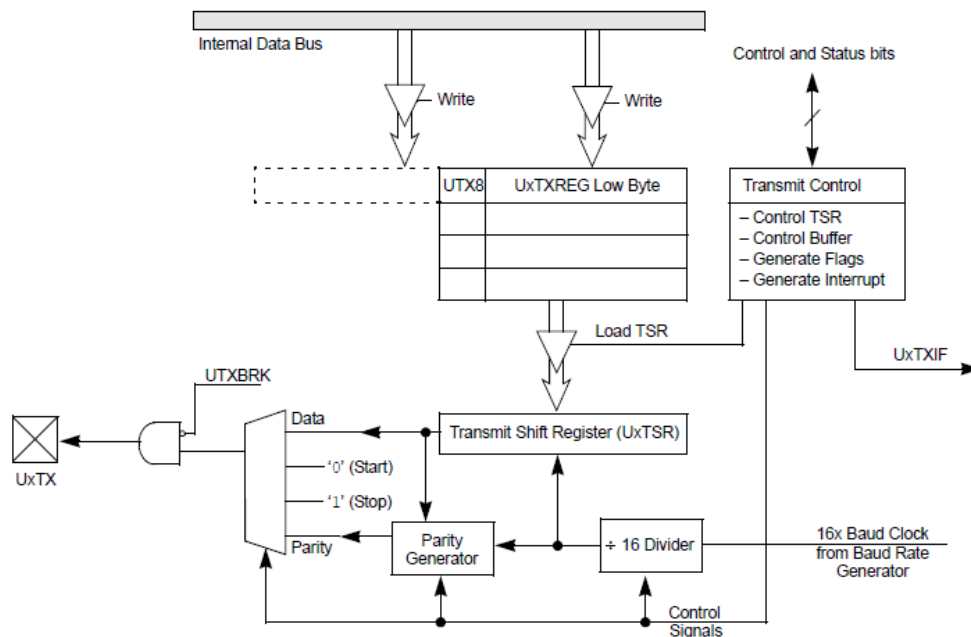


FIGURE 5.15- UART Transmitter Block Diagram [31]

The data reception was made in the HyperTerminal of a computer via USB with a serial port adapter. The register UxBRG is responsible for the choice of the baud rate used in data transmission and its value should be calculated through equation 5.8.

$$UxBRG = \frac{F_{CY}}{16 \cdot BaudRate} - 1 \quad (5.8)$$

The crystal frequency used for the microcontroller clock cycle, allows the use of the standard baud rates with no error, so a baud rate of 115200 was used (UXBRG=15).

The UART module configuration used in the last version of the code is in annex C

5.3.3.3 PWM MODULE

The PWM required for driving the MOSFET that controls the current in the rotor was created using the Output Compare Module of the dsPIC30F4011. This module provides features that are useful in the generation of variable width output pulses like a PWM.

To configure the output compare module for PWM operation the following steps must be performed:

- 1) Set the PWM period by writing to the appropriate Period register.
- 2) Set the PWM duty cycle by writing to the OCxRS register.
- 3) Configure the output compare module for PWM operation.
- 4) Set the TMRx prescale value and enable the timer, TON (TxCON<15>) = 1.

The control bits OCxCON<2:0> are equal to 110, which is the PWM mode of operation without fault protection. The PWM period is specified by writing to the PRx register (Figure 5.16). The PWM period can be calculated using the equation 5.9, the respective frequency of the PWM was set to 1kHz.

$$PWM_{Period} = [(PR_X) + 1] \cdot 4 \cdot T_{OSC} \cdot (TMR_{Xprescale}) \quad (5.9)$$

The dsPIC30F4011 contains four output compare modules, only the output compare 3 was utilized for developing the PWM. Fault protection and CPU Idle modes were disabled. The PWM configuration used in the last version of the code is in annex C.

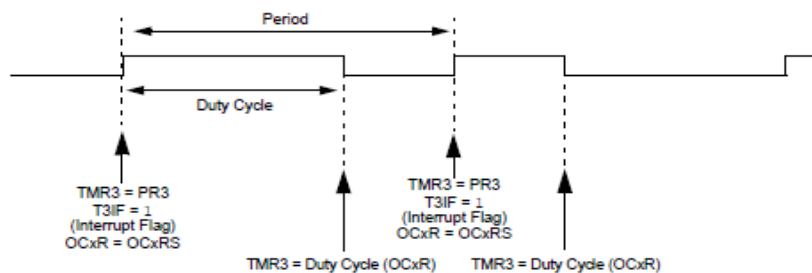


FIGURE 5.16 - PWM Output Timing

5.4 PROTOTYPE TEST RESULTS

The main objective of these prototype tests was to obtain data that would confirm some of the simulation results. In order to obtain the necessary information a computer was connected to the controller by RS232. The data was acquired with a sampling period of 100ms and written in the computer HyperTerminal at a speed of 500ms in order to not overflow the terminal with data and allow looking at the values in real time.

The tests were conducted with the vehicle fixed. The wheel was moved by the engine and then different braking actions were applied to the wheel. The rotor was powered by a 24V battery and the power resistor (0.1Ω) was used as braking load – Dynamic braking. With the motorcycle handle buttons fixed values of PWM duty cycles (which corresponded to a certain amount of current) were applied to the rotor. More specifically duty cycles equal to 99% (about 2.4A), 49% (about 1.2A) and 25% (about 600mA).



FIGURE 5.17 – Assembly to Test the Prototype

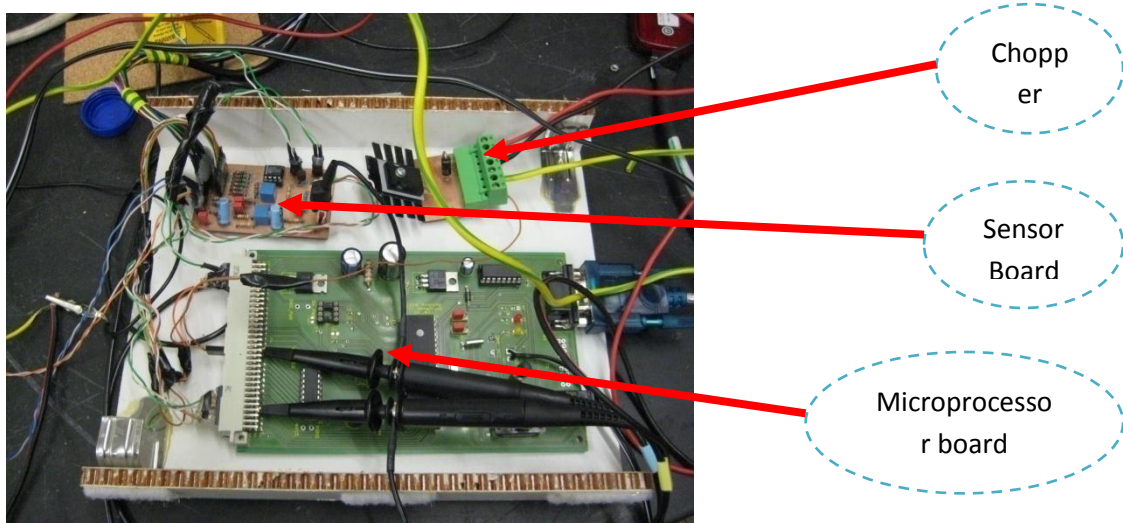


FIGURE 5.18 – Controller Assembly to Test the Prototype

5.4.1 POWER

In Figure 5.19 is represented the power dissipated versus the speed for different duty cycle values. The power dissipated curve is, as expected, higher for high values of duty cycle since as more current flows in the rotor higher is the flux and more current is induced in the stator. Also it is possible to see that the power rising slowly with the speed.

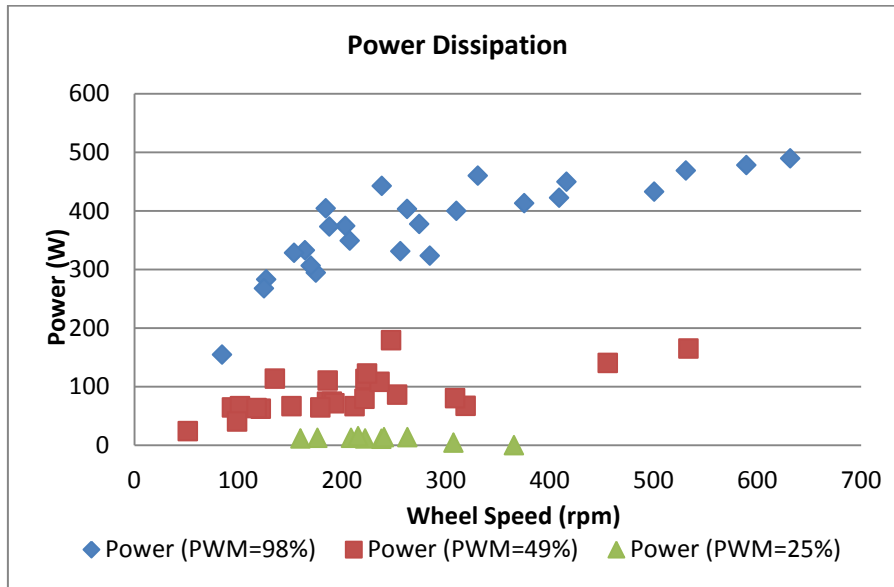


FIGURE 5.19 – Measured Power Dissipated Vs Speed

5.4.2 TORQUE

In the following graphic (Figure 5.20) is possible to verify the values of torque obtained for different values of angular velocity and for different rotor currents (PWM duty cycles). The results obtain and the ranges of values are also characteristic of an alternator (high torque values for low angular velocities, and low torque values for higher angular velocities).

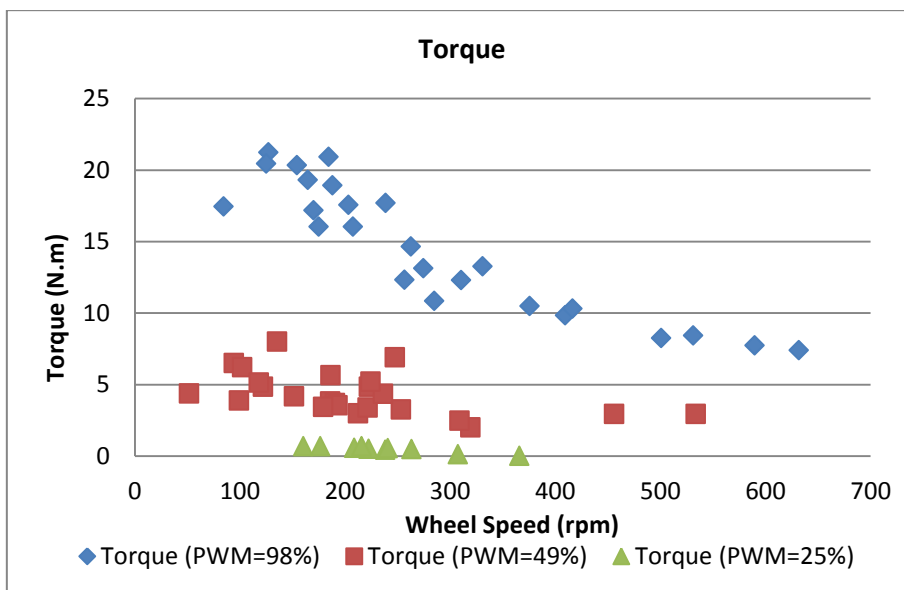


FIGURE 5.20 – Measured Torque Vs Speed

5.5 DISCUSSION AND LIMITATIONS

The previous tests were the only possible tests made in the prototype since the engine had technical problems during this test. That is also why in the previous test so few measured points were taken. Nevertheless these test results already help to experimentally validate some of the simulations results.

In the following section the measured values of Torque and Power were correlated with simulation results. For that a simulation with the same parameters as the real test was realized.

5.5.1 POWER

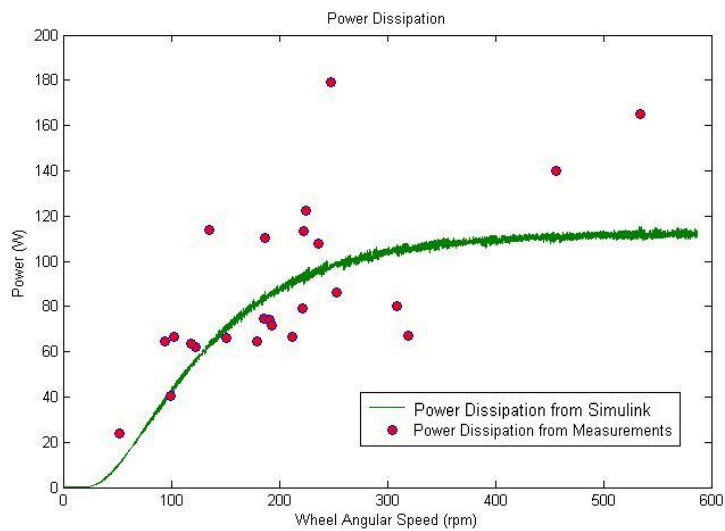


FIGURE 5.21 - Power Dissipation (Duty Cycle =49%)

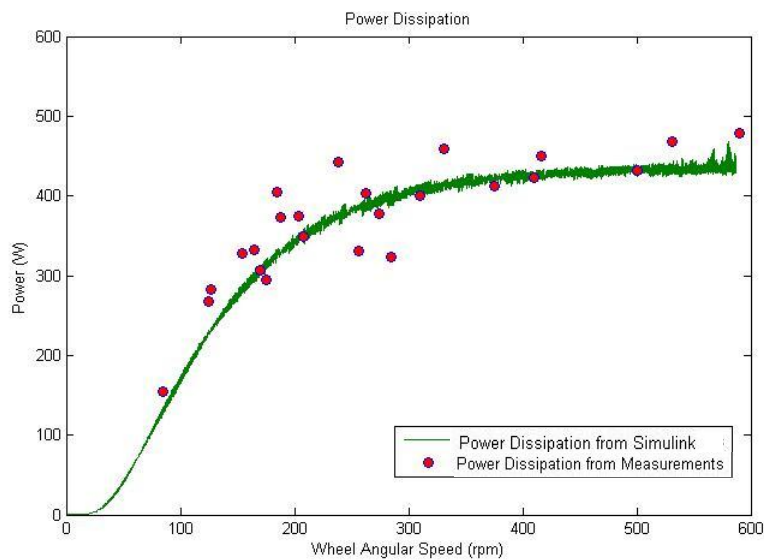


FIGURE 5.22 - Power Dissipation (Duty Cycle =99%)

Comparing the power dissipation graphics in Figure 5.21 and Figure 5.22 is possible to verify that the measured values are approximated to the simulated curve.

5.5.2 TORQUE

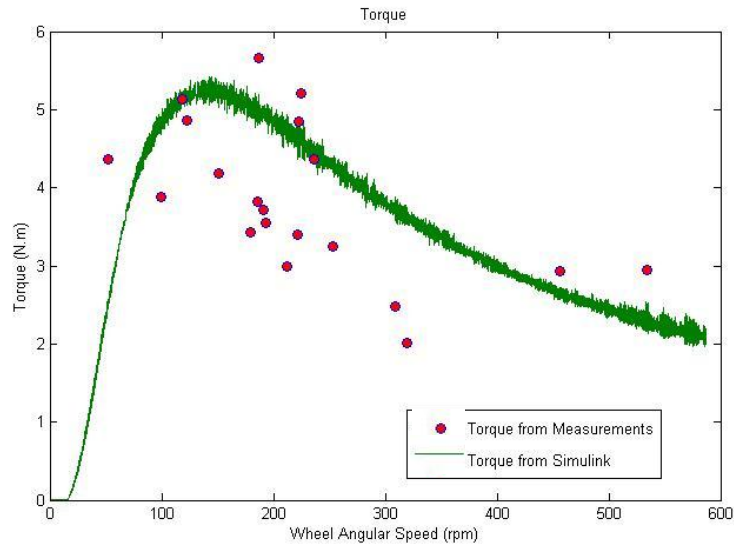


FIGURE 5.23 - Electromagnetic Torque (Duty Cycle =49%)

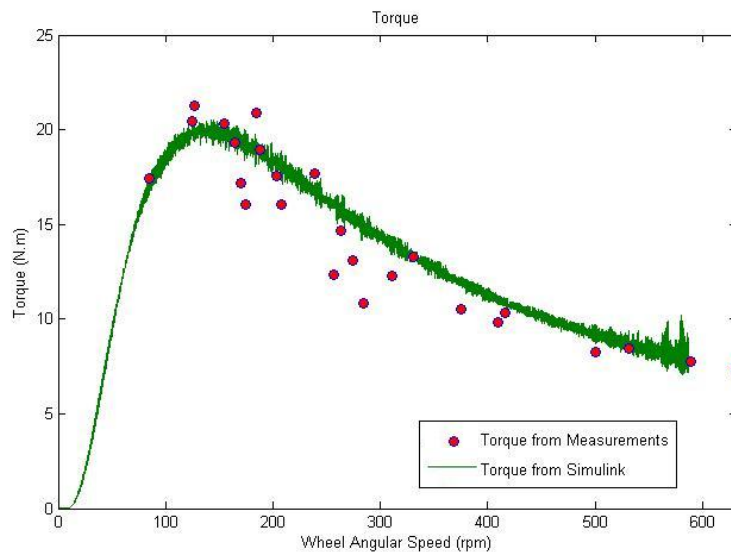


FIGURE 5.24 - Electromagnetic Torque (Duty Cycle =99%)

The torque curves combined with measured values are represented in Figure 5.23 and Figure 5.24. It is possible to verify that there is also a good matching between the torque curves with the experimental values like what was verified with the power profiles.

These results help to validate the simulation models employed. It also help to demonstrate the functioning of the physical equipment and circuitry.

CHAPTER 6

CONCLUSIONS AND FUTURE WORK

6.1 CONCLUSIONS

There is a huge amount of energy involved every time an aircraft brakes. This energy is completely wasted as heat in the disc brakes. Considering the More Electric Aircraft initiative this is an area where the electrification of aviation could help by recurring to an electromagnetic braking system which would be able to regenerate this energy and reduce the wear of the disc brakes. When successful tests of electric taxi concepts are starting to appear, this is the appropriate time to also study the electromagnetic braking possibility.

Preliminary analysis showed that no system of regenerative braking is able to independently stop the landing of aircraft, due to the short time for braking and huge amount of kinetic energy that the airplane possesses. However it might be possible to recover a small amount of energy in this phase beyond the possibility of braking in taxi procedures where the aircraft travels slowly and the braking window is wider. Therefore it was designed a small scale prototype where the testing of the braking control possibility was made. First was developed a simulation in Simulink and afterward a real prototype tests were conducted.

Concerning the Simulink simulation, a complete model of the prototype was implemented and the braking control system was successfully designed, regulating the prototype vehicle deceleration and current. However the maximum deceleration values obtained were not enough to meet the requirements of other vehicles, which would require a more powerful machine.

The real prototype system consisted of a chopper circuit board, a signal processing board for the sensors and a microprocessor board. The equipment was mounted in the vehicle and an open loop test was conducted where the PWM, the signal acquisition and the communication through RS232 were all successfully functioning. Unfortunately limited data was taken.

The Power and Torque results obtained in the open loop prototype tests resemble the simulation results validating the models there. Despite the short amount of experimental data, the author is confident that the closed loop simulation results obtained would be also successful in the prototype given the similarity obtained.

Concerning the aircraft feasibility of this type of concept a few conclusions can be taken:

Bearing in mind that the braking control system for the prototype works, it would also work for the aircraft with the appropriate ratio in the dimensions of the equipment. However unless high powered machines are used, it is very hard to achieve the though braking demands imposed by these vehicles only with regenerative or dynamic braking. Because of this is mandatory that both friction brakes and electromagnetic brakes are controlled in a single integrated system.

Also, a system of this type face a huge weight restriction, which can only be faced with the evolution of technology and with lower weight batteries or even hydrogen powered aircrafts where the regenerated energy would be used to generate hydrogen. Conceptually this is an interesting feature to be added to an aircraft; however the technology necessary to make it a possibility is still not available.

6.2 FUTURE WORK

The prototype vehicle technical problems should be fixed for testing purposes. Also the equipment in the vehicle should be re-arranged in order to test a closed loop braking control. Besides the fact that the alternator was well suited in the motorcycle, other equipment such as the batteries, the controller and all the wiring didn't fit naturally and were hard to attach to the vehicle making it impossible to safely run the vehicle on the road.

Concluded the prototype tests and the expected success of them should be made the simulation of an aircraft specifically with a control system that also include the integrated control the friction brakes.

APPENDIX A

MATLAB SIMULINK MODELS

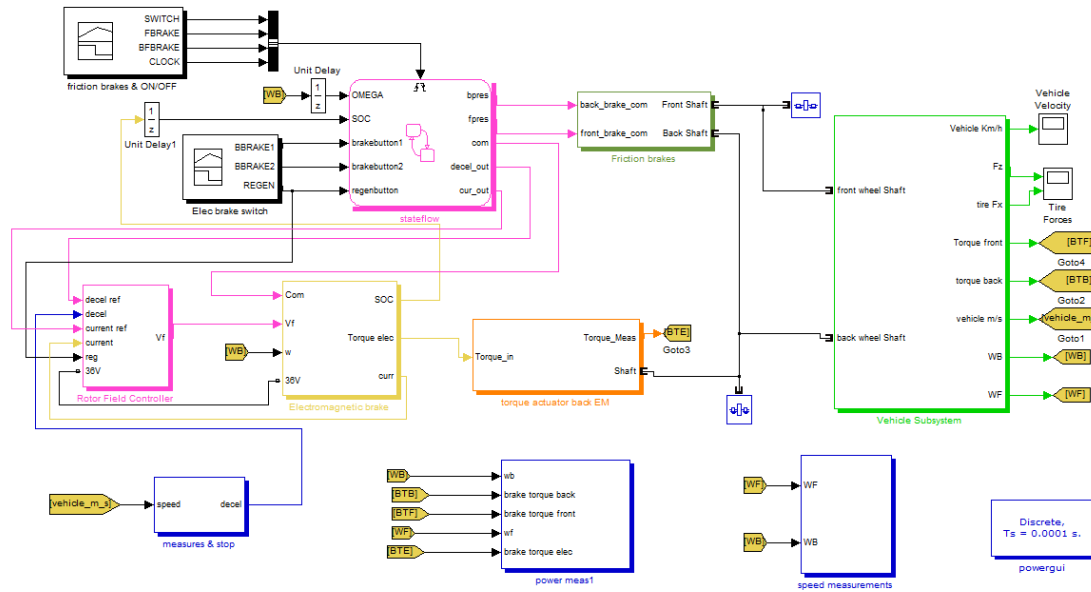


FIGURE A.1 - Simulink Model Overview

Object: Model Overview	
Inputs:	Outputs:
<ul style="list-style-type: none"> BRAKE Button 1; BRAKE Button 2; REGEN Button 	<ul style="list-style-type: none"> Measurements: Velocity; Torque; Power; etc...
<p>Description: In blue is represented the measurements, in pink the controller, in green the vehicle, in yellow the electric system and in orange the torque actuator. This system receives commands from three buttons and measures the effects on the vehicle and the electric system products.</p>	

TABLE A.1 - MODEL OVERVIEW

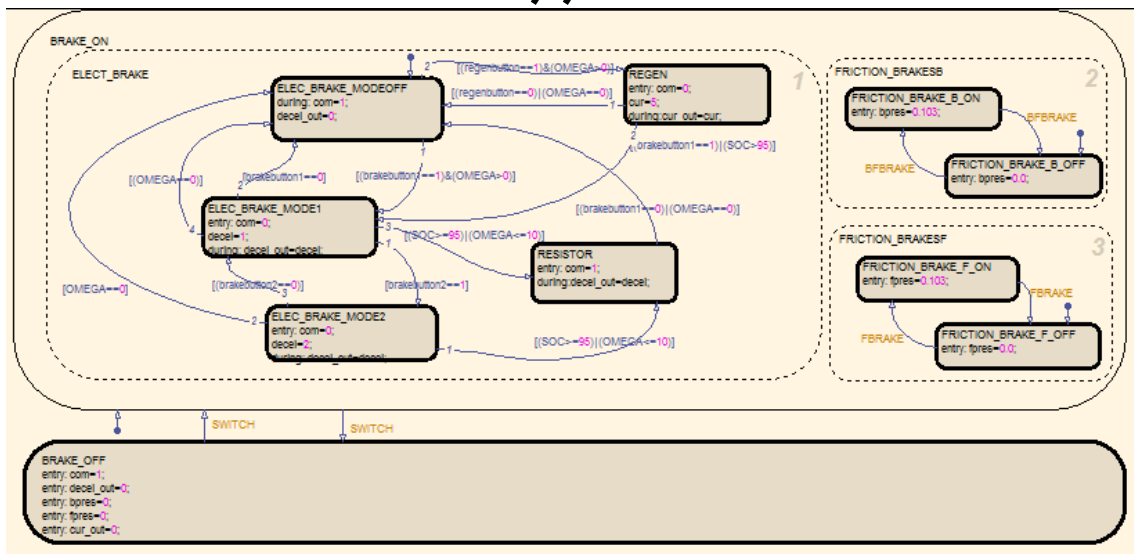


FIGURE A.2 - Main Controller Stateflow

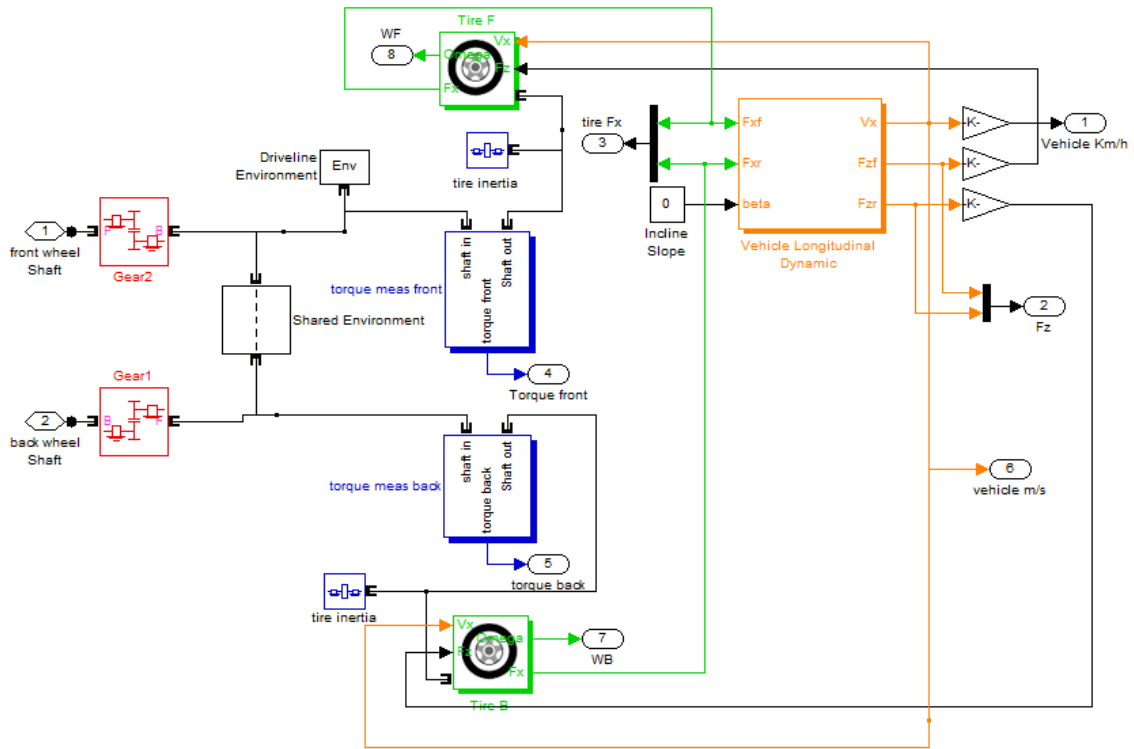


FIGURE A.3 - Vehicle Subsystem Models

Object: Vehicle Subsystem	
Inputs:	Outputs:
<ul style="list-style-type: none"> Front Shaft; Back Shaft. 	<ul style="list-style-type: none"> Velocity; Back and front Torque; Vertical and horizontal Forces; Back and front velocity.
Description: These blocks implement the vehicle dynamics and two wheels. Receives two independent and virtual shafts where the braking torque is applied, and returns the instantaneous values of the vehicle speed, forces and torque.	

TABLE A.2 - Model Overview

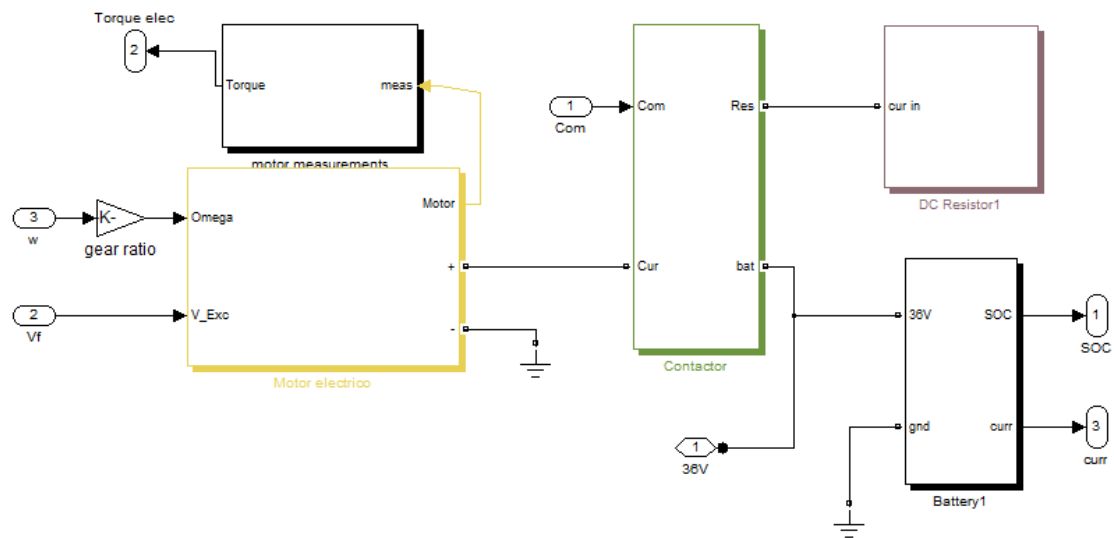


FIGURE A.4 - Electromagnetic Braking System

Object: Electromagnetic Braking System	
Inputs:	Outputs:
<ul style="list-style-type: none"> Angular Speed, Excitation voltage. 	<ul style="list-style-type: none"> Electromagnetic torque; SOC; Deceleration.
Description: This system consists in the machine model, battery model; resistor model, relay model and measurements. The relay connects the load (resistor or battery).	

TABLE A.3 - Electromagnetic Braking System

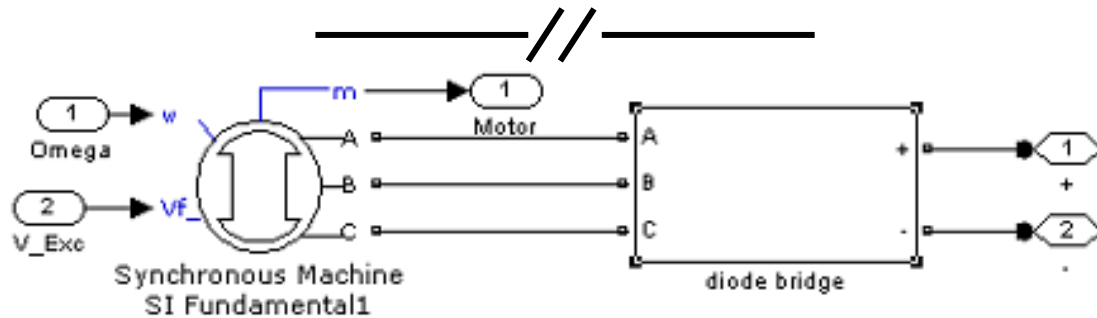


FIGURE A.5 – Alternator And Bridge Rectifier

Object: Alternator and Bridge rectifier	
Inputs:	Outputs:
<ul style="list-style-type: none"> Angular Speed, Excitation voltage. 	<ul style="list-style-type: none"> DC voltage Source, Electromagnetic torque; electric power.
Description: These systems consist in the alternator model and the bridge rectifier model. The alternator receives the angular speed and the excitation, returning a 3-phase voltage source that is rectified in the bridge. Torque and power are measured directly from the motor model	

TABLE A.4 - Alternator And Bridge Rectifier

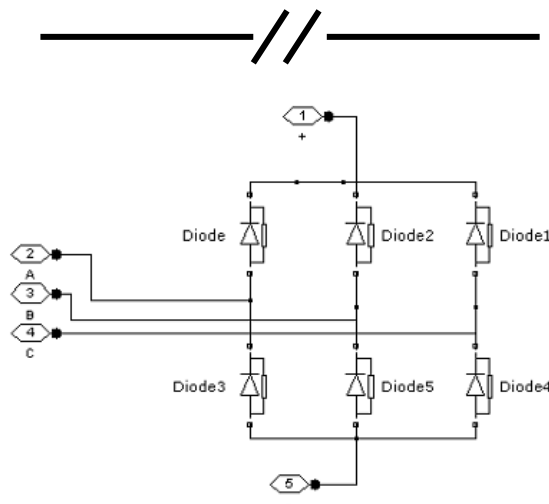


FIGURE A.6 - Bridge Rectifier

Object: Bridge Rectifier	
Inputs:	Outputs:
<ul style="list-style-type: none"> 3 Phase AC Voltage Source 	<ul style="list-style-type: none"> DC Voltage Source
Description: These block implements a bridge made with diodes that are responsible for rectifying the 3-phase AC voltage source.	

TABLE A.5 – Bridge Rectifier



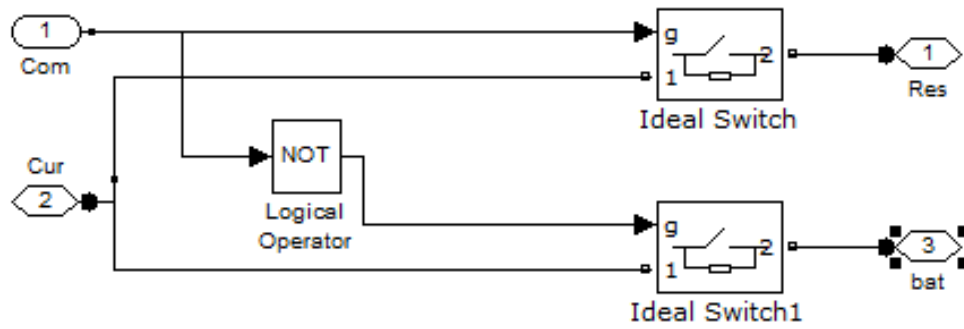


FIGURE A.7 - Relay

Object: Relay	
Inputs:	Outputs:
<ul style="list-style-type: none"> • Command signal; Current 	<ul style="list-style-type: none"> • Battery Current; Resistor Current
Description: The relay block selects which load is used to deploy the current generated in the alternator (battery or resistor). The command signal is given by the main controller.	

TABLE A.6 - Relay

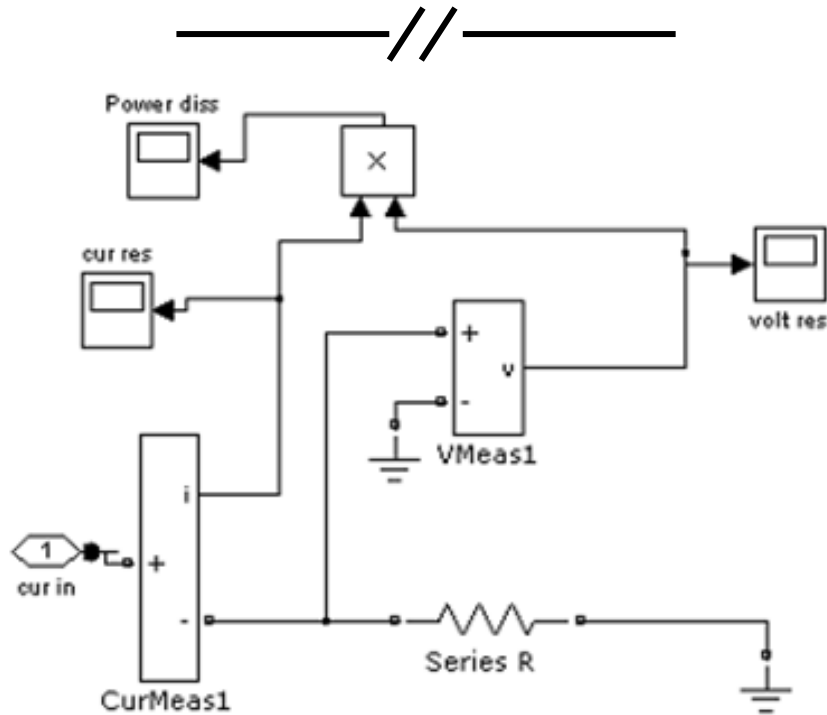


FIGURE A.8 - Resistor and Measurements

Object: Resistor and Measurements	
Inputs:	Outputs:
<ul style="list-style-type: none"> • Current 	<ul style="list-style-type: none"> • N/A
Description: This block implements the model of a resistor and the respective voltage and current measurements.	

TABLE A.7 - Resistor and Measurements



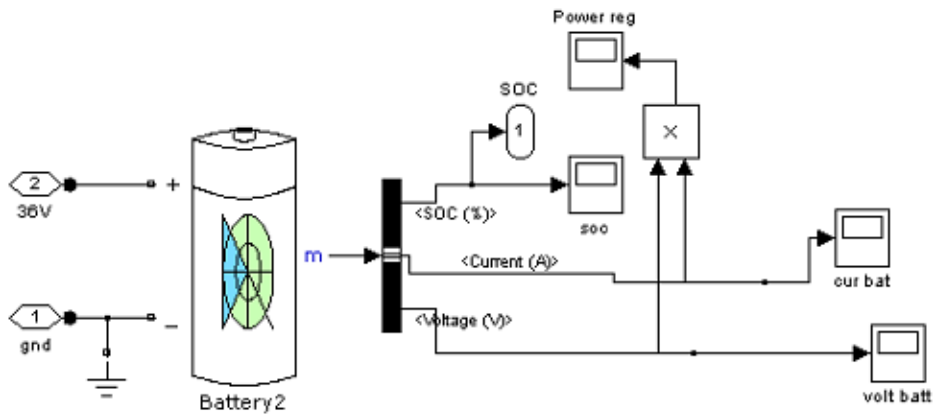


FIGURE A.9 - Battery and Measurements

Object: Battery And Measurements	
Inputs:	Outputs:
<ul style="list-style-type: none"> DC voltage Source 	<ul style="list-style-type: none"> SOC
Description: This block models the battery and the respective voltage and current measurements.	

TABLE A.8 - Battery and Measurements

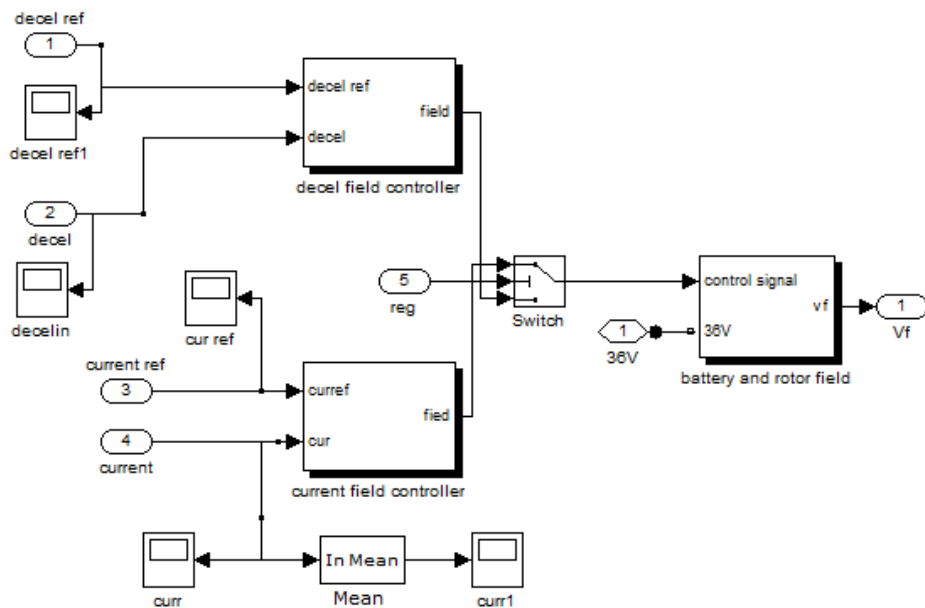


FIGURE A.10 - Braking Controller Block

Object: Braking Controller Block	
Inputs:	Outputs:
<ul style="list-style-type: none"> Deceleration Reference; Deceleration; Current regenerated Reference; Current regenerated; REGEN button; Battery Voltage Source. 	<ul style="list-style-type: none"> Excitation Voltage
Description: This block enclosures 3 sub-blocks: 2 field controllers (current regenerated and deceleration controllers) controlled by the REGEN Button state, and one Rotor field block where the excitation is produced.	

TABLE A.9 - Braking Controller Block

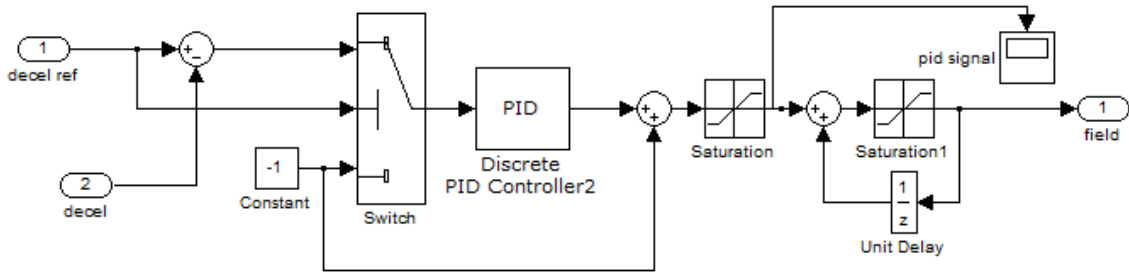


FIGURE A.11 – Deceleration Field Controller

Object: Deceleration Field Controller	
Inputs:	Outputs:
<ul style="list-style-type: none"> Deceleration Reference; Deceleration; 	<ul style="list-style-type: none"> Duty Cycle
<p>Description: In this block a PID controller is applied to the error between the deceleration of the vehicle and a deceleration reference value given by the main controller. Generates the duty cycle of the chopper circuit that regulates the current that pass to the rotor.</p>	

TABLE A.10 - Deceleration Field Controller

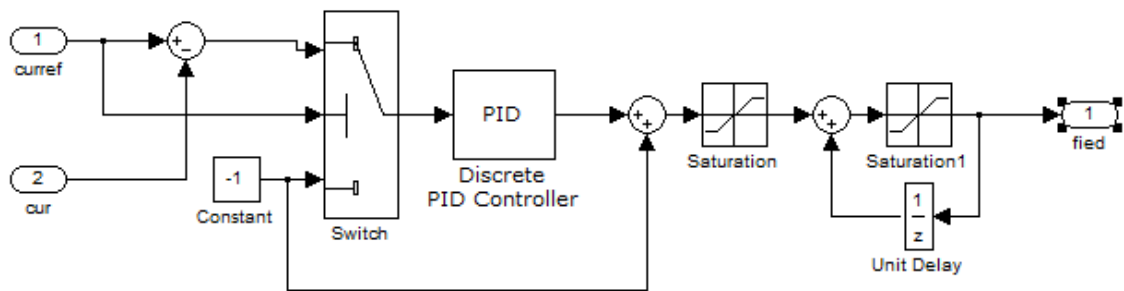


FIGURE A.12 - Current Field Controller

Object: Current Field Controller	
Inputs:	Outputs:
<ul style="list-style-type: none"> Current regenerated Reference; Current regenerated; 	<ul style="list-style-type: none"> Duty Cycle
<p>Description: In this block a PID controller is applied to the error between the current regenerated and a current regenerated reference value given by the main controller. Generates the duty cycle of the chopper circuit that regulates the current that pass to the rotor.</p>	

TABLE A11 – Current Field Controller



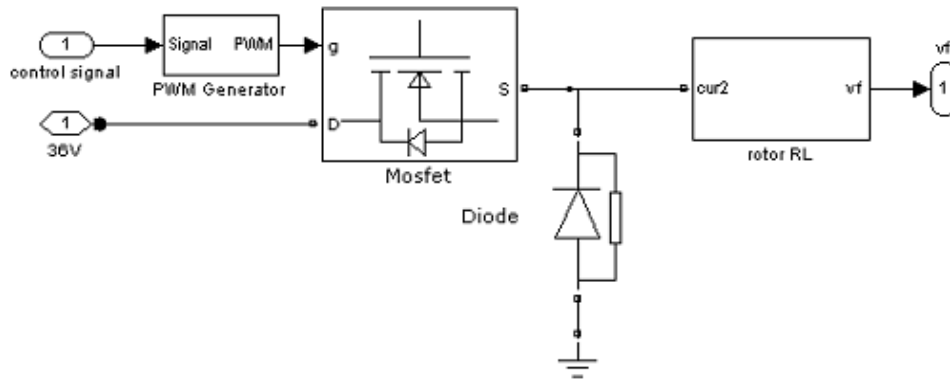


FIGURE A.13 - PWM and Chopper

Object: PWM and Chopper	
Inputs:	Outputs:
<ul style="list-style-type: none"> Duty Cycle; Battery voltage Source. 	<ul style="list-style-type: none"> Excitation Voltage.
Description: In this block the duty Cycle signal is received by the PWM generator and a .a PWM is produced to control a Mosfet that regulates the current that passé to the rotor coil replica. The excitation voltage is then generated by measuring the rotor coil replica.	

TABLE A.12 - PWM and Chopper

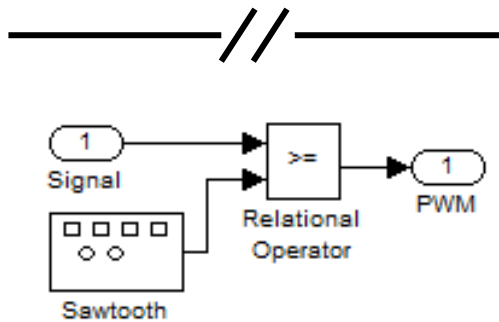


FIGURE A.14 - PWM Generator

Object: PWM Generator	
Inputs:	Outputs:
<ul style="list-style-type: none"> Duty Cycle 	<ul style="list-style-type: none"> PWM.
Description: Generates a fixed period PWM when the duty cycle signal is supplied.	

TABLE A.13 - PWM Generator

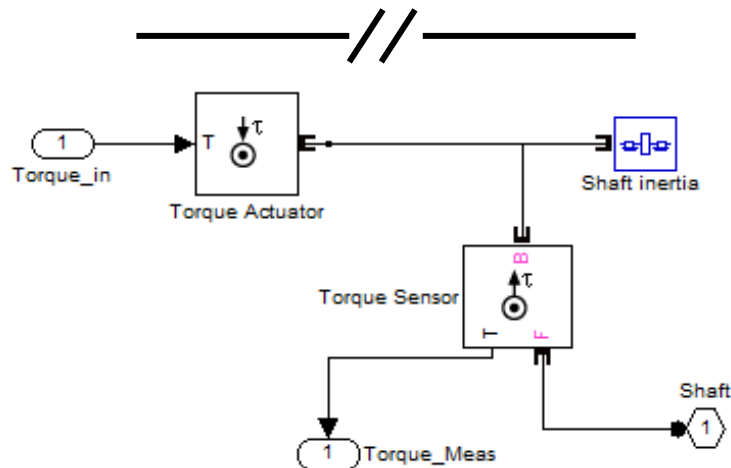


FIGURE A.15 - Torque Actuator

Object: Torque Actuator	
Inputs:	Outputs:
<ul style="list-style-type: none"> Electromagnetic Torque 	<ul style="list-style-type: none"> Shaft; Torque applied.
Description: This blocks actuates the torque produced by the alternator into a virtual shaft connected to the wheel.	

TABLE A.14 - Torque Actuator

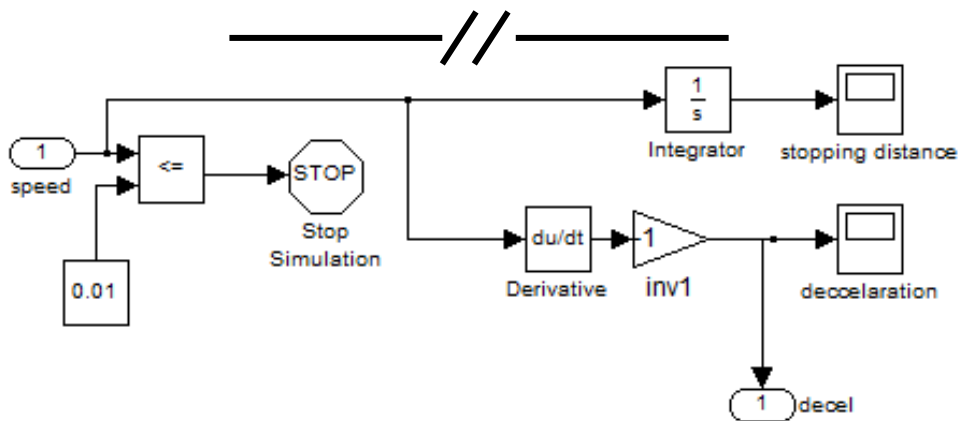


FIGURE A.16 - Simulation Measurements AND STOP Simulation

Object: Simulation Measurements and Stop Simulation	
Inputs:	Outputs:
<ul style="list-style-type: none"> Vehicle speed. 	<ul style="list-style-type: none"> Deceleration.
Description: In this block is calculated the vehicle deceleration and the simulation is stopped if the velocity of the vehicle I close to 0.	

TABLE A.15 - Simulation Measurements and Stop Simulation



APPENDIX B

SENSOR AND CONTROL SYSTEM

GRAPHICS

CURRENT SENSOR

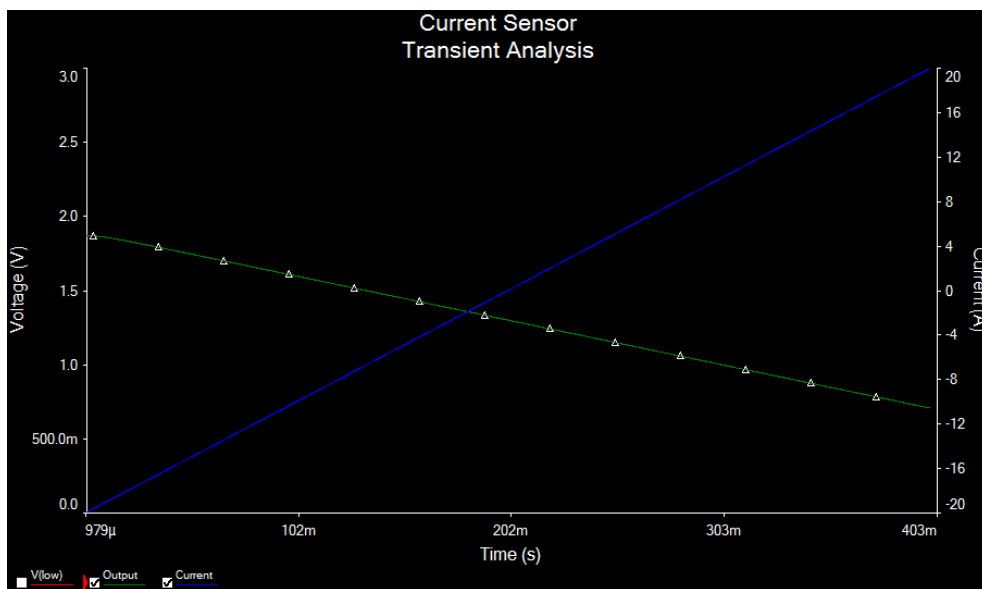


FIGURE B.1 - Current Sensor Performance (Blue - Current, Green Output)

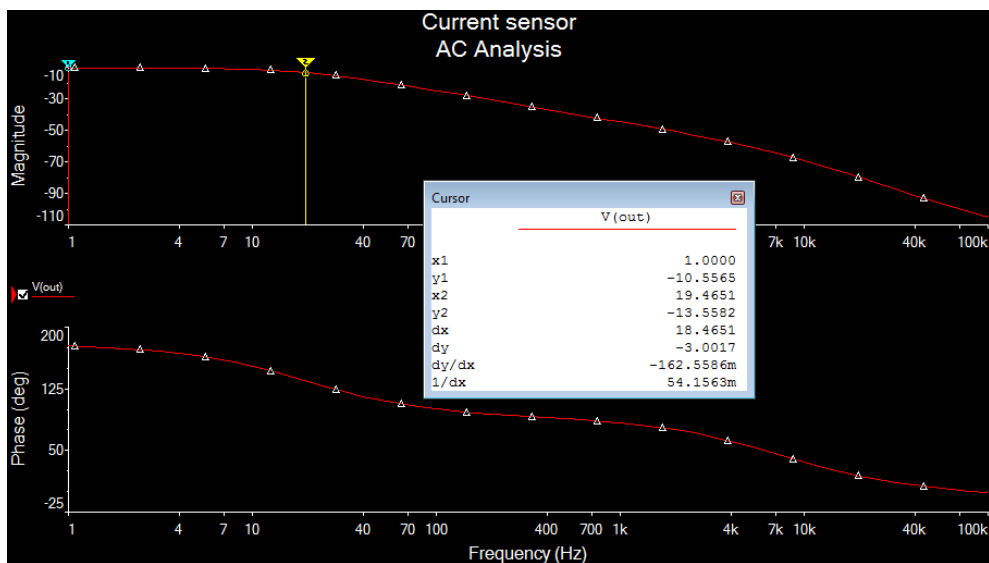


FIGURE B.2 - current output AC Analysis (F-3DB =19,46HZ)

ANGULAR SPEED SENSOR

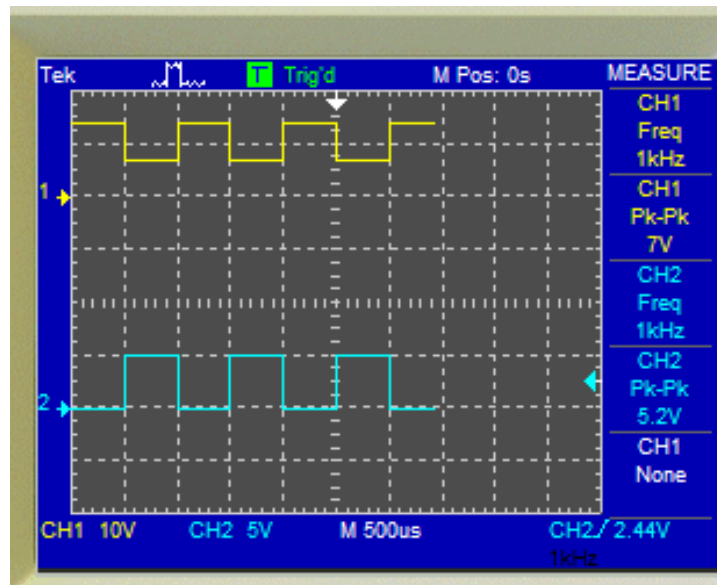


FIGURE B.3 – Angular Speed Sensor Performance (current in Yellow with 1 MA/V and Voltage Output in Blue)

CHOPPER CIRCUIT

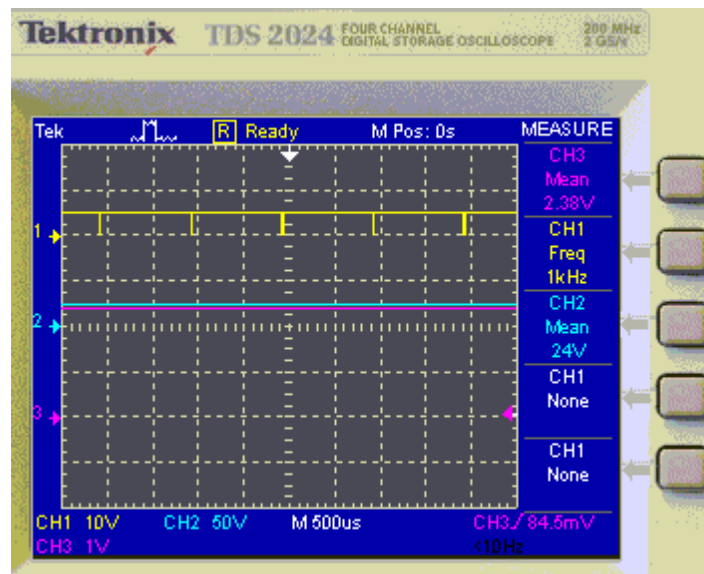


FIGURE B.4 - Chopper Circuit Measurements (Current in Purple with 1 A/V = 2.38A, Chopper Freq = 1KHZ, Duty CYCLE=99% and 24V Battery in Blue)

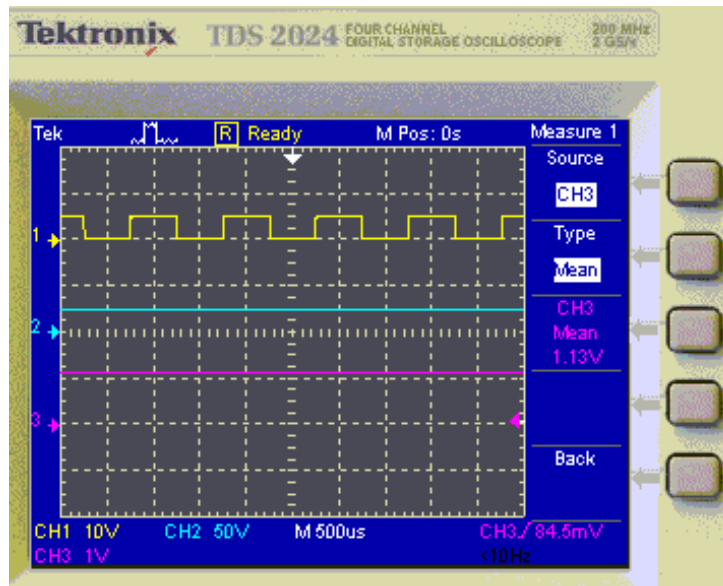


FIGURE B.5 - Chopper Circuit Measurements (Current in Purple with 1 A/V = 1.13A, Chopper Freq = 1KHZ, Duty Cycle=50% and 24V Battery in Blue)

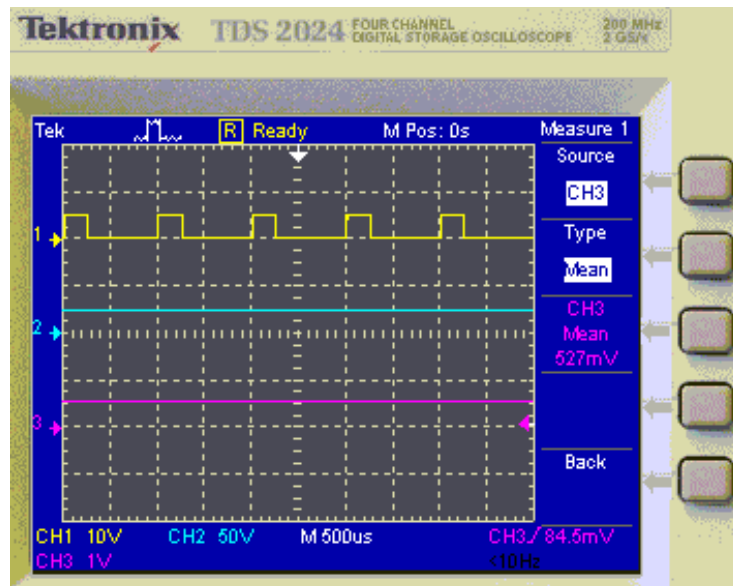


FIGURE B.6 - Chopper Circuit Measurements (Current in Purple with 1 A/V = 527MA, Chopper Freq = 1KHZ, Duty Cycle=99% AND 24V Battery in Blue)

APPENDIX C

PROGRAMMING CODES

```
*/
/***** MAIN FUNCTION *****/

int main(void)
{
    ConfigIO();          // Initialize I/O's
    SerialOpen();
    open_timer2_for_rotorPWM();
    config_rotor_PWM();
    open_input_capture();
        open_adc();          // Initialize ADC
    _ADON = 1;          //Start ADC Module
    T2CONbits.TON = 1;  //Star Timer1 module - 1Khz for PWM and velocity
    calculation

    while(1)
    {
        braking();
        send_data();
    }
    return 0;
}

*/
/***** DEFINES *****/

#define INPUT 1
#define OUTPUT 0

#define BAUD_RATE 115200 //frequency of communication in 100bits/s
#define TOOTH_NUMBER 12

//-----FRQUENCIAS-----
#define FCY 29491200 // External Oscilator = 7.3728 MHz ||| FCY = 7.3728 * 4 MHz ||
FCY = (7.3728 MHZ * PLL 16)/4 || FCY = (FOSC/4)
#define FPWM_ROTOR 1000 // Rotor PWM Frequency 1 KHz

//----- UART -----
#define SEND_DATA_T2MS 500

//----- BRAKING -----

#define BRAKE_TORQUE_CONST (PORTDbits.RD1) //0->5 V
```

```

#define BRAKE_MAX_ACEL (!PORTDbits.RD0)           //5->0 V
#define BRAKE_MED_ACEL (PORTEbits.RE8)           //0->5 V
#define TORQUE_REF 2.0
#define ALPHA_REF 0.5
#define IBAT_REF 1.0

//----- ADC -----

#define READ_ADC1_T2MS 100
#define IBAT_FACTOR 28.0
#define IBAT_OFFSET 1.27
#define VBAT_FACTOR 8.47

*/
/***** ADC CONFIG *****/

void open_adc(){

    _ADON = 0; // 0 - ADC off, 1- ADC on

    /* ADCON1 */
    _DONE = 0; // Indicates that the reading ended (just reading)
    _ASAM = 0; // 1 - Automatic acquisition
    _SSRC = 7; // 7 - conversion started automatically at the end of the ADC clock,
    _SAMP = 0; // 0 - begins the conversion if SSRC == 0. 1 - begins the sampling
    _FORM = 0; // 0-3 selects the format of the data writing
                // 0-full; 1, with full signal; 2-fractional; 3-fraccinal with signal
    _ADSIDL = 0; // 0-The ADC operates when the processor is IDLE

    /* ADCON2 */

    _ALTS = 0; // 0 - only the inputs of the MUXA are chosen, 1 if SMPI == 0 the inputs
of MUX A and B are read alternately

    _BUFM = 0; // 1, the results are written alternately in the first 8 buffers and in the
second 8 buffers on each interruption, 0 - the results are always written in buffers in order
starting from 0

    _SMPI = 0; // 0-15 number of acquisitions-1 before an interruption occurs

    _ADIF=0; // Flag of interruption is put on 1 when the read ends
    _ADIE = 0; //interrupt enable
    _ADIP = 1; //interrupt priority

    _CSCNA = 0; // 1 - the inputs are read sequentially over MUX A. Inputs are chosen
by ADCSSL

    _VCFG = 0; // 0 - + AVdd -Avss;
    _SAMC = 1; // 1-31 number of TAD, acquisition
    _ADRC = 0; // 1 - Clock of the ADC is RC and ADC can operate during the SLEEP
mode, the conversion takes one more TAD

```

```

        _ADCS = 3 ;    //((( long) TAD) * FCY) / 500-1; // 0-63 of the ADC clock TAD TCY = *
(ADCS +1) / 2

        /* ADCHS */

        _CH0SA = 0; // Select the input of the MuxA
        _CH0NA = 0; // 0-Chan 0 neg i / p sel for SAMPLE-A is Vref ,1-Chan 0 neg i / p sel for
SAMPLE A is AN1

        _CH0SB = 0; // Select the input of the Mux B
        _CH0NB = 0;

    }

int read_adc(int channel){
    int x;
    _CH0SA = channel;
    _SAMP=1;
    while(_SAMP);
    while(!_DONE);
    x=ADCBUF0;

    return x;
}

*/
/***** UART CONFIG *****/

void SerialOpen(){
    __C30_UART = 2;

    Serial.receiveddata=Serial.rbuf;
    Serial.transmitdata=Serial.tbuf;
    Serial.datatransmitted=1;

    // The receive buffer has space for 4 characters plus 1
    //The maximum baud rate possible is FCY / 16 (for UxBRG = 0),
    //and the minimum baud rate possible is FCY / (16 * 65536).
    U2BRG = 15 ;//FCY/BAUD_RATE/16-1; // set the baud rate

    U2MODEbits.UARTEN = 1, //enable uart
    U2STAbits.UTXEN = 1, //enable transmission
    U2MODEbits.STSEL = 0; // 0 - 1 stop bit, 1-2 stop bits
    U2MODEbits.PDSEL = 0; // 0-8bits without parity ,1-8bits odd 2-8bits even, 3-9bits
without parity

    U2MODEbits.ALTIO = 0; // 0 - uses pins U2RX, U2TX, 1 - uses the pin U2ARX,U2ATX
    U2STAbits.UTXBRK = 0; // 1-Put pin of transmission in 0 regardless of what is
transferring (used to send breaks)

    U2STAbits.UTXISEL = 1; // 1-interruption when the transmission buffer is empty
    U2STAbits.URXISEL = 2; // 0,1-interruption of receive is made when a byte is received

```

```

        // 2-interruption when missing a byte to fill reception buffer
        // 3-interruption when the the reception buffer is full

        U2MODEbits.LPBACK = 0; // 0-no loopback 1-with loopback (Tx and Rx are linked and
Rx ceases to function normally)
        U2MODEbits.WAKE = 0; // 0-nothing happens in sleep mode, 1-in sleep mode the
reception of a byte generates an interruption

        U2MODEbits.USIDL = 0; // 0 -UART works when dsPIC is in idle mode, 1-ceases to
operate in idle mode

        U2STAbits.ADDEN = 0; // 0-Reception of data, 1-Reception of addresses of memory
(valid only for 9-bit)

        // Variables of warning
        U2STAbits.URXDA = 0, //indicates that there are no characters in the reception buffer
        U2STAbits.OERR = 0; // indicates that the reception buffer is full, and a byte was
received but couldn't enter the buffer
        // If it is 1, the reception stops

        U2STAbits.UTXBF = 0; // indicates that the transmit buffer is full

        // Interruptions
        _U2RXIE = 1; //0-Interruption off, 1-Interruption on
        _U2TXIE = 1;
        _U2RXIP = 3; // Priority for the interruption 0-lowest priority, 7-highest priority
        _U2TXIP = 2; // If two interruptions have the same priority, who has priority is decided
by the table of natural priorities (see manual dsPIC pg. 58)
    }

void SerialWrite(const char * string) {
    while(!U2STAbits.TRMT);
    Serial.datasend=string;
    Serial.datatransmitted=0;
    _U2TXIF = 1;
}

void print_string(const char * s){
    while(!U2STAbits.TRMT);
    while(*s!='\0') *(Serial.transmitdata++)=*(s++);
    *Serial.transmitdata='\t';
    Serial.transmitdata++;
}

void Serial_print() {
    while(!U2STAbits.TRMT);
    if(Serial.transmitdata>Serial.tbuf)
        if(*(Serial.transmitdata-1)=='\t')
            Serial.transmitdata--;
    *Serial.transmitdata='\0';
    Serial.transmitdata=Serial.tbuf;
    Serial.datasend=Serial.tbuf;
}

```

```

        Serial.datatransmitted=0;
        _U2TXIF = 1;
    }

char SerialInstruction_transmitted(){
    if(U2STAbits.TRMT) return 1;
    return 0;
}

void __attribute__((__interrupt__,auto_psv)) _U2TXInterrupt(void)
{
    _U2TXIF = 0;
    if(!Serial.datatransmitted){
        while(!U2STAbits.UTXBF){ //fill transmit buffer until it is full
            if(*(Serial.datasend)=='\0'){ //or until the end string character is read
                U2TXREG='\r';
                // Serial.last_char_transmitted=1;
                Serial.datatransmitted=1;
                break;}
            else {U2TXREG=*(Serial.datasend)++;}
        }
    }
}

*/
/***** PWM CONFIG *****/

void config_rotor_PWM(void){

    OC3CONbits.OCSIDL = 1; // 0 = Output compare x will continue to operate in
CPU Idle mode // 1 = Output compare x will halt in CPU Idle mode

    OC3CONbits.OCFLT = 0; // 0 = No PWM Fault condition has occurred
// 1 = PWM Fault condition has occurred

    OC3CONbits.OCTSEL = 0; // 0 = Timer2 is the clock source for compare x
// 1 = Timer3 is the clock source for compare x

    OC3CONbits.OCM = 110;

    OC3R = 0; // No initial delay
    OC3RS = 0;

}

*/

```

```
/****** BRAKING *****/
```

```
void __attribute__((__interrupt__,__auto_psv)) _T2Interrupt(void){
    _T2IF=0;
    t2counter_vel++;
    t2counter_adc1++;
    t2counter_send_data++;
    //measure routine
    if(t2counter_adc1==READ_ADC1_T2MS){
        vbat = read_adc(0);
        ibat = read_adc(2);
        //vbat = (vbat/1024.0)*(VBAT_FACTOR*5.0);
        ibat = (ibat/1024.0)*5.0;
        ibat = (ibat-IBAT_OFFSET)*(IBAT_FACTOR);
        if (ibat<0) ibat = 0;
        t2counter_adc1=0;
    }
    if(t2counter_send_data==SEND_DATA_T2MS){
        send_adc1 = 1;
        t2counter_send_data = 0;
    }
}
```

```
void __attribute__((__interrupt__,__auto_psv)) _IC7Interrupt(void){
    _IC7IF = 0;
    delta_t_tooth = (t2counter_vel)*((double)(FCY/FPWM_ROTOR)) + ((double) IC7BUF);
    delta_t_tooth = (delta_t_tooth/((double) FCY)); //Real time (milliseconds)
    if (delta_t_tooth!=0) {
        w_vel_aux = w_vel;
        w_vel = (2.0*3.14159)/(delta_t_tooth*((double) TOOTH_NUMBER));
    }
    else
        SerialWrite("\nDivision by ZERO: delta_t_tooth\n\n");
    if(w_vel!=0){
        alpha_vel = (w_vel-w_vel_aux)/delta_t_tooth;
    }
    else
        SerialWrite("\nDivision by Zero: w_vel\n\n");
    t2counter_vel = 0;
}
```

```
void braking(void){
    if(BRAKE_MAX_ACEL && BRAKE_MED_ACEL) {
        SerialWrite("ELEC_BRAKE_MODE2!!\n");
        while(BRAKE_MAX_ACEL && BRAKE_MED_ACEL) {
            OC3RS = (int) (0.99*PR2);
            send_data();
        }
    }
}
```

```

        OC3RS = 0;
        return;
    }
    if(BRAKE_MED_ACEL) {
        SerialWrite("ELEC_BRAKE_MODE1!!\n");
        while(BRAKE_MED_ACEL && !BRAKE_MAX_ACEL) {
            OC3RS = (int) (0.50*PR2);
            send_data();
        }
        OC3RS = 0;
        return;
    }
    if(BRAKE_TORQUE_CONST) {
        SerialWrite("REGEN!!\n");
        while(BRAKE_TORQUE_CONST && !BRAKE_MAX_ACEL &&
!BRAKE_MED_ACEL) {
            OC3RS = (int) (0.25*PR2);
            send_data();
        }
        OC3RS = 0;
        return;
    }
}

void send_data(void){

    if(send_adc1){
        print_int((int) (vbat)); print_string(";"); //print vbat in milivolts
        print_int((int) (ibat*100.0)); print_string(";"); //print ibat in milivolts
        //print_int((int) (delta_t_tooth*1000)); print_string(";");
        //print gear tooth gap time in milliseconds
        print_int((int) (w_vel*10.0)); print_string(";");
        //print radial velocity
        //print_int((int) (torque*10.0)); print_string(";");
        ///print_int((int) (error_aux*10.0)); print_string(";");
        //print_int((int) (pid_value_torque*1000.0));
        print_int((int) (((double) OC3RS)/((double) PR2))*100);
        if (teste==1){
            teste=0;
        }
        print_string("\n");
        Serial_print();
        //vbat=0;ibat=0;w_vel=0;torque=0;error_aux=0;pid_value_torque=0;
        send_adc1 = 0;
    }
}

```

APPENDIX D

MANUFACTURED PIECES

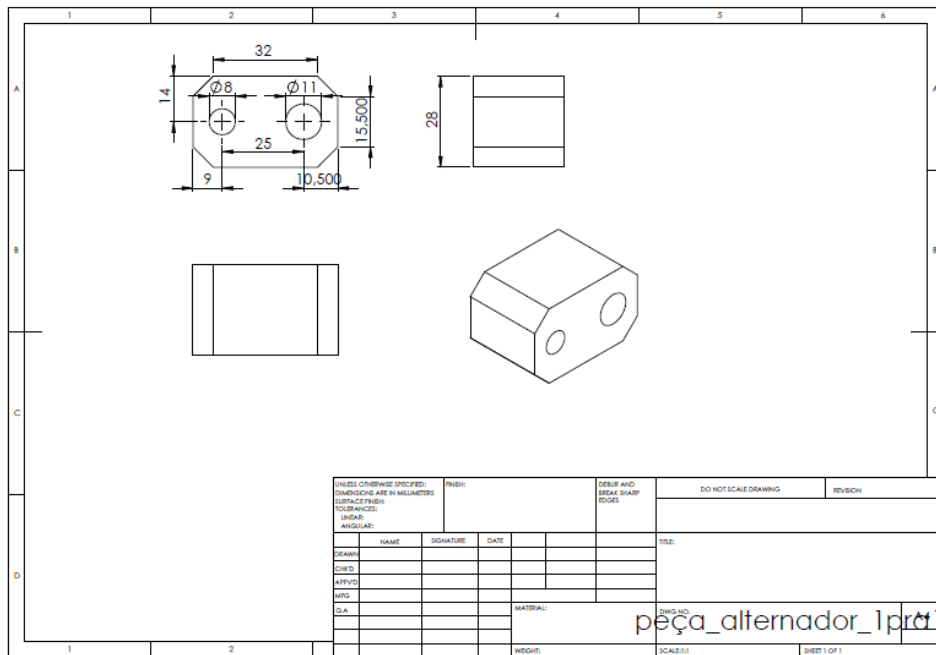


FIGURE C.1 – Alternator Support Piece

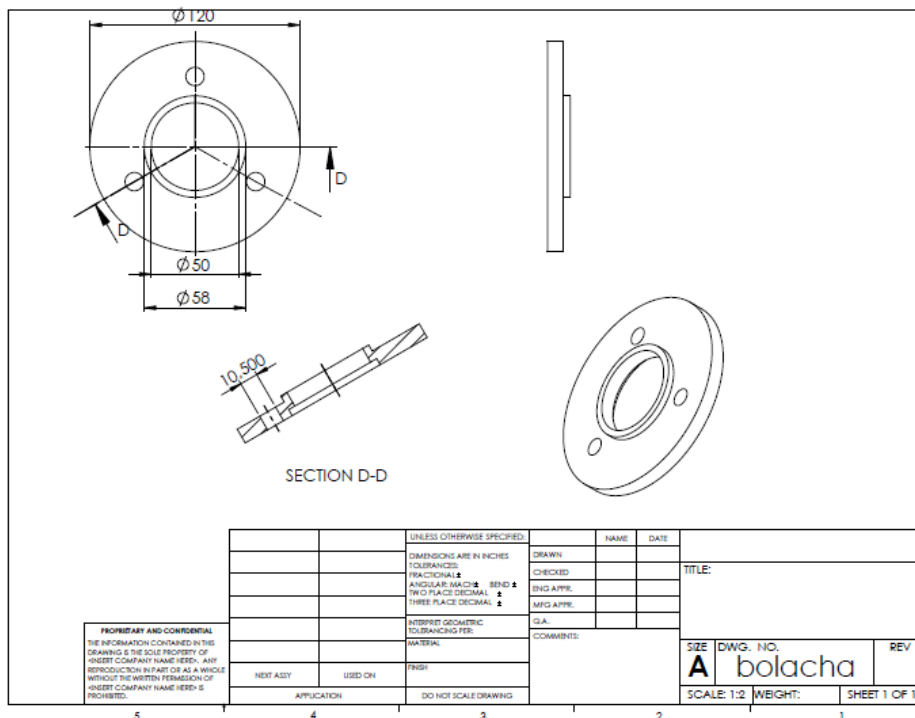


FIGURE C.2 – Separation Disc for the Wheel's Gear

BIBLIOGRAPHY

- [1] **Boeing**. news. *boeing.com*. [Online] 2005.
http://www.boeing.com/news/releases/2005/q3/nr_050801a.html.
- [2] "*The More Electric Aircraft: the past and the future?*", **R. I. Jones**. Colloquium on Electrical Machines and Systems for the More Electric Aircraft, IEEE, London Nov. 1999.
- [3] "*Boeing Commercial Airplanes Current Product Overview*," **Gervais, E.L.** San Diego, CA : Presented at San Diego County Regional Airport Authority Advisory Committee Meeting,, Jul12, 2007.
- [4] *Aircraft Electrical Power Systems – Charged with Opportunities*. **Srimoolanathan, Balaji**. 2008.
- [5] **Chorus Motors**. Wheeltug. <http://www.wheeltug.gi/index.shtml>. [Online]
- [6] **designnews**. Electric_WheelTug_System. *designnews.com*. [Online]
http://www.designnews.com/article/14474-Electric_WheelTug_System_to_Move_Planes_on_the_Ground.php.
- [7] **weekly, electronics**. Innovative motor powers aircraft landing wheels.
electronicsweekly.com. [Online]
<http://www.electronicweekly.com/Articles/Article.aspx?liArticleID=37359&PrinterFriendly=true>.
- [8] **Borealis**. Airport Report. [16]
http://www.borealis.gi/press/WT_Marketing_Partners_Airports_FAQ1_ECOhand.pdf. [Online]
- [9] **Aviation Unit Maintenance**. Aircraft Brake Systems. *TM-1-1500-204-23-2 General Aircraft Maintenance (Pneudraulics Maintenance and Practices) Volume 2 Manual*.
- [10] **Safran Group - Messier Buggati**. Electric brakes. http://www.messier-buggati.com/IMG/pdf/frein_en-2.pdf. [Online]
- [11] *Propulsion Systems for Hybrid Vehicles*. **John M. Miller – Peter Peregrinus Ltd**. Dec. 2003.
- [12] *Electric Motor Handbook*. **James Kirtley, H. Beaty**. 1976
- [13] *Power Electronic Circuits*. **Batarseh, I**. West Sussex, England : John Wiley and Sons, Ltd., 2003.
- [14] **US Department of energy**. Energy and Power by type.
http://www1.eere.energy.gov/vehiclesandfuels/facts/2010_fotw607.html. [Online] Jan 2010.
- [15] **Cadex Electronics Inc**. Battery University. <http://www.batteryuniversity.com/partone-3.htm>. [Online] 2006.

- [16] **conceptcarz**. Mercedes-Benz-SLS-AMG-E-Cell-Prototype. *conceptcarz.com*. [Online] 2010. <http://www.conceptcarz.com/z18535/Mercedes-Benz-SLS-AMG-E-Cell-Prototype.aspx>.
- [17] **Wheeltug System**. Benefits. *Wheeltug.gi*. [Online] <http://www.wheeltug.gi/benefits.shtml>.
- [18] **The MathWorks**. Simdriveline™ 1 User's Guide. [Online] <http://www.mathworks.com/industries/auto/>.
- [19] **Husain, I.** *Electric and Hybrid Vehicles, Design Fundamentals*. s.l. : CRC, 2003.
- [20] **Gillespie, T. D.** "Fundamentals of vehicle dynamics," Ch. 1-4. [book auth.] SAE. 1992.
- [21] **Cossalter, Vittore.** *Motorcycle Dynamics (Second Edition)* . 2006.
- [22] *Load Dump Transient Control of a 42V Automotive Generator*. **Chandra S. Namuduri, Balarama V. Murty, Michael G. Reynolds**. Germany : 35th Annual IEEE Power. Electronics Specialists Conference, 2004.
- [23] **International Rectifier**. *IRFP4310ZPbF POWER MOSFET datasheet*. 2008.
- [24] **JIE SHU, YONG ZHANG, CHENGLIANG YIN**. *Longitudinal control of hybrid electric buses using traction motor and pneumatic braking system*. WSEAS Transactions on Circuits and Systems – volume 8, issue 11, November 2009.
- [25] **Inc., The MathWorks**. Design and simulate state machines and control logic. [Online] 2007. <http://www.mathworks.com/products/stateflow/>,.
- [26] **Tham, M.** study notes on Digital Control. *Discretised PID Controllers*. [Online] <http://lorien.ncl.ac.uk/ming/digicont/digimath/dpid1.htm>.
- [27] *Ziegler-Nichols' Open-Loop Method*. **Haugen, Finn**. s.l. : TechTeach, Jul/2010.
- [28] **Lepkowski, Jim**. *Application Note 894: Motor Control Sensor Feedback Circuits*. s.l. : Microchip Technology Inc, 2003.
- [29] **Allegro MicroSystems, Inc.** *Two-Wire True Zero Speed Miniature Differential Peak-Detecting Gear Tooth Sensor IC with Continuous Calibration*. May 4, 2009. ATS642LSH.
- [30] **Microchip Technology Inc**. DSPIC30F Family Reference Manual. 2006.
- [31] **Microchip Technology Inc**. DSPIC30F4011 Data sheet. 2008.
- [32] MPLAB C30 C Compiler User's Guide. 2007.